Incorporation of the prosthetic heme group into cytoplasmic and membrane proteins

Von der Fakultät für Lebenswissenschaften

der Technischen Universität Carolo-Wilhelmina

zu Braunschweig

zur Erlangung des Grades einer

Doktorin der Naturwissenschaften

(Dr. rer. nat.)

genehmigte

D i s s e r t a t i o n

von Simone Huhn
aus Wolfenbüttel

1. Referent: Professor Dr. Dieter Jahn
2. Referentin: Dr. Gunhild Layer
eingereicht am: 21.12.2011
mündliche Prüfung (Disputation) am: 07.03.2012

Druckjahr 2012

Vorveröffentlichungen der Dissertation

Teilergebnisse aus dieser Arbeit wurden mit Genehmigung der Fakultät für Lebenswissenschaften, vertreten durch den Mentor der Arbeit, in folgenden Beiträgen vorab veröffentlicht:

Tagungsbeiträge

Huhn, S., Jahn, M. & Jahn, D.: Heme Transport (Poster) VAAM-Jahrestagung, Hannover, Germany (2010).

Huhn, S., Jahn, M. & Jahn, D.: Heme Transport (Poster) Tetrapyrrole Discussion Group Meeting (TPDG), Berlin, Germany (2010).

Huhn, S., Jahn, M. & Jahn, D.: Heme Transport (Poster) VAAM-Jahrestagung, Karlsruhe, Germany (2011).

TABLE OF CONTENTS

ABBREVIATIONS

A	Ampere
A_λ	absorption at wavelength λ in nm
Å	Ångström
ALA	5-aminolevulinic acid
amp	ampicillin
APS	ammonium peroxodisulfate
ATP	adenosine triphosphate
BACTH	Bacterial Adenylate Cyclase Two Hybrid
BCIP	5-bromo-4-chloro-3-indolylphosphate
bfrA	bacterioferritin A
bp	base pair
C	Celsius (° C)
cAMP	Cyclic adenosine monophosphate
CAP	catabolic activator protein
carb	carbenicillin
cm	chloramphenicol
COPROGEN	coproporphyrinogen III
CPDH	coproporphyrinogen III dehydrogenase
CPO	coproporphyrinogen III oxidase
Da	Dalton
DMF	dimethylenformamide
DMSO	dimethylsulfoxide
DNA	deoxyribonucleic acid
(d)dNTP	(di)deoxyribonucleotide triphosphate
DTT	1,4-dithio-D,L-threitol
EDTA	ethylenediamine tetraacetic acid
e.g.	*exempli gratia* (for instance)
et al.	*et alteri* (and others)
F	Farad
FLP	flippase recombination enzyme
Fnr	fumarate and nitrate reduction regulator

FRT sites	FLP recognition target sites
for	forward
g	→ *centrifugation*: earth gravity
	→ *weight*: gram
GluTR	glutamyl-tRNA reductase
gm	gentamicin
GSA	glutamate-1-semialdehyde
GSAM	glutamate-1-semialdehyde-2,1-aminomutase
GST	glutathione S-transferase
h	hour
HEPES	4-(2-hydroxyethyl)-piperazine-1-ethane sulfonic acid
HemF	oxygen-dependent coproporphyrinogen III oxidase
HemH	ferrochelatase
HemN	oxygen-independent coproporphyrinogen III oxidase
HemY	protoporphyrinogen IX oxidase
HemZ	proposed oxygen-independent coproporphyrinogen III oxidase
HPLC	high performance liquid chromatography
i.e.	*id est* (that is to say)
IPTG	isopropyl-b-D-thiogalactopyranoside
IRP	iron regulatory protein
K	Kelvin
k	kilo
kan	kanamycin
katA	catalase A
kDa	kilo Dalton
KOAc	potassium acetate
l	liter
lac	lactose
λ	wavelength
LB	Luria Bertani
m	milli
M	molar (mol/l)
µ	micro
MCS	multiple cloning site

min	minute
MOPS	3-morpholinopropane-1-sulfonic acid
Mr	relative molecular mass
n	nano
n.d.	not detectable
n.t.	not tested
NAD(P)H	nicotinamide adenine dinucleotide (phosphate), reduced form
NBT	nitroblue-tetrazolium
Ω	Ohm
OD_λ	optical density at wavelength λ in nm
ONPG	*o*-nitrophenol-β-galactoside
Pa	Pascal
p.a.	*pro analysi*
PBG	porphobilinogen
PBGD	porphobilinogen deaminase
PBGS	porphobilinogen synthase
PBS	phosphate-buffered saline
PCA	perchloric acid
PCR	polymerase chain reaction
PLP	pyridoxal-5'-phosphate
PPIX	protoporphyrin IX
PPO	protoporphyrinogen IX oxidase
PROTOGEN	protoporphyrinogen IX
p.s.i.	pounds per square inch
PVDF	polyvinylidenfluorid
rev	reverse
rpm	rotations per minute
RT	room temperature
s	second
SDS	sodium dodecyl sulfate
SDS-PAGE	sodium dodecyl sulfate polyacrylamide gel electrophoresis
spc	spectinomycin
strep	streptomycin
T	Tesla

TAE	Tris-acetate/EDTA
TE	Tris-EDTA
TEMED	tetramethylen diamine
tet	tetracycline
T_M	annealing temperature
TMB	tertramethylbenzidine
TRAP	tripartite ATP-independent periplasmic
Tris	tris-(hydroxymethyl)-aminomethane
(t)RNA	(transfer) ribonucleic acid
U	unit
UV	ultraviolet
V	volt
via	by (means of)
vol.	volume
vs.	versus
v/v	volume per volume
w/v	weight per volume
x-gal	5-bromo-4-chloro-3-indolyl-beta-D-galactopyranoside
∞	infinite

1 INTRODUCTION

1.1 Tetrapyrroles

Tetrapyrroles are essential compounds for nearly all living organisms. The iron containing tetrapyrrole heme acts as a prosthetic group for many different proteins. As a cofactor of hemoglobin it coordinates molecular oxygen and carbon dioxide transport. Heme-containing cytochromes are part of various electron transfer chains (Panek and O'Brian, 2002), whereas in catalases and peroxidases it mediates redox-reactions. Magnesium containing chlorophyll is responsible for the conversion of light energy to chemical energy, during photosynthesis (Jahn *et al.*, 1996; Beale, 1999; Vavilin and Vermaas, 2002; Frankenberg *et al.*, 2003; Layer *et al.*, 2010). It is also responsible for the green color of leaves as heme is responsible for the red color of blood. Therefore, tetrapyrroles are also called "pigments of life" (Battersby, 2000).

1.1.1 Structure and Function of Tetrapyrroles

The basic tetrapyrrole structure is a macrocycle of four pyrrole rings covalently attached by four methine bridges, as shown in Fig. 1. Corrinoids are the exceptions with one carbon bridge lacking. The numbering of the pyrrole rings as well as of the carbon and nitrogen atoms is in a clockwise orientation (Fig. 1). The carbon atoms C1 and C4 of ring A are termed α-carbons due to their direct bond to a nitrogen atom. Carbon atoms not adjacent to nitrogen atoms are β-carbons, such as C2 and C3 of ring A. The carbon atom within the methine bridges between the pyrrole rings are in meso-position (C5).

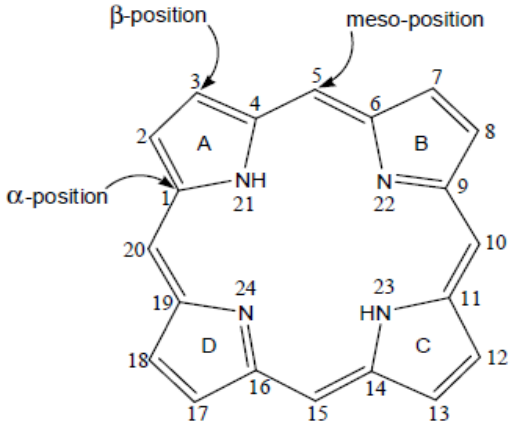

Fig. 1: Basic structure of cyclic tetrapyrroles, the porphyrin ring.
Pyrrole rings are donated A-D, carbon and nitrogen atoms are numbered 1-20 and 21-24 respectively. α- position: carbon atom adjacent to nitrogen atoms. β-position: remaining carbon atoms without direct bond to nitrogen. Meso-position: carbon atom within the methine bridges.

Tetrapyrroles can be divided in eight different groups: hemes, chlorophylls, bacteriochlorophylls, siroheme, heme d_1, corrinoides, coenzyme F_{430} and linear tetrapyrroles, respectively (Fig. 2). They differ in the saturation of the ring system, the chelated metal ion in the center of the porphyrin ring und the sidechain substituents (Frankenberg *et al.*, 2003; Heinemann *et al.*, 2008; Layer *et al.*, 2010). In the beginning of the 20th century the structures of heme and chlorophyll were the first to be determined. From then on more and more structural information has been obtained (Battersby, 2000). The structures of representatives of the different groups of tetrapyrroles are shown in Figure 2. The variations in the ring system, the central metal atom and the sidechains, are the reasons for the diverse functions of tetrapyrroles.

Iron chelating heme acts as a prosthetic group of e.g. hemoglobin, cytochromes, catalases and peroxidases, were it mediates gas transport and detection as well as electron transfer (Munro *et al.*, 2009). Magnesium containing chlorophylls and bacteriochlorophylls function as photoreceptors during photosynthesis (Beale 1999). Siroheme and heme d_1 both contain iron as central atom and are the cofactors of assimilatory sulfite and nitrite reductase and of dissimilatory nitrite reductase, respectively (Chang, 1994; Warren *et al.*, 1994). Nickel chelating coenzyme F_{430} is a yellowish cofactor of methylcoenzyme M reductase involved in methane formation (Thauer and Bonacker, 1994). The cobalt containing corrinoids like vitamin B_{12} catalyze radical-dependent reactions such as methyl transfer reactions or nucleotide reduction (Banerjee and Ragsdale, 2003). They are characterized by their missing methine bridge

between pyrrole ring A and D (Friedmann and Thauer, 1992; Warren *et al.*, 1992; Scott *et al.*, 1993; Layer *at al.*, 2010).

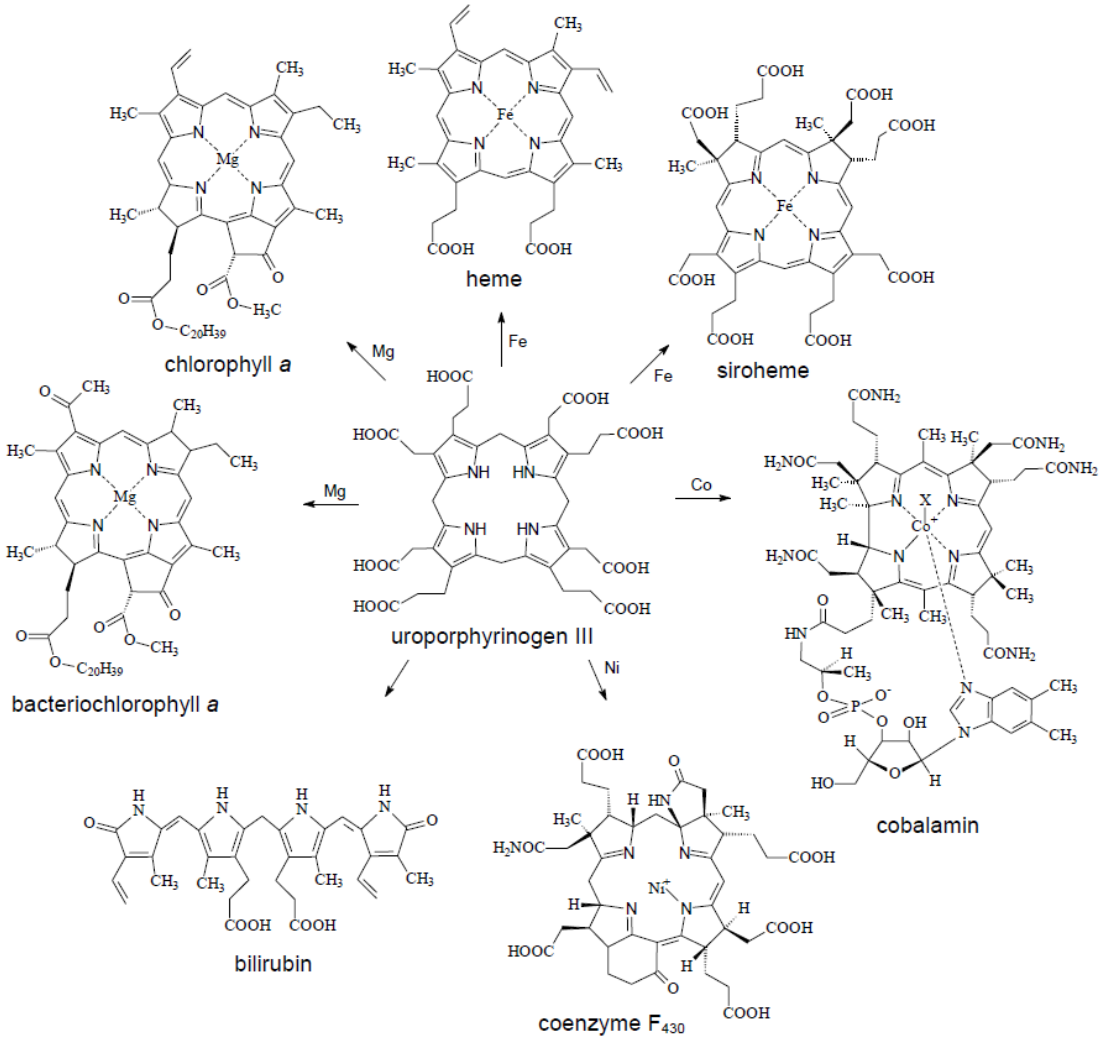

Fig. 2: Structures of important representatives of tetrapyrroles and their common precursor uroporphyrinogen III.

Linear tetrapyrroles such as bilirubin result from the cleavage of previously cyclic tetrapyrroles. They contain only three bridge carbons and no tightly bound metal ion. Linear tetrapyrroles serve as precursor for the biosynthesis of phycobilins and phytochrome chromophores (Beale, 1993; Beale and Yeh, 1999) and serve as chromophoric photoreceptors in cyanobacterial and higher-plant light-harvesting systems (Frankenberg and Lagarias, 2003).

1.1.2 Biosynthesis of Tetrapyrroles

The overall structural analogousness of tetrapyrroles suggests a shared biosynthetic pathway (Fig. 3). The general precursor of all known tetrapyrroles is 5-aminolevulinic acid (ALA). The following steps in tetrapyrrole biosynthesis are highly conserved. After the formation of the first cyclic intermediate, uroporphyrinogen III, the first branching point occurs. Uroporphyrinogen III is either converted into pecorrin 2, the precursor for the porphinoids (siroheme, coenzyme F_{430} and vitamin B_{12}) or protoporphyrin IX the precursor of hemes and chlorophylls.

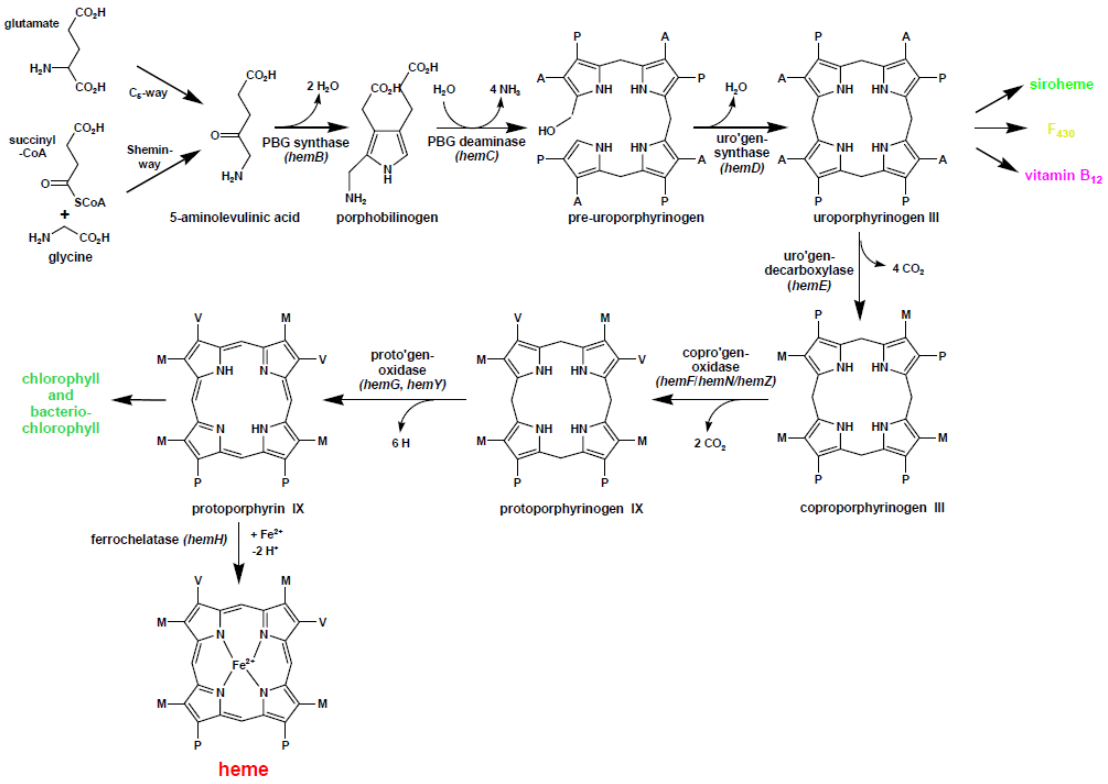

Fig. 3: Biosynthesis of heme.
The names of the enzymes and their respective genes (bacterial) are given below/above the arrows. A = acetate side chain; P = propionate side chain; M = methyl group; V = vinyl group.

Tetrapyrrole biosynthesis in eukaryotes is limited to the formation of heme, siroheme, chlorophyll and bilins, while prokaryotes are able to synthesize complicated tetrapyrroles as corrinoids, coenzyme F_{430} and heme d_1 (Jahn *et al.*, 1996).

1.1.3 Heme Biosynthesis

1.1.3.1 Biosynthesis of 5-aminolevulinic acid

In all organisms heme biosynthesis starts with the synthesis of 5-aminolevulinic acid. ALA contains all carbon and nitrogen atoms required for the formation of the tetrapyrrolic macrocycle and it can be formed *via* two routes.

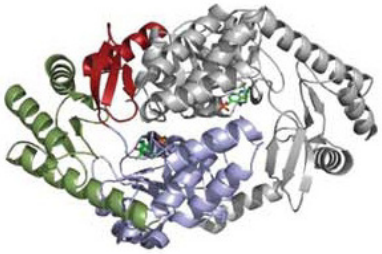

Fig. 4: 5-Aminolevulinic acid synthase. Crystal structure of ALAS from *R. capsulatus* (Astner, 2005), a homodimeric protein. Each monomer (shown in color or grey) consists of three domains (red, green, blue). In the active site of the enzyme the PLP cofactor is covalently attached, displayed as green-blue-red stick-and-ball molecules (Layer *et al*., 2010).

Animals, fungi and the α-group of proteobacteria employ the "Shemin pathway" (Shemin and Russell, 1953). The pyridoxal-5'-phosphate (PLP) dependent enzyme ALA synthase (ALAS; encoded by *hemA*; EC 2.3.1.37; Fig. 4) synthesizes ALA in a one step reaction through condensation of glycine and succinyl-CoA (Kikuchi *et al*., 1958). The reaction starts with binding of glycine to the active site and aldimine formation between glycine and the PLP cofactor. Afterwards, the pro-*R* proton of glycine is removed and succinyl-CoA is bound, resulting in the formation of an α-amino-β-keto adipate intermediate. Decarboxylation of this intermediate leads to formation of an enol intermediate, which is in equilibrium with a second quinonoid and with the ALA bound external aldimine upon protonation of the C-5 position. In the end, ALA is released and the internal aldimine is restored. The release of ALA represents the rate limiting step of the reaction (Hunter and Ferreira, 2009, Hännig, 2011).

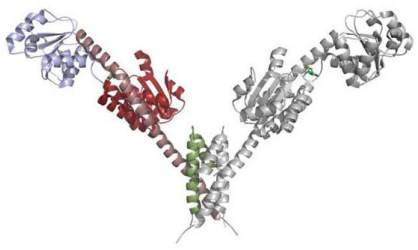

Fig. 5: Glutamyl-tRNA reductase. Crystal structure of *M. kandleri* GluTR (Moser *et al*., 2001) showing the V-shaped form of the dimeric enzyme. In the active site of GluTR the substrate, is displayed as green - blue - red stick - and - ball molecules (Layer *et al*., 2010).

Plants, algae, archaea and all other bacteria use the later discovered "C5-pathway" (Beale and Castelfranco, 1973). The name refers to the incorporation of the 5-carbon skeleton of glutamate into ALA. The reaction is catalyzed by two different enzymes: glutamyl-tRNA

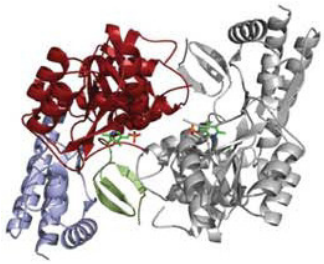

Fig. 6: Glutamate-1-semialdehyde-2,1-aminomutase.
Crystal structure of *T. elongatus* GSAM (Schulze *et al*., 2006). In the active site the PLP cofactor is displayed as green-blue-red stick-and-ball molecules (Layer *et al*., 2010).

reductase (GluTR; encoded by *hemA*; EC 6.1.1.17, Fig. 5) and glutamate-1-semialdehyde-2,1-aminomutase (GSAM; encoded by *hemL*; EC 5.4.3.8, Fig. 6). GluTR is NADPH dependent and catalyzes the reduction of glutamyl-tRNA to the instable glutamate-1-semialdehyde (GSA) (Jahn *et al.*, 1991, Moser *et al.*, 1999). Subsequently, GSA is transaminated by pyridoxamine 5´-phosphate (PMP)-dependent GSAM to yield ALA (Ilag and Jahn, 1992). Since GSA is a highly reactive aldehyde a coordinated action of the two enzymes is required. A GluTR/GSAM complex was proposed, based on the structural complementarity of the two enzymes (Moser *et al*., 2001) and was shown to exist *in vivo* (Schauer, 2003). It allows for direct channeling and thus prevents solvent exposure of the instable intermediate. One of the known organisms using both pathways, the Shemin- and the C5-pathway, for heme biosynthesis is *Euglena gracilis*, a photosynthetic phytoflagellate. Mitochondrial tetrapyrroles are synthesized by the Shemin-pathway, while plastidic pigments are derived from the C5-pathway.

1.1.3.2 The central pathway from ALA to uroporphyrinogen III

The next three initial biosynthetic steps are highly conserved. Porphobilinogen synthase (PBGS; encoded by *hemB*; EC 4.2.1.24, Fig. 7) catalyzes the asymmetric condensation of two molecules of ALA to form the monopyrrole porphobilinogen (PBG). Metal-dependent PBGS from different organisms share a high sequence identity, but are variable in their utilized metal ions, requiring zinc or magnesium ions or both (Frankenberg *et al.*, 1999a and 1999b; Mitchell and Jaffe, 1993; Gibbs *et al.*, 1985; Senior *et al.*, 1996 and 1997). Additionally, some PBG proteins were reported to be metal-independent (Bollivar *et al.*, 2004).

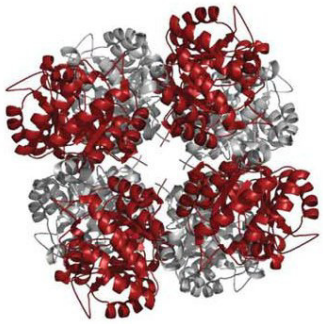

Fig. 7: Porphobilinogen synthase.
Crystal structure of *P. aeruginosa* PBGS (Frankenberg *et al*., 1999) showing the octameric assembly of the protein representing a tetramer of homodimers (Layer *et al*., 2010)

Fig. 8: Porphobilinogen deaminase. Crystal structure of *E. coli* PBGD (Louie *et al*., 1996). In the active site of the enzyme the dipyrromethane cofactor is covalently attached, displayed as green-blue-red stick-and-ball molecules (Layer *et al*., 2010).

Consecutively four molecules of PBG are linked to form the unstable linear tetrapyrrole pre-uroporphyrinogen (Jordan, 1994). The reaction is catalyzed by porphobilinogen deaminase (PBGD; encoded by *hemC*; EC 4.3.1.8, Fig. 8). PBGD requires the cofactor dipyrromethane, a PBG dimer (Jordan and Warren, 1987). This makes PBG the substrate and the cofactor of PBGD. Through its free amino group the dipyrromethane cofactor is covalently attached to PBGD and starts the tetramerization of PBG, by stepwise condensation under deamination. The formed pre-uroporphyrinogen is passed directly from porphobilinogen deaminase to the next enzyme, uroporphyrinogen III synthase (UROS; encoded by *hemD*; EC 4.2.1.75, Fig. 9). Here the inversion of ring D of pre-uroporphyrinogen, subsequent cyclization of the molecule and thus formation of uroporphyrinogen III takes place. Uroporphyrinogen III is the first cyclic intermediate of the pathway and is the last common precursor for two distinct groups of tetrapyrroles: the porphinoids (siroheme, coenzyme F_{430} and vitamin B_{12}), and of hemes and chlorophylls.

Fig. 9: Uroporphyrinogen III synthase. Crystal structure of *T. thermophilus* UROS (Mizohata *et al*., 2005), a monomeric protein consisting of two α/β domains connected by a flexible, two-stranded linker (Layer *et al*., 2010).

1.1.3.3 Conversion of Uroporphyrinogen III into Heme

To synthesize porphyrins, the four acetate side chains of uroporphyrinogen III are decaboxylized by uroporphyrinogen III decarboxylase (UROD; encoded by *hemE;* EC 4.1.1.37, Fig. 10) to form the methyl groups of the product coproporphyrinogen III (COPROGEN). The decarboxylations begin with the acetate side chain of ring D followed by A, B and C (Akhtar, 1991).

The exact reaction mechanism is still unknown. The next step is the conversion of coproporphyrinogen III to protoporphyrinogen IX. The propionate side chains of rings

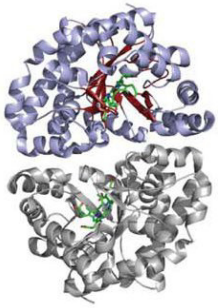

Fig. 10: Uroporphyrinogen III decarboxylase.
Crystal structure of human UROD in complex with the reaction product COPROGEN, displayed as green-blue-red stick-and-ball molecules (Whitby *et al.*, 1998). UROD is a dimeric enzyme in which the two single-domain subunits are orientated head-to-head (Layer *et al.*, 2010).

A and B are oxidatively decarboxylated to the corresponding vinyl groups (Dailey, 2002). This reaction can be catalyzed by two enzymes, the oxygen dependent coproporphyrinogen III oxidase (CPO; encoded by *hemF/hemN*; EC 1.3.3.3, Fig. 11) HemF and the oxygen independent HemN. In eukaryotes the O_2-dependent HemF is the most common CPO, while in bacteria the O_2-independent HemN is dominant. HemN is a 'Radical-SAM' enzyme and should rather be named coproporphyrinogen III dehydrogenase (CPDH, encoded by *hemN*, EC 1.3.99.22; Fig. 11; Breckau *et al.*, 2003; Layer *et al.*, 2002).

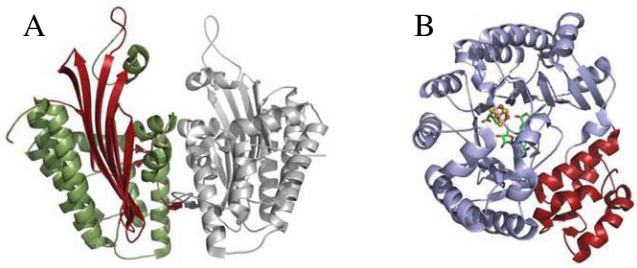

Fig. 11: Coproporphyrinogen III oxidase and coproporphyrinogen III dehydrogenase.
A: Crystal structure of yeast CPO, a homodimeric protein (Phillips *et al.*, 2004). B: Crystal structure of *E. coli* CPDH (Layer e*t al.*, 2003). In the active site of the enzyme the [4Fe–4S] cluster (orange-yellow stick-and-ball molecules) is coordinated by the three cysteine residues of the conserved CX3CX2C sequence motif and by one of the two bound SAM molecules (green-blue-red stick-and-ball molecules) (Layer *et al.*, 2010).

The conversion of protoporphyrinogen IX (PROTOGEN) to protoporphyrin IX is catalyzed by protoporphyrinogen IX oxidase (PPO; encoded by *hemG/hemY*; EC 1.3.3.4, Fig. 12). The result is the abstraction of six electrons and the formation of a planar system of completely conjugated double bonds. A flavin containing oxygen-dependent PPO (HemY) employing molecular oxygen was found in eukaryotes and some bacteria (Hansson and

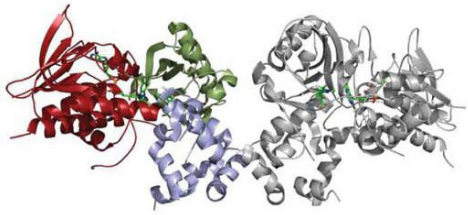

Fig. 12: Protoporphyrinogen IX oxidase.
Crystal structure of tobacco PPO (Koch *et al.*, 2004). In the active site the inhibitor acifluorfen (AF, green-blue-red stick-and-ball molecules) was observed to bind indicating the approximate position of the substrate PROTOGEN (Corradi *et al.*, 2006; Layer *et al.*, 2010).

Hederstedt, 1994; Koch *et al.*, 2004; Heinemann *et al.*, 2007). The oxygen-independent PPO (HemG) contains a flavin mononucleotide (FMN) as cofactor, which transfers electrons to various electron acceptors (fumarate, nitrate, O_2) *via* ubiquinone and menaquinone (Jacobs and Jacobs, 1976, Sasarman *et al.*, 1979, Sasarman *et al.*, 1993, Möbius *et al.*, 2010*).* The last step of heme biosynthesis is the insertion of iron into protoporphyrin IX catalyzed by ferrochelatase (Dailey, 2002).

1.1.4 Conversion of Protoporphyrin IX to Protoheme

The generation of protoheme by insertion of a ferrous iron into protoporphyrin IX (PPIX) is a conserved process, even though substrate specificity differs slightly among species (Dailey, 1996). This reaction is catalyzed by the enzyme ferrochelatase (FC; encoded by *hemH*; EC 4.99.1.1), as shown in figure 13. In eukaryotes ferrochelatase is a membrane-associated homodimer, while in bacteria it is monomeric (Wu *et al.*, 2001; Wang *et al.*, 2001; Grzybowska *et al.*, 2002). In the Gram positive bacterium *Bacillus subtilis* even a soluble version of ferrochelatase was detected in the cytoplasm (Hansson and Hederstedt, 1994). Except for plant enzymes, the eukaryotic ferrochelatases were described containing one [2Fe-2S] cluster per subunit (Dailey *et al.*, 1994; Day *et al.*, 1998), while bacterial enzymes were reported to have one or no Fe-S cluster (Dailey, 2002; Shepherd *et al.*, 2006).

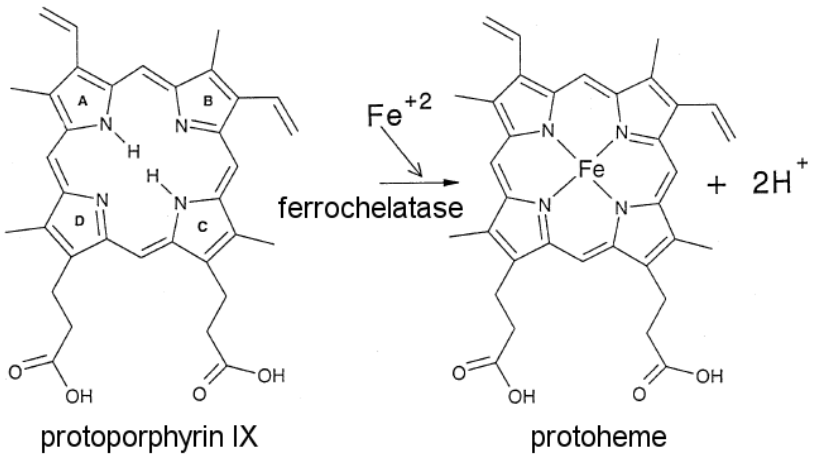

Fig. 13: Conversion of protoporphyrin IX to protoheme catalyzed by ferrochelatase.
(Dailey *et al.*, 2000)

The first step of the proposed reaction mechanism is the binding iron to ferrochelatase (Dailey and Fleming, 1983), followed by the distortion of the porphyrin to a non planar conformation (Sigfridsson, 2003). The incoming metal forms a so called “sitting atop” complex on the porphyrin macrocycle (Fig. 14). The insertion of the metal in the distorted porphyrin is isochronic to the abstraction of the pyrrole protons from the opposite side of the active site (Takeda *et al*, 1992; Hambright, 1975). While variation of the substituents on rings A and B is allowed to a certain degree, the position of the propionate side chains on rings C and D seems to be critical for catalysis.

A

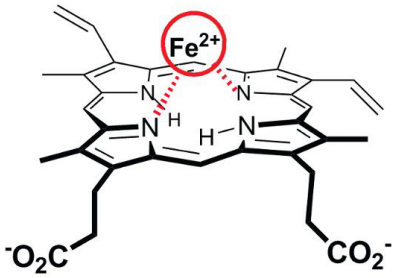

B

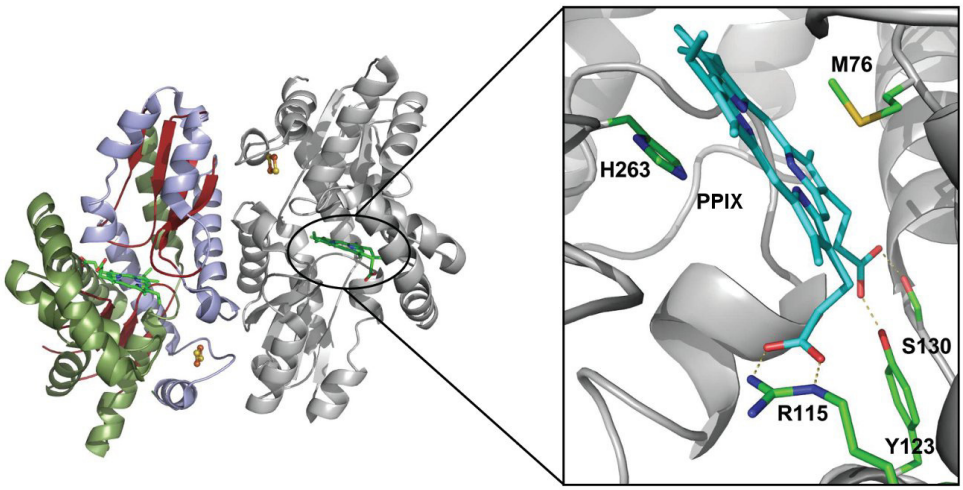

Fig. 14: Crystal structure of ferrochelatase-PPIX complex.
A: The proposed “sitting-atop” complex during iron insertion into PPIX catalyzed by ferrochelatase. B: Crystal structure of human ferrochelatase in complex with its substrate PPIX (left; Medlock *et al*., 2006). PPIX bound in the active site of ferrochelatase exhibited only a slight distortion of about 11.5° adopting a modest saddle conformation (right). Structure representation adapted from Layer *et al*., 2010.

Several key interactions between ferrochelatase and PPIX are responsible for the coordination of PPIX in the active site pocket (Fig. 14). A salt bridge is formed between the propionate carboxylate group of PPIX ring D with Arg115 of ferrochelatase. The propionate carboxylate group of PPIX ring C is involved in hydrogen bonding with the side chains of Ser130 and Tyr123. On the opposite site of the macrocycle His263 and

Met76 assist in positioning of the substrate. The ferrochelatase-PPIX complex structure revealed that PPIX is distorted by *ca*. 11.5° to adopt a modest saddle conformation. It was reported for the human ferrochelatase-PPIX complex that after metal insertion His263 swings away from the metalated porphyrin. Furthermore, the hydrogen bonds between the product ring C propionate side chain and Ser130 and Tyr123 are broken (Medlock *et al*., 2007).

One important question is the mechanism of reduced iron delivery to ferrochelatase, since ferric iron is no substrate. It was reported for *Haemophilus influenzae* that ferrochelatase also functions in the reverse direction, catalyzing the release of Fe^{2+} from PPIX (Loeb, 1995). With Ferrochelatase being the only enzyme of the heme biosynthetic pathway present in this pathogen, it is probably a mechanism to obtain Fe^{2+} from its host. Without doubt there will be several other alternatives for ferrochelatase to receive iron.

1.1.5 HemW

Lactococcus lactis is a Gram positive, facultative anaerobe bacteria extensively used in food industries which possesses a fermentative metabolism (Holt, 1994). Genome sequencing of *L. lactis* strain Il1403 (Bolotin, 2001) showed an incomplete heme biosynthesis pathway. Only genes annotated as homologues of ferrochelatase, protoporphyrinogen IX oxidase and oxygen-independent coproporphyrinogen III oxidase were found, suggesting that *L. lactis* has no respiratory metabolism for heme synthesis. A closer look revealed that the protoporphyrinogen oxidase gene was mis-annotated. It was shown that oxygen had negative effects of growth and survival of *L. lactis* (Codon, 1987; Duwat, 1995). On the other hand, the genes *cydA* and *cydB* coding for cytochrome *bd* were detected. Cytochrome *bd* is normally produced under oxygen-limited conditions or in the stationary phase of growth, where it is involved in the forming of electron transport chains with oxygen as terminal electron acceptor (Cotter, 1990).

Studies showed respiratory growth was possible for *L. lactis*, when the *cydA* and *cydB* genes were intact, and heme was supplemented to the cells. Furthermore, the production of cytochrome *bd* was induced by the uptake of heme, while a deletion mutant of cytochrome *bd* had no effect on the heme uptake (Duwat *et al.*, 2001). That means the

production of cytochrome *bd* depends directly on the presence of heme, but the cytochrome itself plays no role in heme transport.

Just recently it was shown that *L. lactis* HemW, previously annotated as HemN (coproporphyrinogen III dehydrogenase, EC 1.3.99.22.), displayed characteristics of a heme chaperone responsible for heme transfer to cytochrome *bd* (Abicht *et al*., 2012). A *L. lactis* Δ*hemW* mutant accumulated free heme in the membranes. HemW displayed no HemN activity, making it implausible for it to be an actual coproporphyrinogen III oxidase. Further analysis showed the presence of an oxygen sensitive iron-sulfur cluster, and the ability to covalently bind one molecule heme per monomer HemW with a K_D of 8 µM. The same HemW-heme complex could be isolated from *L. lactis* wild type cells. In a NADH dependent reaction *L. lactis* membranes triggered the dissociation of heme from HemW, supporting its presumed function as heme chaperone in the cytochrome *bd* maturation pathway (Abicht *et al.*, 2012).

Sequence comparison of *L. lactis* HemW showed an important difference to the well characterized *E. coli* HemN. *E. coli* HemN possesses an extra 47 N-terminal residues, containing the conserved 21-PRYTSYPTA-motif with arginine22 as the proposed critical factor for substrate binding. An extensive phylogenetic analysis of HemW- and HemN-type proteins divided the two proteins in two clades, grouping "short" HemW-type proteins in one clade and "long" HemN-type proteins in the other (Tab. 1). The HemW clad also contained the *E. coli* protein YggW. An *E. coli* Δ*yggW* mutant (Kitagawa *et al.*, 2005) was successfully complementated with *L. lactis hemW*. These findings suggest that *E. coli* YggW, which will be named HemW in this work, has similar characteristics as *L. lactis* HemW regarding its heme chaperone properties.

Tab. 1: Occurrence of genes encoding HemW- and HemN-type proteins in different bacteria.

Organism	HemW	HemN
Gram-negative bacteria		
α-proteobacteria		
Agrobacterium tumefaciens	+	+
Magnetospirillum magneticum	+	+
Zymomonas mobilis	+	+
Agrobacterium tumefaciens	+	+

Organism	HemW	HemN
δ-proteobacteria		
Bdellovibrio bacteriovorus	+	+
γ-proteobacteria		
Escherichia coli	+	+
Pseudomonas aeruginosa	+	+
Salmonella typhimurium	++	+
Vibrio cholera	++	+
Yersinia pestis	++	+
Gram-positive bacteria		
Bacillus anthracis	++	
Bacillus subtilis	++	
Clostridium botulinum	++	
Frankia alni	++	
Streptomyces griseus	++	
Cyanobacteria		
Nostoc sp.	+	+
Synechocystic sp.	+	+

Modified from Abicht. + = one encoding gene, ++ = two encoding genes, - = no coding gene

1.1.6 Heme Transport

Heme proteins are ubiquitous in pro- and eukaryotic cells. They have been detected in all compartments and organelles. Due to their hydrophobic nature, heme molecules readily aggregate in aqueous solutions and bind unspecific to lipids and proteins (Vincent, 1988). In addition, free heme mediates lipid peroxidation and thus damages DNA by oxidative stress (Vincent, 1988). For these reasons the amount of free heme in the cells has to be kept extremely low. Transport across membranes and through cyto- and periplasm has to be tightly controlled. A summary of the cellular interaction of heme with lipids and proteins is shown in figure 15.

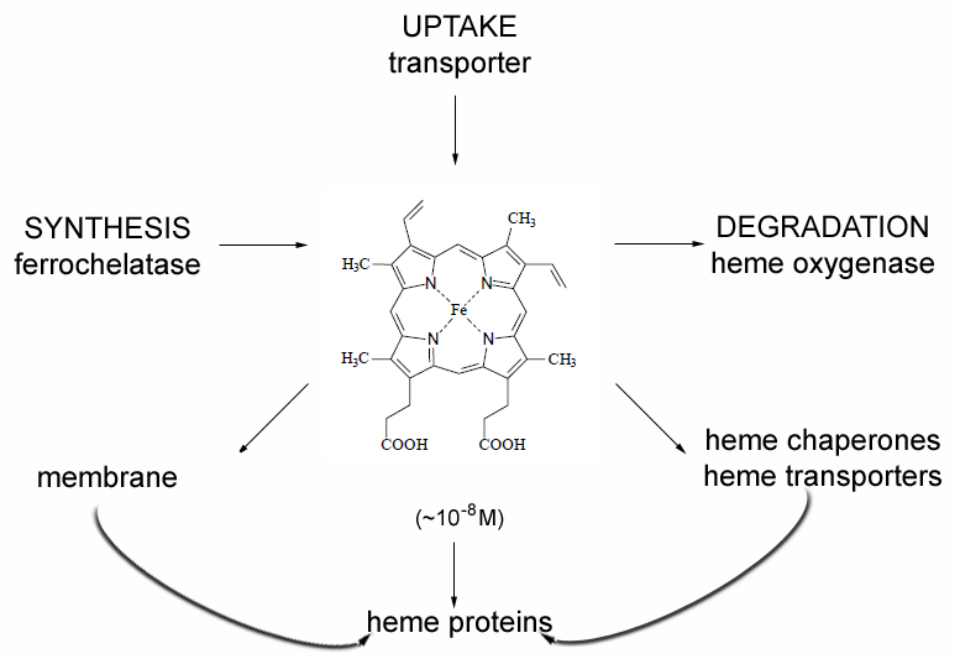

Fig. 15: Cellular interaction of heme.
(adapted from Warren and Smith, 2009)

Heme transport is rather specific, depending on the heme protein and the organism in which the transport takes place. The formation and uptake as well as the transfer of heme to various target proteins is illustrated in figure 16.

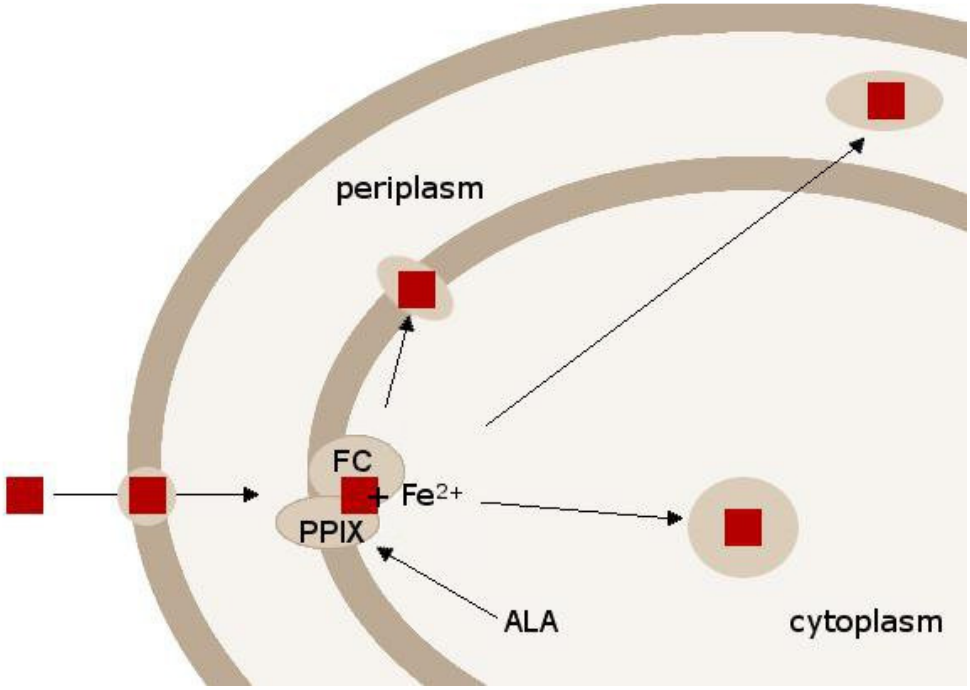

Fig. 16: Heme traffic in bacterial cells.
Heme (red square) is synthesized from ALA, the last step taking place in the cytoplasm by insertion of Fe^{2+} into protoporphyrin IX (PPIX) catalyzed by ferrochelatase (FC), or is taken up by specific transport systems. In the following heme is transferred to cytoplasmic, inner membrane and periplasmic proteins (adapted from Warren and Smith, 2009).

In most prokaryotes heme is formed in the cytoplasm *via* insertion of Fe^{2+} into protoporphyrin XI catalyzed by ferrochelatase. Heme auxotrophes like *Streptococcus agalactiae* (Glaser *et al*, 2002) require specific heme uptake systems to assimilate heme from the environment. Pathogens use similar systems to capture heme as an iron source (Wandersman and Stojiljkovic, 2000; Genco and Dixon, 2001; Stojiljkovic and Perkins-Balding, 2002).

Different strategies for heme uptake exist. Some bacteria possess heme or heme protein receptors in the outer membrane that bind their target molecule. Transport into the cell is then accomplished by TonB/ExbBD proteins (Braun and Killmann, 1999). Other Gram-negative bacteria excrete small hemophores to catch heme from the environment. HasA from *Pseudomonas aeruginosa* and *Serratia marcescens* was shown to be such a hemophore, transporting hemoglobin-bound heme to the outer membrane receptor HasR (Ghigo *et al*., 1997; Létoffé *et al*., 1999). In this process, HasA binds its cognate outer membrane receptor HasR in a heme independent fashion (Létoffé *et al*., 2001). The binding is mediated by two HasA β-strands (Létoffé *et al*., 2003) and heme is bound to HasR by two conserved histidine residues (Izadi-Pruneyte *et al*., 2006). In all characterized systems, heme transport by the outer membrane receptors requires the inner membrane protein complex TonB or a TonB analog, probably to provide the required energy for opening a gated channel in the outer membrane receptor (Braun, 1995; Klebba and Newton, 1998). The TonB complex is also essential for the hemophore release (Létoffé *et al*., 2004).

Once in the periplasm, heme is bound by a periplasmic heme binding protein, e.g. HemT from *Yersinia enterocolitica*, and transported to an inner membrane ABC transporter. The exact transport mechanism is unknown, but it is believed that the periplasmic heme binding proteins interact with the permease subunit of the inner membrane ABC transporter and under consumption of two ATPs transfers heme (reviewed by Rees *et al.*, 2009).

Only few cytoplasmic heme transporting proteins are described until now. This is partly due to their low sequence identity. While many heme-binding proteins in the periplasm share a common motif such as CXXCH or CXXC, it takes a single residue in the right environment to bind heme, as evidenced by the heme chaperone CcmE (Severance and Hamza, 2009; Stevens *et al.*, 2003). This makes it difficult to identify heme-binding proteins by structural genome annotation. One described chaperone is *Pseudomonas aeruginosa* PhuS, which delivers heme to a specific heme oxygenase. Analysis of PhuS

indicates that, *in vitro*, the protein exists as a mixture of dimer (M_r = 78,000) and monomer (M_r = 39,000), and binds one heme per monomer (Lanksky *et al.*, 2006). It is proposed that changes in both the spin-state (low-spin to high-spin) and axial heme coordination occur during the transfer reaction (Bhakta and Wilks, 2006). One has to keep in mind that heme binding proteins like PhuS are involved in iron acquisition from heme and are limited to few pathogenic bacteria. Therefore, they cannot be seen as representing class of heme binding proteins for heme insertion into cytoplasmic target proteins.

Heme transport from cytoplasm to periplasm is necessary for biosynthesis of periplasmic *b*- and *c*-type cytochromes, and probably facilitated by ABC-type putative heme exporters (Thöny-Meyer , 1997; Page *et al.*, 1998; Kranz *et al.*, 1998; Beckman *et al.*, 1992; Ramseier *et al.*, 1991; Goldman and Kranz, 2001).

The posttranslational maturation of *c*-type cytochromes is the best investigated example of heme incorporation so far. Four distinct systems can be distinguished, with prokaryotes and plants using either system I or II and fungi, invertebrates and vertebrates using system III, differing mostly in the transport of apo-cytochrome *c* and heme to the periplasm. Recently, a fourth pathway was detected in the chloroplast of *Arabidopsis thaliana* (Lezhneva, 2008). The main feature of all *c*-type cytochromes is the covalently bound heme molecule. They possess a CXXCH motive. The two cysteinyl residues are bound via thioether bounds to the two vinyl groups of the heme. The histidinyl residue acts as a ligand to the iron of heme (reviewed by Kranz *et al*., 1998). In many Gram negative bacteria using system I for cytochrome *c* maturation the membrane anchored heme chaperone CcmE transports heme from the heme *b* transporter subunit CcmC to the putative heme lyase CcmF (Schulz *et al.,* 1998, Sanders *et al.,* 2010, Bonnard *et al.,* 2010). Heme *b* release from the heme chaperone CcmE requires additional proteins. In Gram positive bacteria using system II for cytochrome *c* maturation a complex of ResB/CcsB and ResC/CcsA binds heme *b* in the cytoplasm and delivers it to the extracytoplasmic side. Here, heme *b* is integrated into apocytochromes (Ahuja *et al*., 2009). As of today, it is unknown how heme is inserted into cytochromes with non- covalently attached heme, e.g. cytochrome *bd*.

In 1999, Hassett and coworkers reported that *P. aeruginosa* catalase A (KatA) requires bacterioferritin A (BfrA) for full activity, proposing that BfrA stores iron that is incorporated into heme the necessary prosthetic group for KatA activity. BfrA is an ubiquitously found iron storage protein. It consists of 24 subunits and was shown to

bind 3 to 9 heme groups *in vivo* as well as up to 24 heme groups *in vitro* (Kadir and Moore, 1190). These findings suggest that BfrA could function as a heme transporter between HemH, the last enzyme of heme biosynthesis and the heme *b* accepting protein KatA (Fig. 17).

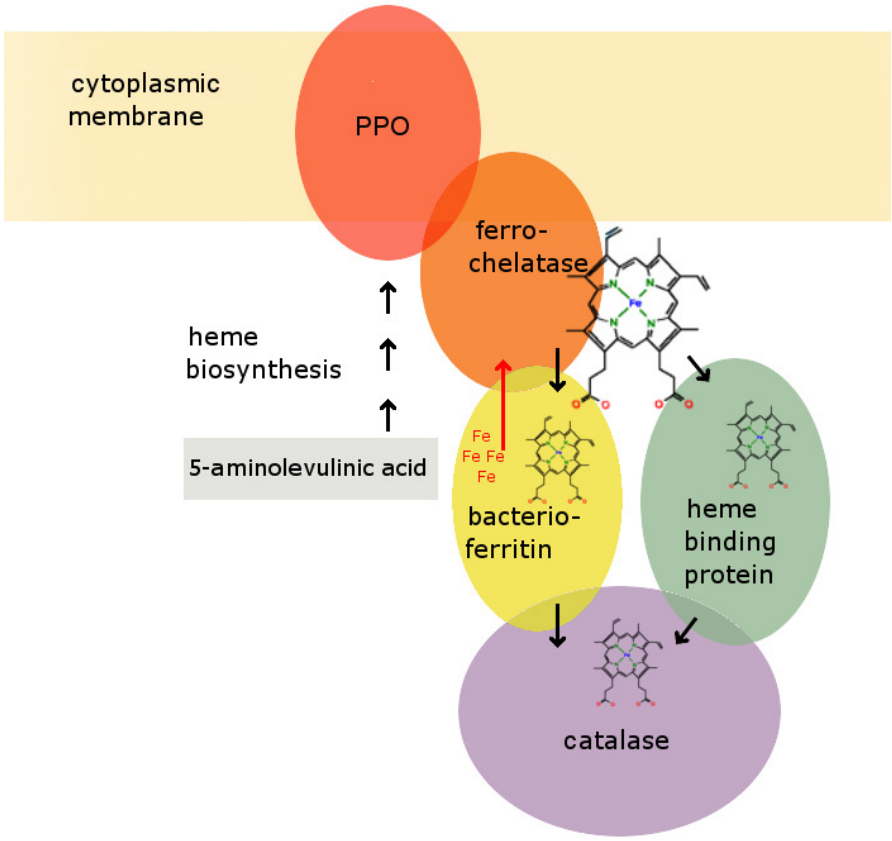

Fig. 17: Working hypothesis for the function of the heme chaperone BfrA in *E. coli*.
Heme is formed from 5-aminolevulinic acid. The last two enzymes of the heme biosynthetic pathway protoporphyrinogen IX oxidase (PPO) and ferrochelatase are forming a complex (Masoumi *et al.*, 2008). Heme is subsequently bound by BfrA or an alternative heme binding protein and directed to catalase A.

1.2 Objectives of the Work

The aim of this work was the identification of putative heme transporter proteins, and the further characterization with regard to their function and their interaction partners. One approach was to screen a *Pseudomonas aeruginosa* DNA library with suitable heme proteins, to fish for probable heme chaperones. The assessment of BfrA being a heme chaperone was also conducted by testing for protein-protein interactions between BfrA, HemH and KatA *via* a bacterial two hybrid system. Knock-out mutants of possible candidates were to be generated for further investigation of their functional role in heme transport.

Another approach was the characterization of *Escherichia coli* HemW, a proposed heme chaperone. HemW was to be produced, purified und tested for heme binding and transporting activity. Also the nature of heme binding was to be determined by spectrometric analysis.

2 MATERIALS AND METHODS

2.1 Instruments and Chemicals

2.1.1 Instruments

Tab. 2: instruments

Instrument	Model	Source
Agarose gel electrophoresis	Agagel	Biometra
Agarose gel documentation	GelDoc	Bio-Rad
Anaerobic chamber	Type B flexible vinyl chamber	Coy Laboratories
Autoclave	LVSA 50/70	Zirbus
Blotting equipment	Semidry-Blot Trans-Blot®SD	Bio-Rad
Centrifuges	5804	Eppendorf
	Avanti®J-30I	Beckmann Coulter
	Biofuge primoR	Hereaus
	Minispin	Eppendorf
	Optima L-90K Ultracentrifuge	Beckmann Coulter
	Qik Spin QS 7000	Edwards instruments
	Speed Vac SPD 110B	Savant
DNA sequencing	Genetic Analyzer ABI Prism™ 310	Applied Biosystems
Electrophoresis power supply	PowerPac 300	Bio-Rad
EPR spectrometer	Bruker Spin R ESP 300 E	Bruker
Homogenizer	FastPrep®24 Instruments	MP Biomedicals
pH determination	pH meter C 6840 B	Schott
Photometer	Ultrospec 2000	Amersham Bioscience
Pipettes	BioPette	Labnet
Protein concentration cells	Amicon 8050	Millipore
Scales	BL 1500	Sartorius
	BL 61S	Sartorius
	SBA 52	Scaltec
SDS-PAGE system	Mini-Protean II	Bio-Rad
Spectral scanning multimode reader	Varioskan flash	Thermo scientific
Spectrophotometer	NanoDrop™ 1000	PeQlab
Spectropolarimeter	Jasco J810	Jasco®
Thermocycler	Tpersonal	Biometra
	96 universal peQSTAR	PeQlab
Thermomixer	Thermomixer compact	Eppendorf
	Thermomixer comfort	Eppendorf
UV/visible Spectrophotometer	Jasco V-550	Jasco®
	Jasco V-650	Jasco®
Vortex	Vortex Genie 2	Scientific Industries
Water purification	Milli-Q-System	Millipore

2.1.2 Chemicals and Kits

Tab. 3: chemicals and kits

	Product	Source
Antibodies	Anti-Glutathion-S-Transferase (rabbit-anti-GST)	Sigma
	Anti Rabbit IgG, Alkaline Phophatase Conjugated	Pierce
Blotting material	Gel blotting paper	Roth
	Roti-PVDF-membrane	Roth
Chemicals	5-aminolevulinic acid	Sigma
	Bradford reagent	Sigma
Crystal Screens	Cryos Suit	Qiagen
Enzymes	Phusion DNA Polymerase	Finnzymes
	PreScission™ Protease	GE Healthcare
	T4 DNA Ligase	New England Biolabs
	Taq DNA Polymerase	New England Biolabs
	Restriction enzymes	New England Biolabs
Kits	BACTH System	Euromedex
	BigDye Terminator v1.1 cycle	Applied Biosystems
	QIAquick Gel Extraction Kit	Qiagen
	QIAquick PCR Purification Kit	Qiagen
	QIAprep® Spin Miniprep Kit	Qiagen
	NucleoSpin® Soil	Macherey-Nagel
Molecular weight standards	GeneRuler™ DNA LadderMix	MBI Fermentas
	PageRuler™ Prestained Protein Ladder	MBI Fermentas
	Unstained protein molecular weight marker	MBI Fermentas
PCR materials	Oligonucleotides	Metabion
	Deoxynucleotide Solution Mix	New England biolabs
Other materials	Dialysis visking, tybe 27/32 exclusion 14'000	Roth
	Glutathion Sepharose™ 4 Fast Flow	GE Healthcare
	Instant*Blue*™	Expedeon
	Lysing Matrix B Bulk	MP Biomedicals
	Steril filter (0.2 µm)	Millipore
	Ultrafiltration membrane, NMWL: 10000	Millipore

Chemicals and reagents not specifically listed were purchased from following companies: Amersham Biosciences, Applichem, Fluka, GE Healthcare, Merk, Roth, Sigma, MP Biomedicals.

2.2 Strains and Plasmids

All bacterial strains and plasmids used for this work are listed in Tab. 4 and Tab. 5.

Tab. 4: bacterial strains

Strain	Genotype	Reference
Escherichia coli BL21(DE3)	F^- *dcm ompT hsd*S(rB^- mB^-) *gal* l(DE3)	Stratagene
Escherichia coli BTH101	F^-, *cya-99*, *araD139, galE15, galK16, rpsL1 (*Str^r*), hsdR2, mcrA1, mcrB1.*	Euromedex
Escherichia coli BW25113	*lacI*^{q} *rrnB*$_{T14}$ D*lacZ*$_{WJ16}$ *hsdR514 ΔaraBAD*$_{AH33}$	Datsenko &

Strain	Genotype	Reference
	ΔrhaBAD$_{LD78}$	Wanner
Escherichia coli DH10β	F- *mcr*A Δ(*mrr-hsd*RMS-*mcr*BC) Φ80*lac*ZΔM15 *lac*X74 *rec*A1 *end*A1 *ara*Δ139 Δ(*ara*, *leu*)7697 *gal*U *gal*K λ$^-$ *rps*L (Str^R) *nup*G	GibcoBRL (Invitrogen)
Escherichia coli JW2922	*lacI*^{q} *rrnB*$_{T14}$ D*lacZ*$_{WJ16}$ *hsdR514 ΔaraBAD*$_{AH33}$ *ΔrhaBAD*$_{LD78}$ Δ*yggW*	Baba (2006)
Escherichia coli ST18	*pro thi hsdR*$^+$ Tp^r Sm^r; chromosome::RP4-2 Tc::Mu-Kan::Tn7λ*pir* Δ*hemA*	Thoma & Schobert (2009)
Escherichia coli XL1-Blue	*rec*A1 *end*A1 *gyr*A96 *thi-1 hsd*R17 *sup*E44 *rel*A1 *lac* [F´*pro*AB *lacI*^{q}Z_M15 Tn*10* (Tet^r)]	Stratagene
Pseudomonas aeruginosa PAO1	Wildtype	Dunn & Holloway (1971)
SH01	*Pseudomonas aeruginosa* PAO1 PA3851 mutant	this work

Tab. 5: plasmids

Plasmid	Description	Reference
pGEX-6P-1	Expression vector carrying N-terminal sequence for GST from *Schistosoma japonicum* and recognition sequence for PreScission™ Protease, *lac* promoter, *amp*^{r}	Amersham Biosciences
pEX18Ap	*amp*^{r} *oriT*$^+$ *sacB*$^+$; gene replacement vector with MCS of pUC18	Hoang *et al.* (1998)
pKNT25	derivative of the low copy-number plasmid pSU40, encodes the T25 fragment (corresponding to the first 224 amino acids of CyaA), lac promoter, *kan*^{r}. A multicloning site sequence (MCS) is inserted at the 3' end of T25.	Euromedex
pKT25	derivative of the low copy-number plasmid pSU40, encodes the T25 fragment (corresponding to the first 224 amino acids of CyaA), *lac* promoter, *kan*^{r}. A MCS is inserted at the 5' end of T25.	Euromedex
pUT18	derivative of the high copy number vector pUC19, *amp*^{r}, encodes the T18 fragment (amino acids 225 to 399 of CyaA), *lac* promoter. A MCS is inserted at the 5' end of T18.	Euromedex
pUT18C	derivative of the high copy number vector pUC19, amp^r, encodes the T18 fragment (amino acids 225 to 399 of CyaA), *lac* promoter. A MCS is inserted at the 3' end of T18.	Euromedex
pCA24N-yggW$_{E.c.}$	high copy number vector carrying N-terminal sequence for HIS, *lac* promoter, *cm*^{r} with HemW from *E. coli*	Kitagawa (2005)
pGEX-hemW $_{E.c.}$	pGEX-6P-1 derivative, encodes N-terminal fusion of GST with HemW from *E. coli*	Katrin Grage (2005)
pKNT25-hemH $_{E.c.}$	pKNT25 derivate, encodes C-terminal fusion of HemH with the T25 fragment	this work
pKNT25-katA $_{E.c.}$	pKNT25 derivate, encodes C-terminal fusion of KatA with the T25 fragment	this work
pKNT25-bfrA $_{E.c.}$	pKNT25 derivate, encodes C-terminal fusion of BfrA with the T25 fragment	this work
pKT25-hemH $_{E.c.}$	pKT25 derivate, encodes N-terminal fusion of HemH with the T25 fragment	this work
pKT25-katA $_{E.c.}$	pKT25 derivate, encodes N-terminal fusion of KatA with the T25 fragment	this work
pKT25-bfrA $_{E.c.}$	pKT25 derivate, encodes N-terminal fusion of BfrA with the T25 fragment	this work
pUT18C- hemH $_{E.c}$	pUT18C derivate, encodes C-terminal fusion of HemH with the T18 fragment	this work

Plasmid	Description	Reference
pUT18C- katA $_{E.c.}$	pUT18C derivate, encodes C-terminal fusion of KatA with the T18 fragment	this work
pUT18C-PA3851	pUT18C derivate, encodes C-terminal fusion of BfrA with the T18 fragment	this work
pUT18- bfrA $_{E.c}$	pUT18 derivate, encodes N-terminal fusion of HemH with the T18 fragment	this work
pUT18- katA $_{E.c.}$	pUT18 derivate, encodes N-terminal fusion of KatA with the T18 fragment	this work
pUT18- bfrA $_{E.c}$	pUT18 derivate, encodes N-terminal fusion of KatA with the T18 fragment	this work
pPS858	*amp*^{r} *gm*^{r}; source of gentamicin cassette	Hoang *et al.* (1998)
pSH1	*amp*^{r} *gm*^{r}; pEX18Ap with 550 bp fragment upstream of PA01 PA3851, Gm^r-*gfp* fragment from pPS858 and 633 bp fragment downstream of PA3851 between EcoRI and XbaI	this work
pUT18C-PA3851	pUT18C derivate, encodes C-terminal fusion of PAO1 PA3851 with the T18 fragment	this work

2.3 Growth Media and Media Additives

2.3.1 Growth Media

For the cultivation of *E. coli* cells the nutritionally rich medium Luria Bertani (LB) (Sambrook *et al*., 1989) was used.

LB-Medium:

trypton	10	g/l
NaCl	10	g/l
yeast extract	5	g/l

Solid medium required the addition of 15 g/l agar before sterilization.

For electroporation the nutrient rich SOC medium (Hanahan, 1983) was used.

SOC medium:

trypton	20	g/l
yeast extract	5	g/l
NaCl	0.5	g/l
250 mM KCl	10	g/l

in H_2O_{dest}, pH 7.0 adjusted with 5 N NaOH

sterile filtered additives after autoclaving

2 M $MgCl_2$	5	ml/l
1 M glucose	20	ml/l

For Screening and selection of specific bacteria different minimal media were used.

M63 Medium (Ausubel *et al.*, 1994):

$(NH_4)_2SO_4$	2	g/l
KH_2PO_4	13.6	g/l
$FeSO_4 \cdot 7H_2O$	0.5	mg/l

in H_2O_{dest}, pH 7.0 adjusted with 7.0 with KOH

sterile filtered additives after autoclaving

$MgSO_4 \cdot 7H_2O$	1	ml/l
20 % maltose	10	ml/l
0.05 % vitamin B1	2	ml/l

For solid medium 15 g/l agar were added.

M9 Medium (Clowes, 1968):

Na_2HPO_4	6	g/l
KH_2PO_4	3	g/l
NaCl	0.5	g/l
NH_4Cl	1	g/l

sterile filtered additives after autoclaving

1M $MgSO_4$	2	ml/l
1M $CaCl_2$	0.1	ml/l
1M glucose	4	ml/l
0.1 % casaminoacids	2	ml/l
0.005 % tryptophan	25	ml/l

2.3.2 Media Additives

Media additives were prepared as stock solutions, sterile filtrated, and added to the media after sterilization by autoclaving. All stock solutions were stored at –20 °C.

Tab. 6: media additives

medium additive	stock solution	end concentration
5-aminolevulinic acid hydrochloride (ALA)	50 mg/ml in H_2O_{dest}	50 µg/ml
5-bromo-4-chloro-3-indolyl- β-D-galactopyranoside (x-gal)	20 mg/ml in dimethyl formamide	40 µg/ml
ampicillin (amp)	100 mg/ml in H_2O_{dest}	100 µg/ml
carbenicillin (carb)	100 mg/ml in H_2O_{dest}	100 µg/ml
chloramphenicol (cm)	34 mg/ml in 70 % ethanol (v/v)	34 µg/ml
gentamicin (gm)	80 mg/ml in H_2O_{dest}	80 µg/ml 10 µg/ml
Isopropyl-1-thio-β-D-galactoside (IPTG)	1 molar in H_2O_{dest}	500 µM
kanamycin (kan)	50 mg/ml in H_2O_{dest} 10 mg/ml in H_2O_{dest}	50 µg/ml 10 µg/ml
o-nitrophenol-β-galactoside (ONPG)	4 mg/ml in H_2O_{dest}	941 µg/ml
spectinomycin (spc)	50 mg/ml in H_2O_{dest}	50 µg/ml
streptomycin (strep)	100 mg/ml in H_2O_{dest}	100 µg/ml
tetracycline (tet)	5 mg/ml in 70 % ethanol (v/v)	10 µg/ml

2.4 Microbiological Techniques

2.4.1 Sterilization

If not otherwise stated all media and solutions were vapor sterilized for 20 min at 120 °C and 1 bar overpressure, or sterilized by filtration (pore width 0.2 µm).

2.4.2 Cultivation of Bacteria

Bacterial cells for recombinant protein production were grown under aerobic conditions. Pre-cultures of *E. coli* BL21 (DE) containing the corresponding plasmids were grown in 100 ml LB including the required additives. Cultivation was carried out at 37 °C and 200 rpm over night. Main cultures (500 ml) were inoculated with a 1:100 dilution of pre-culture and incubated at 37 °C and 200 rpm. The induction of protein production by IPTG was initiated at an optical density (OD) at the wavelength 578 nm of 0.6 – 0.8. Further growth occurred at 17 °C and 200 rpm. Cultivation on agar-plates occurred as plating 50 – 100 µl of cell suspension with a Drygalski spatula, or streaking cells with an inoculating loop from liquid culture or a single colony. Plates were incubated aerobically at 37 °C.

2.4.3 Determination of Cell Density

Cell density of bacterial solutions was determined by measuring the OD_{578} nm. For cell densities with an OD_{578} nm $\geq$ 1 1:10 dilutions were prepared. An OD_{578} nm of 1 corresponds to approximately 1 x 10^9 *E. coli* cells per ml.

2.4.4 Storage of Bacterial Cells

Storage on agar-plates occurred at 4 °C, not exceeding 4 weeks. Long term storage of bacterial strains was accomplished by preparing glycerol stocks. Therefore, 800 µl of a

bacterial culture was mixed with 350 µl of sterile 80 % (v/v) glycerol, instantly frozen and stored at -80 °C.

2.5 Molecular Biology Techniques

2.5.1 Preparation of Genomic DNA

The respective strains were grown over night to yield a culture of high density. 3 ml were harvested in two steps by centrifugation at 11'000 g for 5 min.
Cell disruption and DNA purification with the NucleoSpin® Soil Kit was carried out according to manufacturer's instructions. Purified DNA was stored in H_2O_{dest} at 4 °C.

2.5.2 Preparation of Plasmid DNA (mini prep)

Three ml of an overnight culture were harvested by centrifugation at 11'000 g for 5 min in two steps. The sediment was resuspended in 300 µl buffer P1. 300 µl buffer P2 were added and the sample carefully mixed, by inverting the tube. Incubation for 5 min at room temperature was followed by addition of 300 µl buffer P3 und again careful mixing of the sample. The mixture was incubated for 5 min on ice before centrifugation for 15 min at 11'000 g and 4 °C occurred. 800 µl supernatant was transferred in a new reaction tube to repeat the centrifugation step and loose all precipitated protein. Subsequently, 600 µl supernatant was added to 600 µl isopropanol in a fresh tube. Incubation for 10 min at room temperature allowed the DNA to precipitate. Centrifugation for 15 min at 11'000 g and 4 °C led to sedimented DNA, which in the following was washed with 70 % (v/v) ethanol. After all traces of ethanol had evaporated, the DNA was solubilized in 60 µl H_2O.

P1:

Tris-HCL, pH 8.0	50 mM
EDTA	10 mM
RNAse A	100 µg/ml

P2:

NaOH	200 mM
SDS	1 %

P3:

KOAc, pH 5.5	3 M

2.5.3 Determination of DNA Concentration

Concentration and purity of DNA solutions were determined by measuring the absorbance at 260 nm and 280 nm, respectively. The ratio of OD_{260} to OD_{280} provides information of the DNA solutions purity, as in an OD_{260}/OD_{280} ratio of 1.8 - 2.0 was considered as pure.

2.5.4 Production and Transformation of Rubidium Chloride Competent *Escherichia coli* Cells

For the production of rubidium chloride competent *E. coli* cells 250 ml LB medium was inoculated with a 1:100 dilution of the respective pre-culture. Cells were harvested after reaching an OD_{578} nm of 0.6 by centrifugation for 5 min at 4 °C and 4'500 g. The cell sediment was suspended in 0.4 volume ice-cold TFB1 (referring to the volume of the original culture) and incubated for 5 min on ice. After another centrifugation step for 5 min at 4 °C and 4'500 g the cell sediment was suspended in 0.04 volume ice-cold TFB2 and incubate for 15 - 60 min on ice. Aliquots of 50 µl were loaded into pre-cooled reaction tubes and stored at -80 °C. For transformation one aliquot of competent cells was thawed for 30 min on ice, before ~ 50 µg/ml plasmid DNA was added. After another 30 min on ice the mixture was subjected to a heat shock at 42 °C for 45 sec and cooled on ice for 2 min. 500 µl LB were added and the cells were incubated at 37 °C for 15 - 45 min. Depending on cell density and used plasmid DNA different amounts of cell solution were plated on agar-plates containing the respective antibiotics and incubated at 37 °C over night.

TFB1:

KOAc	30 mM
$CaCl_2$	10 mM
$MnCl_2$	50 mM
RbCl	100 mM
glycerol	15 % (v/v)
in H_2O_{dest}, pH 5.8	

TFB2:

MOPS	10 mM
$CaCl_2$	75 mM
RbCl	10 mM
glycerol	15 % (v/v)
in H_2O_{dest}, pH 6.5	

2.5.5 Production and Transformation of Electrocompetent *Escherichia coli* Cells

For the production of electrocompetent *E. coli* cells, 250 ml LB medium was inoculated with a 1:100 dilution of the respective pre-culture. After reaching an OD_{578} nm of 0.6 the cells were cooled for 10 min in ice-water and harvested by centrifugation for 15 min at 4 °C and 4'500 g. The cell sediment was suspended in 250 ml ice-cold H_2O_{dest}. After another centrifugation step for 15 min at 4 °C and 4'500 g the cell sediment was again suspended in 250 ml ice-cold H_2O_{dest} and centrifuged for 15 min at 4 °C and 4'500 g. The cell sediment was suspended in 10 ml ice-cold sterile 10 % glycerol (v/v) and centrifuged (15 min at 4 °C and 4'500 g). The final cell sediment was suspended in 1 ml ice-cold sterile 10 % glycerol (v/v). Aliquots of 40 µl were loaded into pre-cooled reaction tubes and stored at -80 °C. For transformation one aliquot of competent cells was thawed for a few minutes on ice, before about 5 ng plasmid DNA was added. The mixture was transferred into an ice-cooled electroporation cuvette. In a Gene Pulser (Bio-Rad) the cells were subjected to a short electric pulse (voltage 2.5 kV, capacity 25 µF, resistance 200 Ω) and thereby temporarily rendered permeable for DNA. Immediately afterwards 1 ml SOC medium was added and the mixture was incubated for 1 h at 37 °C and 700 rpm. Depending on cell density and used plasmid DNA different amounts of cell solution were plated on agar-plates containing the respective antibiotics and incubated at 37 °C over night.

2.5.6 Agarose Gel Electrophoresis

To differentiate DNA molecules by their mass proportions gels consisting of 1 % (w/v) agarose in TAE buffer were prepared. Through voltage application of 80 - 120 V (depending on the gel size) the negative charged DNA molecules migrate towards the anode. The velocity is proportional to negative logarithm of their length. Prior to loading, DNA samples were mixed with loading dye to facilitate loading and to indicate the progress of the samples in the gel. GeneRuler™ DNA Ladder Mix was used as size standard according to the manufacturer's instructions. After electrophoresis the gel was stained with an ethidium bromide solution for 10 - 30 min, rinsed with H_2O and the DNA was detected *via* its fluorescence und UV-light at a wavelength of 312 nm. In case of DNA fragment extraction from the gel, the QIAquick Gel Extraction Kit (Qiagen) according to the manufacturer's instructions was used.

TAE buffer:

tris-acetate	40	mM
EDTA	1	mM
in H_2O_{dest}, pH 8.		

5x DNA loading dye :

bromphenol blue	0.35	mM
xylen cyanol FF	0.45	mM
orange G	0.25	% (w/v)
sucrose	115	mM
in TAE buffer		

ethidium bromide solution:

ethidium bromide	1	% (v/v)
in H_2O_{dest}		

2.5.7 Amplification of DNA Fragments by Polymerase Chain Reaction

2.5.7.1 Design and synthesis of oligonucleotide primers

Primers for the amplification of *P. aeruginosa hemH, katA* and *bfrA* genes as well as *E. coli hemW* gene were designed with the aim of subsequent cloning into different vectors. *Via* these primers recognition sites of restriction endonucleases were inserted at

both ends of the genes. Table 7 lists oligonucleotide primers. Recognition sites of restriction endonucleases are underlined.

Tab. 7: Oligonucleotide primers used for amplification of DNA fragments.
Restriction sites are underlined, "for" refers to forward primer and "rev" refers to reverse primer.

Primer	Sequence of oligonucleotide primer (5'→3')	additional information
$hemH_{Ec}$for	ACTCTAGAGATGACCGAGAATGCCCTGCTG	pKT25/pKNT25 for, *XbaI* restriction site
$hemH_{Ec}$oSrev	CATTGAATTCGAGAGCGGCCTGGCCAAGCG	pKNT25 rev, *EcoRI* restriction site
$hemH_{Ec}$rev	CATTGAATTCGATCAGAGCGGCCTGGCCAAGC	pKT25 rev, *EcoRI* restriction site
$katA_{Ec}$for	ACTCTAGAGATGGAAGAGAAGACCCGCCTG	pKT25/pKNT25 for, *XbaI* restriction site
$katA_{Ec}$oSrev	CATTGAATTCGAGTCCAGCTTCAGGCCGAG	pKNT25 rev, *EcoRI* restriction site
$katA_{Ec}$rev	CATTGAATTCGATCAGTCCAGCTTCAGGCCGAG	pKT25 rev, *EcoRI* restriction site
$bfrA_{Ec}$for	ACTCTAGAGATGCAAGGCCATCCGGAAGTC	pKT25/pKNT25 for, *XbaI* restriction site
$bfrA_{Ec}$oSrev	CATTGAATTCGAGATCTGCGATTGCAGGTA	pKNT25 rev, *EcoRI* restriction site
$bfrA_{Ec}$rev	CATTGAATTCGATCAGATCTGCGATTGCAGGTA	pKT25 rev, *EcoRI* restriction site
PA3851for	ACTCTAGAGATGCCGGCGGAGACCCCGC	pKT25 for, *XbaI* restriction site
PA3851rev	CCGAATTCTTCAGCCCAGGCCCACGCCG	pKT25 rev, *EcoRI* restriction site
$hemW_{Ec}$-pGEX for	ACGGGATCCGTAATGGTTAAATTACCTC	pGEX-6P-1 for, *BamHI* restriction site
$hemW_{Ec}$-pGEX rev	CGCCTCGAGCAATACAAGTTTACTCAGC	pGEX-6P-1 rev, *XhoI* restriction site

2.5.7.2 Polymerase chain reaction conditions

The polymerase chain reaction (PCR) serves to amplify specific DNA fragments *in vitro*. For reaction concerning *E. coli* DNA the *Taq* DNA Polymerase was used. The standard composition of the reaction is listed below.

Taq PCR composition:

template DNA	10-100	ng
10 x ThermoPol reaction buffer	2.5	µl
forward Primer	10	pmol
reverse Primer	10	pmol
dNTP mix	50	µM
Taq DNA Polymerase	2.5	U
H_2O_{dest}	ad 25	µl

The amplification of *P. aeruginosa* DNA was archived with Phusion™ high-fidelity DNA Polymerase.

Phusion PCR composition:

template DNA	10-100	ng
5 x Phusion™ HF buffer	5	µl
forward Primer	10	pmol
reverse Primer	10	pmol
DMSO	3	% (v/v)
dNTP mix	25	µM
Phusion™ DNA Polymerase	0.5	U
H_2O_{dest}	ad 25	µl

The reaction started with initial denaturation of the template DNA. Afterwards a cycle consisting of three steps, denaturation, primer annealing and primer elongation, occurred. The reaction was terminated by a final elongation step. The annealing temperature depends on length and GC content of the DNA to be amplified and was calculated as follows.

$$T_m\ [°C] = 69.3 + 0.41\ (\%\ G+C) - 650/n$$

G+C stands for the percental G+C content of the primers while *n* represents the number of nucleotides. The duration of elongation is based upon the length of the DNA fragment to be amplified. All other steps were chosen according to manufacturer's instructions.

Taq PCR program:

95 °C	3 min		
94 °C	40 s		
50 – 65 °C	40 s	↻	35 x
72 °C	1 min		
72 °C	10 min		
10 °C	∞		

Phusion PCR program:

98 °C	30 min		
98 °C	6 s		
50 °C	20 s	↻	30 x
72 °C	1 min		
72 °C	10 min		
10 °C	∞		

2.5.7.3 Purification of PCR products

An aliquot of the amplified DNA was analyzed by gel electrophoresis for quality control. If only one PCR product could be detected the reaction mixture was purified with the QIAquick PCR Purification Kit according to manufacturer's instructions. In the case of more than one PCR product being visible, the DNA fragment of interest was excised from the gel and purified with the QIAquick Gel Extraction Kit according to manufacturer's instructions.

2.5.8 Enzymatic Modification of PCR Products

2.5.8.1 DNA cleavage with restriction endonucleases

Bacteria accumulate restriction endonucleases to protect themselves against external DNA, with class II endonucleases being the most abundant ones. A palindromic DNA sequence is recognized and two phosphordiester bonds inside this sequence are hydrolyzed, leading to 'blunt' or 'sticky' ends. Restriction of vectors and PCR product was carried out using restriction endonucleases purchased from New England Biolabs (Frankfurt am Main, Germany). Concentrations of enzymes and DNA, reaction buffers and incubation temperature was chosen according to manufacturer's instructions. Digestion proceeded for 1 - 3 h and was followed by heat inactivation.

2.5.8.2 Ligation

The DNA Ligase is an enzyme that repairs double-strand breaks by covalently connecting the 3' hydroxyl end of one nucleotide, with the 5' phosphate end of another. The 5' phosphate group of vectors was removed before ligation, to prevent re-circularization. Therefore, 1 U/µg DNA antarctic alkaline phosphatase (New England BioLabs) was added after restriction and the mixture incubated at 37 °C for 30 min. Afterwards the sample was heat inactivated at 65 °C for 15 min. Ligation of DNA was carried out using T4 DNA ligase (MBI Fermentas) in a reaction buffer supplied by the manufacturer. The reaction was executed for 2 - 4 h at 25 °C using 25 - 50 ng of vector

DNA and insert DNA excess (insert to vector ratio with regard to molar concentrations ~5:1) and T4 DNA ligase (MBI Fermentas) in a reaction buffer supplied by the manufacturer.

2.5.9 DNA Sequencing and Analysis

The performed sequencing reaction was a modified version of Sangers chain-terminator method (Sanger *et al*., 1977). DNA sequences were obtained with an Abi Prism™ 310 Genetic Analyzer (Applied Biosystems, Darmstadt, Germany) in our laboratory. The required preparatory PCR with fluorescence-labeled dideoxyribonucleotide triphosphates (ddNTPs) and purification of the PCR product were carried out as described by manufacturer's instruction.

Standard PCR program:

96 °C	1 min	
96 °C	30 s	
50 °C	15 s	25 x
60 °C	4 min	
4 °C	∞ min	

Tab. 8 Oligonucleotide primers used for sequencing of DNA fragments.
"For" refers to forward primer and "rev" refers to reverse primer.

Primer	Sequence of oligonucleotide primer (5'→3')	additional information
pGEX-6P-1for	CCTCCAAAATCGGATCTG	sequencing of pGEX-6P-1, forward
pGEX-6P-1rev	CACCGTCATCACCGAAAC	sequencing of pGEX-6P-1, reverse
oAW009	GTATTCCACTGACGGCGGATATCGAC	sequencing of pKT25, forward
oAW010	TAAGTTGGGTAACGCCAGGGTTTTCC	sequencing of pKT25, reverse
oAW011	AGGCACCCCAGGCTTTACACTTTATG	sequencing of pKNT25, forward
oAW012	CAGGCGGAACATCAATGTGGCGTTTT	sequencing of pKNT25, reverse
oAW013	TATGCTTCCGGCTCGTATGTTGTGTG	sequencing of pUT18, forward
oAW014	ACGCCGATATTCATGTCGCCGTCGTA	sequencing of pUT18, reverse
oAW015	AGTTCTCGCCGGATGTACTGGAAACG	sequencing of pUT18C, forward
oAW016	GGCTGGCTTAACTATGCGGCATCAGA	sequencing of pUT18C, reverse
pCA24N for	CATTAAAGAGGAGAAATTA	sequencing of pCA24N, forward
pCA24N rev	TATCAACAGGAGTCCAAGCTCA	sequencing of pCA24N, reverse

2.5.10 Generation of a Chromosomal PA3851 Knock-Out Mutant in *Pseudomonas aeruginosa* PAO1

To create an unmarked gene deletion, the *sacB* counter selection and FLP recombinase excision (Hoang *et al*., 1998) was used. First the target gene is replaced by a gentamicin resistance cassette, obtained from the vector pPS858. Therefore, the gentamicin cassette was cloned interjacent of two DNA fragments homolog to the up- and downstream regions of the target gene. In the following the complete construct was cloned into the MCS of the suicide vector pEX18Ap. In table 9 the primers, size of the obtained PCR products and restriction sites deployed to create knockout constructs conducted in this study are listed.

Tab. 9: Oligonucleotide primers and restriction sites used for construction of suicide vectors required for deletion of *Pseudomonas aeruginosa* gene PAO1.
Restriction sites are underlined, "for" refers to forward primer and "rev" refers to reverse primer.

region	primer name	sequence (5'→3')	product size	restriction site
upstream of PA3851	KOPA3851for KOPA3850rev	GGAATTCAATTCAGCGGCGTCGAGCAG CGAGCTCCTTCACCTATGGGTTGGGCACC	550 bp	*EcoRI* *SacI*
downstream of PA3851	KOPA3852for KOPA3852rev	CGAGCTCTGCCTCAACGCGCCTCGATG GCTCTAGAACCAGTGGCCGGCATTCATG	480 bp	*SacI* *XbaI*

The finished suicide vectors were controlled *via* restriction analysis and the positive vectors were transferred into *P. aeruginosa* per diparental mating. Selection followed by plating the cells on LB plates containing gentamicin. Since pEX18Ap is not capable of replicating in *P. aeruginosa*, growth only occurs if the gentamicin cassette is integrated into the genome through homologous recombination between upstream and downstream region of the target gene. A single crossover event leads to integration of the plasmid but not to a deletion of the gene itself. To ensure that the strain carries the required double crossover the cells were plated on agar plates containing 5 % (w/v) sucrose and gentamicin. The *sacB* gene encoding for levansucrase on vector pEX18Ap produces a toxic degradation product of sucrose which allows for selection. Thus only carbenicillin sensitive strains with inserted gentamicin resistance cassette and removed vector are able to grow.

To remove the gentamicin resistance cassette from the genome, a FLP-recombinase was used. It binds to the FRT recognition sequences flanking the resistance cassette and removes the interjacent part from the genome. FLP-recombinase is encoded on the plasmid pFLP2 and was first transformed into *E. coli* ST18 before it was transferred

into *P. aeruginosa via* diparental mating. The first selection step occurred on LB containing carbenicillin, to allow FLP-recombinase the excision of the resistance cassette. To remove vector pFLP2 the cells were plated on LB containing 5 % sucrose, which leads to toxic degradation products by the *sacB* gene. Again only cells without vector are able to grow. For further verification of removement of the gentamicin resistance cassette and vector pFLP2, the cells were plated on LB with gentamicin and carbenicillin. Finally, to verify a successful knockout, PCR analysis was carried out using primers binding upstream and downstream of homologous sequences as listed in table 9. DNA upstream and downstream of the excised gene was amplified, and compared with amplified DNA from PAO1 wild type. The fragment of the knockout mutant should be shorter.

2.6 Bacterial Adenylate Cyclase Based Two Hybrid System (BACTH)

The BACTH system is a two hybrid system to detect and characterize protein-protein interactions *in vivo*, using the adenylate cyclase from *Bordetella pertussis*. The catalytic domain of adenylate cyclase includes the first 400 amino acids which code for two complementary fragments, the T18- and T25-fragment. When physically separated these fragments show no cyclase activity.

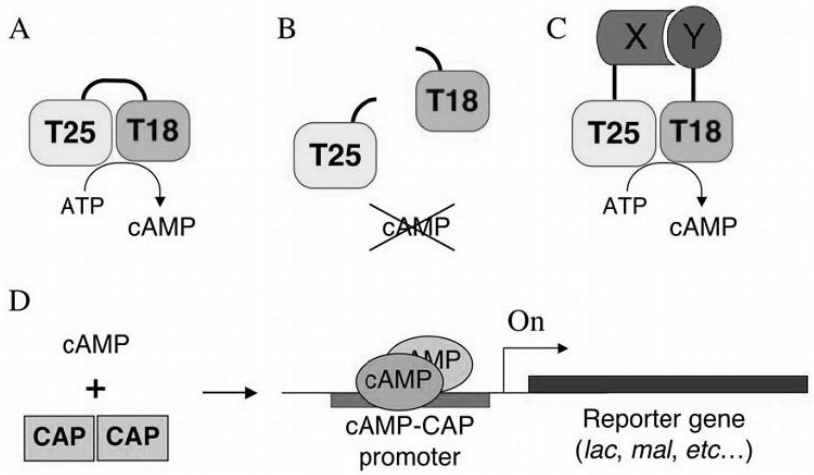

Fig. 18: Principle of the BACTH system (Euromedex)
A) T25- und T18 fragment of *B. pertussis* adenylate cyclase convert ATP to cAMP. B) Physical separation of the T25- and T18 fragment leads to inactivity. C) Catalytic activity results of the interaction of protein "X" and "Y", to which the complementary fragments are fused. D) cAMP binds to the catabolic activator protein (CAP). The cAMP/CAP complex is an activator for several genes, amongst others the reporter gene β-galactosidase.

Interaction mediated reconstitution through fused interacting proteins leads to adenylate cyclase activity and starts the cAMP signal pathway (Fig. 18). The co-transformation was done in adenylate cyclase deficient *E. coli* (*cya*$^-$) BTH101 cells.

LB X-gal was used as indicator medium, where all bacteria can grow. Bacteria expressing interacting hybrid proteins can form blue colonies due to the conversion of X-gal to 5,5‘-dibromo-4,4‘-dichloro-indigo by β-galactosidase. As selective medium M63 medium supplemented with maltose was used. Only bacteria with functional protein-protein interactions can grow, since the only carbon source maltose is utilized by induction of the *mal*-operon. Therefore, all colonies appear blue. Table 4 and 5 give an overview over the used strains and plasmids.

The intention was the detection of *P. aeruginosa* ferrochelatase (*hemH*), catalase A (*katA*) and bacterioferritin A (*bfrA*) interaction partners by screening a genomic *P. aeruginosa* library and the investigation of direct interaction between the three proteins. For this reason *hemH*, *katA* and *bfrA* were cloned into the plasmids pKT25, pKNT25, pUT18 and pUT18C containing the T25-fragment or T18-fragment from adenylate cyclase C-terminal and respectively N-terminal of the MSC. Transcription is controlled by the *lac*-operon. Subsequently, the addition of IPTG is essential to induce the promoter as well as the *lacZ* gene for β-galactosidase expression. The DNA sequences of the genes for detected interaction partners were sequenced and the β-galactosidase activity was measured.

2.6.1 Screening of the *Pseudomonas aeruginosa* BACTH Library

For screening of the genomic *P. aeruginosa* library 5 - 500 ng plasmid DNA of the library and 5 ng of the desalted screening vectors pKT25-*hemH*, - *katA*, -*bfrA* or pKNT25-*hemH*, -*katA*, -*bfrA* were used. Co-transformation was carried out as in section 2.5.4 described. The transformation was washed twice with 1000 µl liquid M63 medium and afterwards was resuspended in 500 µl M63. To define a transformation rate, dilutions (1:10, 1:100; 1:1000) of the transformation were streaked on LB containing amp, kan, IPTG and X-Gal. 300 µl of the transformation was plated on M36. Incubation was done at 30 °C over night on LB and up to 5 days on M36 medium. The vectors pKT25-zip and pUT18C-zip were used as positive control while pKT25 and pUT18C were used as negative control.

Clones featuring a HemH, KatA and BfrA interaction appeared as blue colonies on M63 medium. To obtain a pure culture, the positive clones were streaked on M36 medium twice and incubated by 30 °C. Over-night cultures were made in order to carry out a plasmid preparation. To identify the fragment size a PCR and subsequent purification was done. Through sequencing and alignment of the data with the *P. aeruginosa* PAO1 database (http://www.pseudomonas.com/), the detected interaction partners were identified.

2.6.2 β-Galactosidase Enzyme Assay

LacZ is a reporter gene encoding the enzyme β-galactosidase. It hydrolyzes β-galactosides like *ortho*-nitrophenyl-β-galactoside (ONPG) into monosaccharides. ONPG itself is colorless, while the product of the β-galactosidase reaction *o*-nitrophenol is yellow and can be colorimetrically assayed at 420 nm wavelength. Since the amount of protein interaction in the BACTH system correlates with the amount of β-galactosidase production, the β-galactosidase activity was measured.

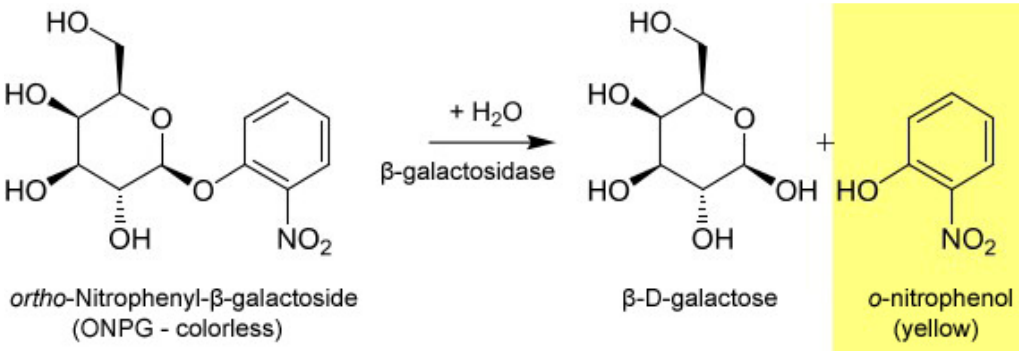

Fig. 19: Hydrolyzation of the ONPG molecule into galactose and ortho-nitrophenol.
ONPG is hydrolyzed into β-D-galactose and *o*-nitrophenol, catalyzed by β-galactosidase. The amount of o-nitrophenol can be messured photometrically at 420 nm wavelength.
(http://www.chemgapedia.de/vsengine/vlu/vsc/de/ch/5/bc/vlus/gentechnik/prak_lacz_test.vlu/Page/vsc/de/ch/5/bc/gentechnik/praktikum/lacz_test/lacz_test.vscml.html)

LB cultures with 100 µg/ml amp, 50 µg/ml kan and 0.5 mM IPTG were incubated over night at 30 °C and 200 rpm. The OD_{578} nm of the over-night cultures was measured and 50 µl of the cultures were sedimented for 5 min at 11'000 g and 4 °C respectively. The supernatant was discarded and sediment stored at – 20 °C. For measurement of the β-galactosidase activity the sediment was thawed and resuspended in 800 µl Z-buffer. To permeabilize the cells one drop of each 0.1 % SDS and chloroform was added and the

solution incubated for 5 min at 30 °C. The reaction was started by the addition of 200 µl ONPG (4mg/ml). Incubation continued at 30 °C till apparent yellow coloring of the mixture and was stopped by 1M Na_2CO_3. A centrifugation step followed for 5 min at 11'000 g and 4 °C. The resulting supernatant was measured at 420 nm wavelength. Calculation of β-galactosidase activity was archived by following arithmetic equation.

$$\text{spec. activity [MU]} = \frac{\Delta E_{420nm} \cdot 1000}{OD_{578nm} \cdot V \cdot t}$$

MU - Miller Unit
ΔE_{420nm} - absorbance difference of the reaction mixture after stopping the reaction compared to the initial absorbance
OD_{578nm} - optical density of employed culture
V - volume (ml) of employed culture
t - time (min) till reaction stop

The specific activity is given in µmol of hydrolyzed substrate ONPG per minute and optical density OD_{578} nm. The measurement unit of specific activity is Miller unit (MU).

Z-buffer:

Na_2HPO_4	60 mM
NaH_2PO_4	40 mM
KCl	10 mM
$MgSO_4$	1 mM
β-mercaptoethanol	50 mM

2.7 Protein Biochemical Methods

2.7.1 Production and Purification of *Escherichia coli* HemW

2.7.1.1 Cell Growth for Protein Production

Five times 500 ml vapour sterilized LB medium containing 100 µg/ml amp in 1 L Erlenmeyer flasks were each inoculated with 5 ml of an overnight culture of *E. coli* BL21 (DE3) carrying pGEX-*hemW*. Cultures were grown at 37 °C and 200 rpm. At an OD_{578} nm of 0.6 expression of *hemW* was induced by addition of 500 µM IPTG. Incubation continued overnight at 17 °C and 200 rpm. Afterwards cells were harvested by centrifugation for 15 min at 4 °C and 4000 x g. Production and harvest of the cells

were carried out under aerobic conditions, while all following steps occurred under strictly anaerobic conditions.

2.7.1.2 Cell Disruption

The cell sediment was resuspended in 10 ml PBS buffer (2.7.1.3). Cells were disrupted by a single passage through a French Press at 19,200 p.s.i. Cell debris and insoluble proteins were removed by centrifugation for 60 min at 25000 x g and 4 °C. The resulting supernatant was loaded onto a Glutathione Sepharose column.

2.7.1.3 Affinity Chromatography Using Glutathione Sepharose

The chromatography was performed in an anaerobic chamber. A 6 ml Glutathione Sepharose column was equilibrated with 10 column volumes of PBS buffer. The supernatant was mixed with the column resin and incubated for 2 h. The flow through was collected and the column washed with 12 column volumes PBS buffer. Subsequently, the column resin with the bound protein was mixed with 7 ml PBS buffer containing 800 U PreScission Protease and incubated overnight, to clip the GST-tag. Afterwards the protein was eluted with 3 column volumes of PBS buffer. Eluates were collected in 1 ml fractions. The final steps were the regeneration of the column with 10 column volumes of regeneration buffer. Fractions containing HemW were identified by SDS-PAGE (2.7.8), pooled and concentrated by ultrafiltration (2.7.2).

PBS buffer:

NaCl	140	mM
KCl	2.7	mM
Na_2HPO_4	10	mM
KH_2PO_4	1.8	mM
DTT	5	mM

in H_2O_{dest}, pH 7.4

regeneration buffer:

NaCl	140	mM
KCl	2.7	mM
Na_2HPO_4	10	mM
KH_2PO_4	1.8	mM
DTT	5	mM
glutathione	10	mM
in H_2O_{dest}, pH 7.4		

2.7.2 Concentration of Protein Solutions

Protein solutions were concentrated in a 50 ml or in a 10 ml stirred ultrafiltration cell with a YM30 membrane at 2.5 bar until a protein concentration of 9 to 11 mg/ml was reached. *E. coli* HemW protein was stored at 4 °C.

2.7.3 Determination of Protein Concentration

Protein concentration was determined by Bradford Protein Assay Method (Bio-Rad, Munich, Germany).

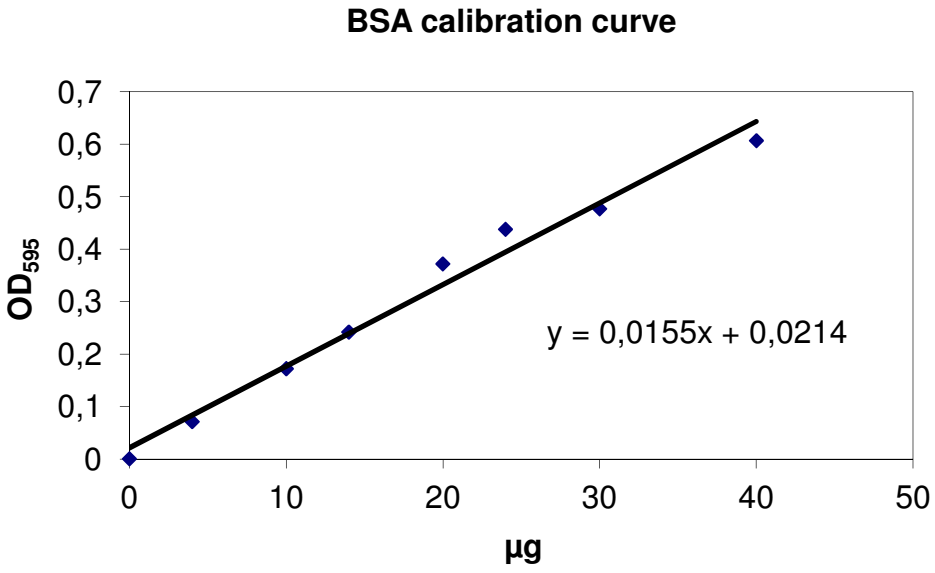

Fig. 20: BSA calibration curve for determination of protein concentrations.
The used amount of BSA was plotted against the absorption at 595 nm after incubation with the Bradford reagent.

This photometric method is based on the complexation of the non-polar, hydrophobic side chains of the proteins with the dye Coomassie-Brillant-Blau G-250 under acidic conditions. The result is a shift in the absorption maximum of the dye from 465 to 595 nm, which is proportional to the protein content. The calibration curve was created using bovine serum albumin (BSA) in the concentrations from 0 to 40 mg/ml.

2.7.4 Determination of Protein Iron Content

The iron content of recombinant, purified HemW was determined colorimetrically with bathophenanthroline (Smith, 1952). Thirty µl of each protein solution were mixed vigorously with 45 µl of 1 M perchloric acid (PCA), and incubated for 15 min at RT. After centrifugation for 5 min at 10'000 x g, 90 µl of the supernatant was vigorously mixed with 72 µl of 3 mM bathophenanthroline disulfate, 36 µl of 192 mM sodium ascorbate and 27 µl saturated ammonium acetate. Incubation for 30 min at RT was preceding centrifugation for 5 min at 10'000 x g. The resulting supernatant was photometrical measured at 535 nm and 680 nm wavelength, respectively. The iron content of the samples was determined via a calibration curve obtained from a series of dilutions of an iron standard (Merck).

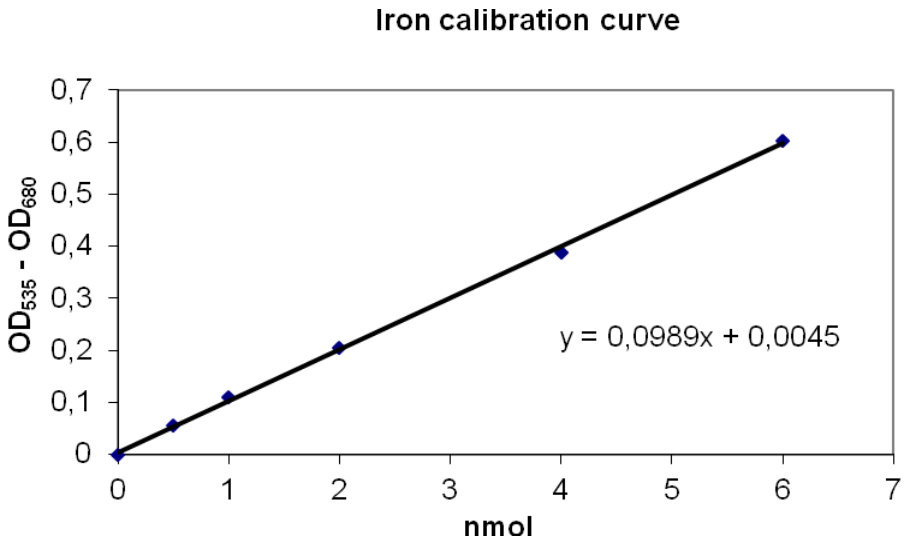

Fig. 21: Iron calibration curve for determination of iron concentrations.
The used amount of iron was plotted against the absorption at 535 nm minus the absorption at 680 nm after incubation.

2.7.5 UV-Visible Light Absorption Spectroscopy

UV-visible light absorption spectra of purified recombinant proteins were recorded under anaerobic conditions using a UV/visible Spectrophotometer (Jasco V-650). The presence of an Fe-S cluster was indicated by an absorption maximum at 420 nm wavelength. 10 µM HemW and hemin in PBS buffer were deployed.

2.7.6 Circular Dichroism Spectroscopy

CD spectra of protein samples (500 µg/ml in PBS buffer) in quartz cuvettes of 2 mm path length were recorded as an average of ten scans with a Jasco J810 spectropolarimeter over a range of 200 - 300 nm on a millidegree ellipticity scale.

2.7.7 Gel Permeation Chromatography

For determination of the oligomerization state of *E. coli* HemW a gel permeation chromatography under strict anaerobic conditions using a 24 ml Superdex 200 HR 10/30 equilibrated with PBS buffer was performed. The column was calibrated using carbonic anhydrase (Mr = 29,000), bovine serum albumin (Mr = 66,200), yeast alcohol dehydrogenase (Mr = 150,000), and β-amylase (Mr = 200,000) as marker proteins. Purified protein of a concentration of 1 mg/ml was chromatographed at a flow rate of 0.25 ml/min. After GPC, collected recombinant HemW was identified by SDS-PAGE analysis and Western Blotting.

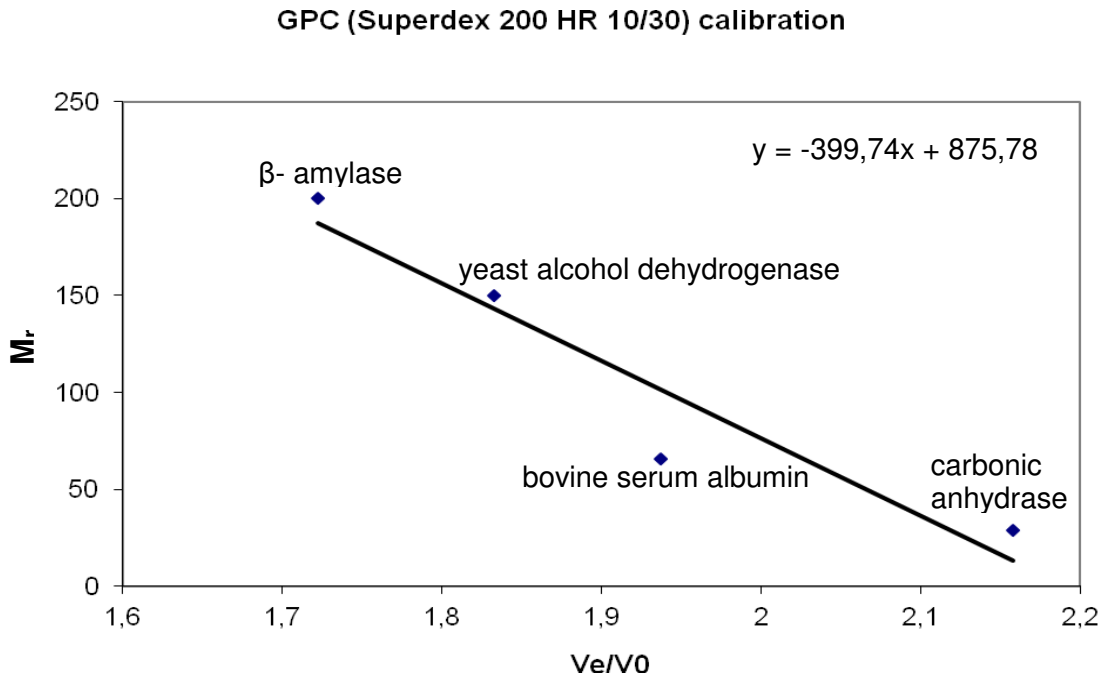

Fig. 22: GPC Superdex 200 HR 10/30 calibration curve for the determination of the oligomerization state of *E. coli* HemW.
The relative molecular mass (M_r) of the marker proteins is plotted against their elution volume (Ve) divided with the 'dead volume' (V0) of the column.

2.7.8 Discontinuous SDS Page

Proteins were analyzed by SDS-PAGE as described by Laemmli (Laemmli, 1970) with modifications by Righetti (Righetti, 1990) for discontinuous SDS-PAGE. Protein samples were denatured by heating to 95 °C for 5 min in SDS loading dye. Samples were loaded onto the gel which was run at 45 mA. During electrophoresis, proteins were first focused in the stacking gel and subsequently separated according to their relative molecular mass in the running gel. The size standard employed was Unstained Protein Molecular Weight Marker (MBI Fermentas). Gels were stained with Instant*Blue*^{TM} (Expedeon) and destained with water until the protein bands were clearly visible.

SDS Page

	running gel [12 % (v/v)]	stacking gel [6 % (v/v)]
acylamide stock solution	2.0 ml	500.0 µl
buffer for running gel	1.25 ml	-
buffer for stacking gel	-	625.0 µl
$H_2O_{deion.}$	1.75 ml	1.375 ml
APS-Solution	5.0 µl	3.0 µl
tetramethylen diamine (TEMED)	50.0 µl	30.0 µl

acrylamide stock solution: Rotiphorese® Gel 30 (37.5:1) (Roth)

APS solution:

Ammonium peroxodisulfate in H_2O_{dest}	10	%

buffer for running gel:

tris-HCl	1.5	M
SDS	0.4	% (w/v)
in H_2O_{dest}; pH 8.8		

buffer for stacking gel:

tris-HCl	0.5	M
SDS	0.4	% (w/v)
in H_2O_{dest}; pH 6.8		

electrophoresis buffer:

tris-HCl	14.5	mM
glycine	1.44	% (w/v)
SDS	1.0	% (w/v)
in H_2O_{dest}; pH 8.4		

SDS loading dye:

tris-HCl	100.0	mM
glycerol	40.0	% (v/v)
β-mercaptoethanol	10.0	% (v/v)
SDS	3.2	% (w/v)
bromphenol blue	0.2	% (w/v)
in H_2O_{dest}; pH 6.8		

Unstained protein molecular weight marker (MBI Fermentas):
(indicated are approximate relative molecular weights)

β-galactosidase, *E. coli*	166,000
bovine serum albumin, bovine plasma	66,200
ovalbumin, chicken egg white	45,000
lactate dehydrogenase, porcine muscle	35,000
restriction endonuclease *Bsp*981, *E.coli*	25,000
β-lactoglobulin, bovine milk	18,400
lysozyme, chicken egg white	14,400

2.7.9 Heme Stain

To confirm *E. coli* HemW is a heme containing protein, the peroxidase activity has been determined. All heme proteins possess peroxidase activity under mild acidic conditions. (Hrycay, 1971). When supplied with exogenous H_2O_2, peroxidase activity catalyzes the oxidation of tetramethylbenzidine (TMB). In acidic conditions this leads to the formation of a TMB cation free radical in equilibrium with a charge-transfer complex of the parent diamine and product diimine, responsible for a blue-green color (Josephy, 1982).

Proteins separated by SDS Page were stained in fresh heme-stain solution for 1h on ice in the dark (modification from Thomas, 1976). Five to 15 min after addition of 2 % H_2O_2 heme proteins were visible by blue-green coloration.

Heme-stain solution:

Sodium acetate, pH 5.0	250	mM
tetramethylbenzidine	0.25	% (w/v)
methanol	25.	% (v/v)

2.7.10 Western Blotting

For further analysis proteins separated during SDS-PAGE were transferred onto a polyvinylidenfluorid (PVDF) membrane, to make them accessible to antibody detection. Hydrophobic and charged interactions between the membrane and protein are responsible for protein binding.

Preparatory, the PVDF membrane was incubated for 10 min in methanol and, simultaneously to the SDS gel and blotting paper, incubated in transfer buffer. Afterwards the different components were assembled in following order in the blotting apparatus: cathode, blotting paper, SDS gel, PVDF membrane, blotting paper, anode (Fig. 23). Proteins were blottet on the membrane by applying a current of 0.8 mA/cm^2 for 30 - 45 min at 10 V. Nonspecific binding sites of the membrane were saturated over night in blocking solution at 4 °C and slight shaking.

Fig. 23: Schematics of a western blotting apparatus.

Primary antibodies were directed against GST or His-tag, secondary antibodies were directed against the primary antibody and were coupled to an alkaline phosphatase. Incubation with the primary antibody was carried out in blocking solution for 1 h at RT and slight shaking. Following three wash steps for 10 min with washing-buffer, the membrane was incubated for 45 min with the secondary antibody. Four additional washing steps with PBS/Tween buffer for 10 min followed before the membrane was incubated for 5 min in alkaline phosphatase buffer and exposed to staining solution until bands became visible. During exposure alkaline phosphatase, the enzyme bound to the antibody, catalyzes the reaction of 5-bromo-4-chloro-3-indolylphosphate (BCIP) with nitroblue-tetrazolium (NBT).

transfer buffer:

tris-HCl	25.0	mM
glycine	192.0	mM
methanol	20.0	% (v/v)
in H_2O_{dest}; pH 8.5		

blocking solution:

Skim milk powder	5.0	% (w/v)
Tween 20	0.1	% (v/v)
PBS	10.0	% (v/v)
in H_2O_{dest}		

washing solution:

Skim milk powder	0.5	% (w/v)
Tween 20	0.1	% (v/v)
PBS	10.0	% (v/v)
in H_2O_{dest}		

PBS/Tween buffer:

Tween 20	0.1	% (v/v)
PBS	10.0	% (v/v)
in H_2O_{dest}		

alkaline phosphatase buffer:

tris-HCl	100.0	mM
NaCl	100.0	mM
$MgCl_2$	5.0	mM
in H_2O_{dest}; pH 9.5		

staining solution:

NBT-solution	0.33	% (v/v)
BCIP-solution	0.33	% (v/v)
in alkaline phosphatase buffer		

NBT-solution:

nitroblue-tetrazolium	10.0	% (w/v)
dimethylenformamide (DMF)	70.0	% (v/v)
in H_2O_{dest}		

BCIP-solution:

5-bromo-4-chloro-3-indolylphosphate	5.0	% (w/v)
DMF		

2.8 Crystallization of *Escherichia coli* HemW

2.8.1 Crystallization Conditions

The crystallization of *E. coli* HemW occurred under strict anaerobic conditions (MACS MG 1000 anaerobic work station, Don Whitley Scientific, Lähden-Holte, Germany), using the vapor diffusion method. This type of method allows for slow and controlled growth of protein crystals. A variety of salts, buffers and precipitants were used, included in the Qiagen cryos suite (Hilden, Germany). The crystallizations were performed in 96-well sitting drop CrystalClear strip racks (Greiner bio-one, Frickenhausen, Germany) with 100 µl reservoir solution. For protein crystallization, 1.5 µl protein solution was mixed with 1.5 ml reservoir solution. Prior to mixing 150 µM DTT was added to the protein solution. The used protein concentration was between 117 mM and 235 mM (5 mg/ml - 10 mg/ml).

2.9 Electron Paramagnetic Resonance (EPR)

Electron paramagnetic resonance spectroscopy is a method for studying samples that have one or more unpaired electrons, like radicals. It is based on the splitting of the energy level of an electron in the outer magnetic field (Zeeman, 1896).

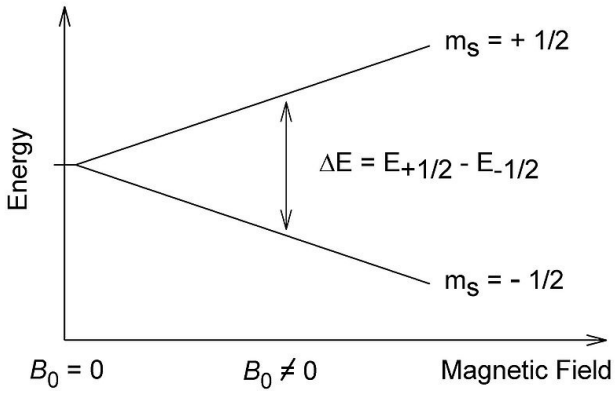

Fig. 24: Splitting of electron spin states.
(http://en.wikipedia.org/wiki/File:EPR_splitting.jpg)

B_0	magnetic field strength
m_S = + ½	upper energy state, antiparallel alignment of the electrons magnetic moment to the field
m_S = - ½	lower energy state, parallel alignment of the electrons magnetic moment to the field
ΔE	energy distance between upper and lower energy state

The splitting of the energy levels is directly proportional to the magnetic fields strength (Fig. 24). In theory a paramagnetic molecule is brought into the outer magnetic field and irradiated with microwaves. Exact correlation of the photon energy with the energy distance of the energy levels results in the biggest effect. At this point the unpaired electrons can move between their two spin states. From the photon frequency, the energy levels of the atom can be determined.

The incubation of 150 µM HemW with equimolar hemin, as well as 80 µM HemW with equimolar Fe^{3+} corrole was carried out over night under strict anaerobic conditions, without prior reduction by dithionate. The samples were transferred into 4 mm EPR tubes, cooled to 4 K and measured by a frequence of 9.2399 GHz using a Bruker Spin R ESP 300 E instrument.

3 RESULTS AND DISCUSSION

This work investigated heme transport and insertion into target proteins by two different ways. First, interaction partners of the last enzyme of heme biosynthesis, ferrochelatase, the heme containing protein bacterioferritin A and of the hemoprotein catalase A were searched via genetic screens. Secondly, based on the findings for the *L. lactis* heme chaperone HemW, *E. coli* HemW was biochemically characterized.

3.1 Determination of Hemoprotein-Protein Interactions

In order to test the hypothesis of BfrA being a heme chaperone, the *P. aeruginosa* genes encoding ferrochelatase (*hemH*), catalase A (*katA*) und bacterioferritin (*bfrA*) were cloned into the corresponding screening vectors (see 2.6). The ferrochelatase HemH is known to catalyze the last step of heme biosynthesis by inserting iron into PPIX to generate heme *b* (Dailey, 2002). It is a plausible candidate for the docking of heme transporting proteins. KatA contains a heme *b* cofactor (Switala and Loewen, 2002) and is the major catalase detected in all phases of growth, responsible for H_2O_2 decomposition (Brown *et al*., 1995; Hassett *et al*., 1992). Consequently, KatA is a heme *b* accepting protein, either directly from ferrochelatase or from a potential heme chaperone.

BfrA consists of 24 subunits able to bind 700 iron atoms (Moore *et al*., 1994). It was also shown to bind 3 to 9 heme groups *in vivo* and up to 24 heme groups *in vitro* (Kadir and Moore, 1990). In 1999, Hassett and coworkers reported that KatA requires BfrA for full activity, proposing that BfrA stores iron that is incorporated into heme the necessary prosthetic group for KatA activity. BfrA is a heme accepting protein also potentially interacting with HemH. In addition it might serve as a heme chaperone for KatA.

To test for potential interactions between HemH, KatA and BfrA a bacterial two hybrid system based on *P. aeruginosa* was employed. Furthermore, a *P. aeruginosa* genomic library was screened for interaction partners of the three proteins.

3.1.1 Vectors for the bacterial tow hybrid system studies

The Bacterial Adenylate Cyclase Two Hybrid System (BACTH) is based on the protein-protein interaction mediated reconstitution of the bacterial adenylate cyclase from *B. pertussis*.

The catalytic domain of adenylate cyclase includes the first 400 amino acids and is composed of two complementary parts, the T18- and T25-fragment. Upon physical separation these fragments alone show no cyclase activity. Only the fused interacting protein-fragments mediate reconstitution of adenylate cyclase and onset of the cAMP pathway. Interaction of both fragments can be achieved by two strongly interacting proteins fused to the T18- and T25-fragments. Consequently, one can search for unknown protein-protein interaction *via* fusion of the known interaction partner to one of the fragments. The resulting reconstituted cAMP pathway allows for the selection of maltose metabolization.

Therefore, the genes *hemH*, *katA* and *bfrA* were amplified from *P. aeruginosa* chromosomal DNA with restriction sites required for cloning as described in MATERIAL AND METHODS. Afterwards the digested and purified genes were cloned into their respective screening vectors, encoding the N- or C-terminal fused adenylatecyclase fragment (Fig. 25). The *P. aeruginosa* DNA library constructed in a pUT18C vector was recently created by Andrea Wesche in our institute (Wesche, 2008). The average insert size of the library was around 700 bp and the genome coverage was over 90 %.

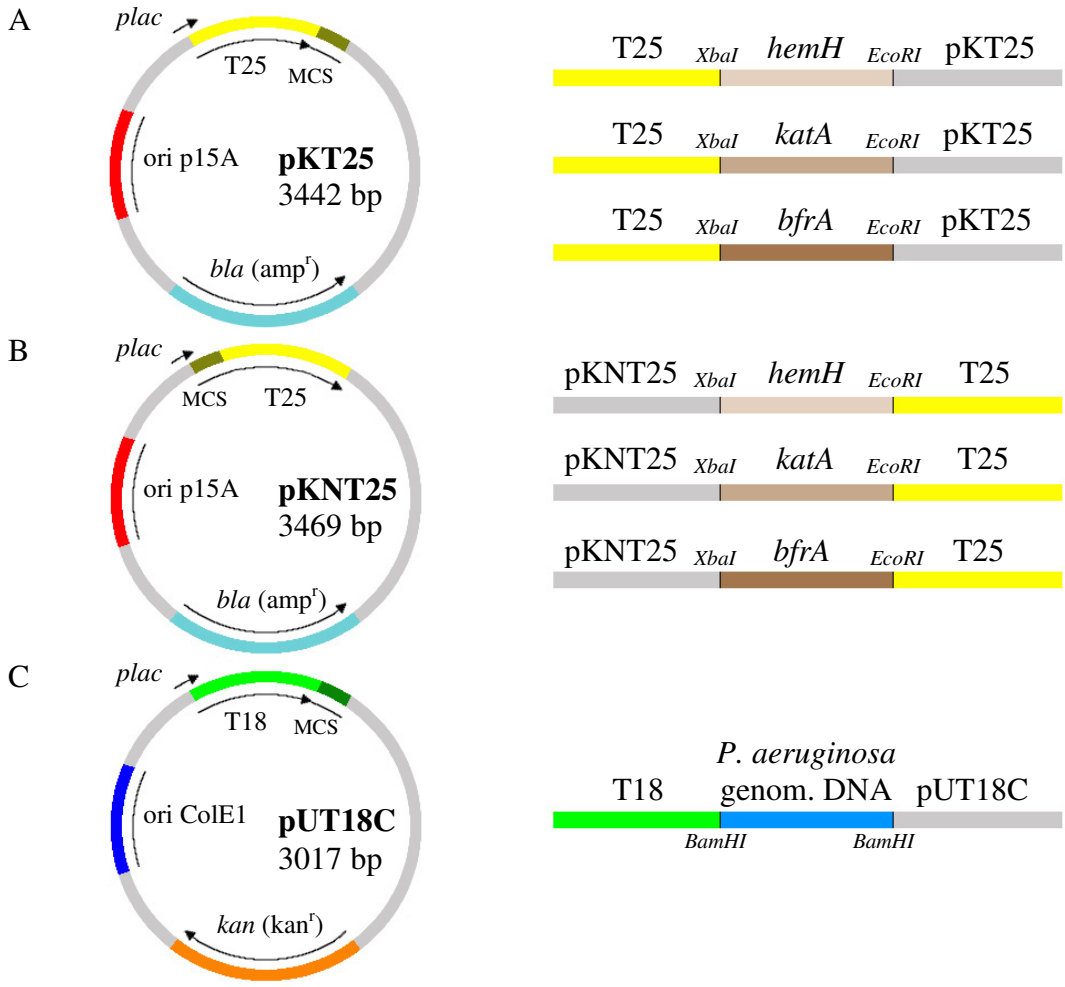

Fig. 25: Method for the construction of vectors for protein-protein interaction studies.
A: On the left the vector map of pKT25 is depicted. The ampicillin resistance gene (*bla*) is shown in light blue, the origin of replication p15A is shown in red, the DNA for the T25 fragment is shown in yellow and the C-terminally adjacent multiple cloning site (MCS) is depicted in olive. The *lac* promoter (*plac*) is indicated. The right side shows a section of the completed vectors for protein-protein interaction studies. The DNA for the T25 fragment is shown in yellow, the bait genes *hemH*, *katA* and *bfrA* are shown in brown with increasing intensities and pKT25 is depicted in grey. The restriction sites for the endonucleases *XbaI* and *EcoRI* are indicated. B: On the left the vector map of pKNT25 is depicted. The ampicillin resistance gene (*bla*) is shown in light blue, origin of replication p15A is shown in red, the DNA for the T25 fragment is shown in yellow and the N-terminally adjacent MCS is depicted in olive. The *lac* promoter (*plac*) is indicated. The right side shows a section of the completed vectors for protein-protein interaction studies. The DNA for the T25 fragment is shown in yellow, the bait genes *hemH*, *katA* and *bfrA* are shown in brown with increasing intensities and pKT25 is depicted in grey. The restriction sites for the endonucleases *XbaI* and *EcoRI* are indicated. C: On the left the vector map of pUT18C is depicted. The kanamycin resistance gene (*kan*) is shown in orange, origin of replication ColE1 modified is shown in dark blue, the DNA for the T18 fragment is shown in green and the C-terminally adjacent MCS is depicted in dark green. The *lac* promoter (*plac*) is indicated. The right side shows a section of the completed vectors for protein-protein interaction studies. The DNA for the T18 fragment is shown in green, the variable prey gene of *P. aeruginosa* is shown in blue and pUT18C is depicted in grey. The restriction sites for *BamHI* are indicated. (Karimova, 1998)

3.1.2 Investigation of protein-protein interaction between *Pseudomonas aeruginosa* HemH, KatA and BfrA

To investigate whether *P. aeruginosa* HemH, KatA and BfrA interact directly with each other, co-transformations of bait and prey vectors were carried out under standard conditions as described under 2.6.1. The results are shown in table 10.

Tab. 10: Occurrence of interaction between *P. aeruginosa* HemH, KatA and BfrA.
The vectors pUT18C-zip and pKT25-zip in which the leucine zipper of the yeast protein GCN4 is genetically fused in frame to the T18- or T25 fragment coding DNA were acting as positive control. The geneless pUT18C and pKT25 vectors were deployed as negative control.

	interaction							
vector	pUT18 *-hemH*	pUT18 *-katA*	pUT18 *-bfrA*	pUT18C *-hemH*	pUT18C *-katA*	pUT18C *-bfrA*	pUT18C *-zip*	pUT18C
pKT25-*hemH*	n.d.	-	-	n.d.	-	-	n.d.	n.d.
pKT25-*katA*	-	n.d.	-	-	n.d.	-	n.d.	n.d.
pKT25-*bfrA*	-	-	n.d.	-	-	n.d.	n.d.	n.d.
pKNT25-*hemH*	n.d.	-	-	n.d.	-	-	n.d.	n.d.
pKNT25-*katA*	-	n.d.	-	-	n.d.	-	n.d.	n.d.
pKNT25-*bfrA*	-	-	n.d.	-	-	n.d.	n.d.	n.d.
pKT25-*zip*	n.d.	n.d.	n.d.	n.d.	n.d.	n.d.	+	n.d.
pKT25	n.d.	n.d.	n.d.	n.d.	n.d.	n.d.	n.d.	-

+ = detected interaction, - = no detected interaction, n.d. = not determined.

No direct interaction between *P. aeruginosa* HemH, KatA and BfrA could be shown *via* the BACTH System. Therefore, there is no indication of BfrA acting as a heme chaperone in the transport of heme from HemH to KatA. There is still the possibility of BfrA being part of the cytoplasmic heme transport process, but obviously not *via* interaction with HemH or KatA. It is also possible that the sole role of BfrA is one of an iron storage protein. Now, the further approach was the identification of alternative putative heme transporting proteins by screening of a *P. aeruginosa* DNA library with the known hemoproteins HemH, KatA and BfrA.

3.1.3 Identification of interaction partners of *Pseudomonas aeruginosa* HemH, KatA and BfrA using the Bacterial Adenylate Cyclase Two Hybrid System

The screens with HemH, KatA and BfrA acting as bait in the described bacterial two hybrid system were carried out under standard conditions as stated under 2.6.1. After up to one week positive clones were identified due to their ability to form blue colonies as a result of the conversion of X-gal to 5,5‘-dibromo-4,4‘-dichloro-indigo by β-galactosidase (Fig. 26).

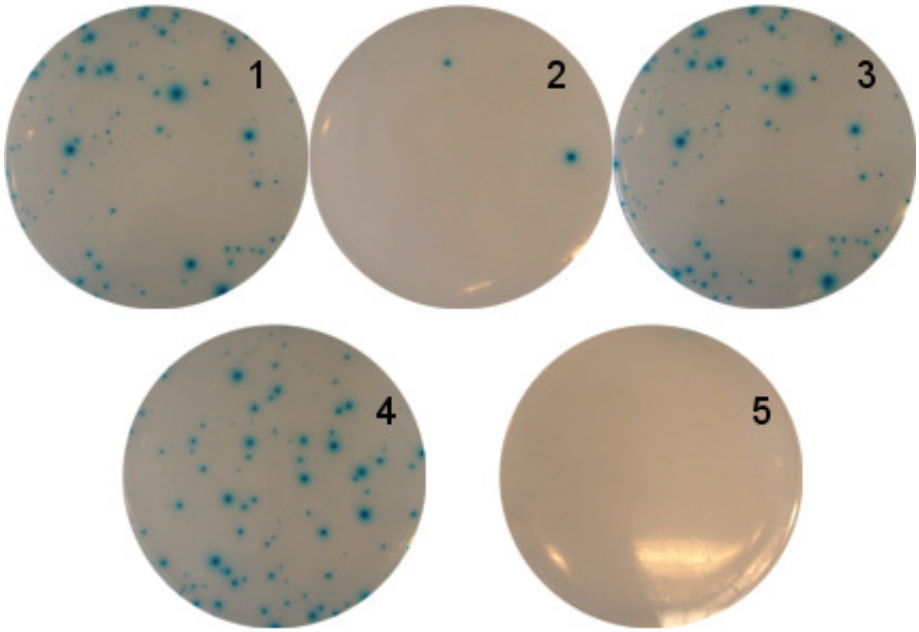

Fig. 26: Detection of interaction partners of *P. aeruginosa* HemH, KatA and BfrA *via* BACTH. Examples of agar plates obtained after a BACTH screen, shown for a screen with HemH (1), KatA (2) and BfrA (3) with the pKT25 vector on M63 medium, respectively. 4: positive control, 5: negative control. Screens conducted with HemH and BfrA as bait showed good growth of positive (blue) colonies, comparable to the positive control. The screen with KatA showed very weak growth, indicating a weak interaction. The negative control showed no growth as expected.

To minimize the chance of false positives the clones were streaked on M36 plates twice consecutively. From the so obtained monocultures the plasmids were derived by preparation (see 2.5.2) and their DNA sequenced (2.5.9). For the HemH screens of the *P. aeruginosa* library 26 clones were found which showed interaction and where the corresponding genes were in the correct reading frame. For KatA and BfrA only two clones with appropriate reading frames were detected. That was expected for KatA, since it already showed low interaction activity in all executed screens.

Table 11 gives an overview of the amount of clones during single steps of the screen.

Tab. 11: Amount of clones showing interaction properties during different steps of the *P. aeruginosa* library screen.
Shown is the merged amount of clones from different screens. The total amount of clones is compared to the amount putative interaction partners after second streaking on M63 media and sequence analysis.

vector	Total amount	2 x M36	in-frame
pKT25-*hemH*	194	96	26
pKNT25-*hemH*	7	-	-
pKT25-*katA*	23	19	2
pKNT25-*katA*	3	1	-
pKT25-*bfrA*	35	25	2
pKNT25-*bfrA*	46	5	-

Interacting clones with in-frame fusions at the C-terminal end of the T25 polypeptide were the only ones detected. Subsequently, the identified putative proteins were analyzed for their potential functions, using the Clusters of Orthologous Groups (COGs) from www.pseudomonas.com. COGs is based on the Reversed Position Specific Blast (RPSBLAST; blast version 2.2.10). Data to all probable interactions partners of HemH, KatA and BfrA are to be found in the Appendices (Tab. 15).

Since no satisfying results could be obtained with regard to *P. aeruginosa* KatA and BfrA, further analyses were focused on HemH. Several detected interaction partners of HemH deserved closer attention, either because they were detected multiple times during the screen or they showed very good sequence coverage and identity to their homolog genes. Table 12 gives an overview of these proteins.

To rule out unspecific interactions mediated by the plasmids pKT25-*hemH* and pUT18C, as well as pUT18C-*hemH* and pKT25; they were co-transformed and tested. No interaction between the protein components encoded by the respective plasmids could be detected, excluding background reactivity.

Interestingly, PA1442 was detected twice as HemH interaction partner. It encodes a conserved hypothetical protein, predicted as flagellar basal body-associated protein belonging to the FliL superfamily (Marchler-Bauer *et al*., 2011). It is typically a cytoplasmic membrane protein associated with the basal body of the flagella. For the trypanosome *Leishmania* it was reported that hemoglobin endocytosis is mediated through a hemoglobin receptor present in the flagellar pocket, probably to generate intracellular heme (Krishnamurthy *et al.*, 2004). Currently, this sort of heme acquisition is only known from trypanosomatids. However, *P. aeruginosa* is also known to utilize external heme. Since FliL is predicted to be a transmembrane spanning protein with the

C-terminus located in the periplasm and the N-terminus in the cytoplasm (Attmannspacher *et al*., 2008; Suaste-Olmos *et al*., 2010) it could be involved in heme transport to HemH.

Tab. 12: Characterization of detected interaction partners of *P. aeruginosa* HemH on protein level.

clone	length of homolog protein [aa]	Coverage of the homolog protein by the interacting protein fragment [aa]	Identity [%]	homolog gene	potential function
pKT25-hemH					
1.1	173	42 – 117	86	PA1442	hypothetical flagellar basal body-associated protein, fliL
1.24	173	42 – 117	86	PA1442	
1.9	250	63 – 250	90	PA3851	Uncharacterized membrane protein, CCC1-like
2.49	250	91 – 190	99	PA3851	
2.147	250	63 – 92	76	PA3851	
2.36	212	1 – 181	84	PA0885	probable C4-dicarboxylate transporter, dctQ
2.53	212	1 – 112	100	PA0885	
2.82	212	1 – 181	84	PA0885	
1.19	81	1 – 81	100	PA0738	conserved hypothetical protein
2.128	117	1 – 117	100	PA0563	

PA0885 was detected thrice. It encodes a probable TRAP-type (Tripartite ATP-independent periplasmic) C4-dicarboxylate transporter DctQ, involved in aerobic carbohydrate transport and metabolism (Marchler-Bauer *et al*., 2011; Forward *et al*., 1997). Its specific function regarding the C4-dicarboxylate transport is unknown. DctQ is a four-helix cytoplasmic membrane protein, with its C- and N-terminus predicted to be located in the cytoplasm (Wyborn *et al*., 2001). Considering this, PA0885 could be part of channeling transport processes from or to HemH.

PA0738 and PA0563 were only detected once, but showed a sequence coverage and identity of 100 %, respectively. PA0738 encodes a predicted cytoplasmic membrane protein. A BLAST search at NCBI showed homology to the DUF1145 superfamily (Marchler-Bauer *et al*., 2011), consisting of several hypothetical bacterial proteins of

unknown function. PA0563 also is a predicted cytoplasmic membrane protein, homolog to the DUF805 superfamily (Marchler-Bauer *et al*., 2011). Since both PA0738 and PA0563 are so called "domains of unknown functions" (DUF) a prediction of the nature of HemH interaction is impossible. Since both are cytoplasmic membrane proteins a role as cytoplasmic chaperone can be excluded.

The situation is similar for the three times detected PA3851, in that it is a predicted cytoplasmic membrane protein of unknown function. However, a BLAST search at NCBI showed homology to proteins of the CCC1-like superfamily (Marchler-Bauer *et al*., 2011), including proteins related to CCC1, a yeast vacuole transmembrane protein responsible for the iron and manganese transport from the cytosol into vacuoles. It also includes the proteins similar to nodulin-21, a plant nodule-specific protein that may be involved in symbiotic nitrogen fixation. All in all, PA3851 shows homology to a set of prokaryotic as well as eukaryotic proteins involved in iron and manganese transport. As a cytoplasmic membrane protein it could be part of channeling transport of iron to HemH.

To further verify these results the protein interaction mediating inserts of the pUT18C plasmids were cloned into the pKT25 plasmid and co-transformed with pUT18C-*hemH*. This way the bait and prey vectors were exchanged for the interaction partners.

For *P. aeruginosa* PA1442 no interaction with HemH was detectable. PA0885 and PA0738 showed interaction with HemH. PA3851 showed strong interaction. PA0563 could not be tested, since the cloning attempts were not successful. These results partly confirmed the results of the first round of screening.

3.1.3.1 Quantification of interaction between HemH and its newly found interaction partners

To quantify the interaction between HemH and the respective interaction partner, β- galactosidase activity was measured as described in MATERIAL AND METHODS (2.6.2). Intensity of interaction affects adenylate cyclase reconstitution and therefore cAMP levels in the cell (Ladant & Karimova, 2000). A high level of cAMP together with CAP induces the expression of β-galactosidase (Vossen *et al.*, 1996). The amount of produced β-galactosidase is proportional to interaction intensity. β-galactosidase activity was measured for HemH and its respective interaction partners.

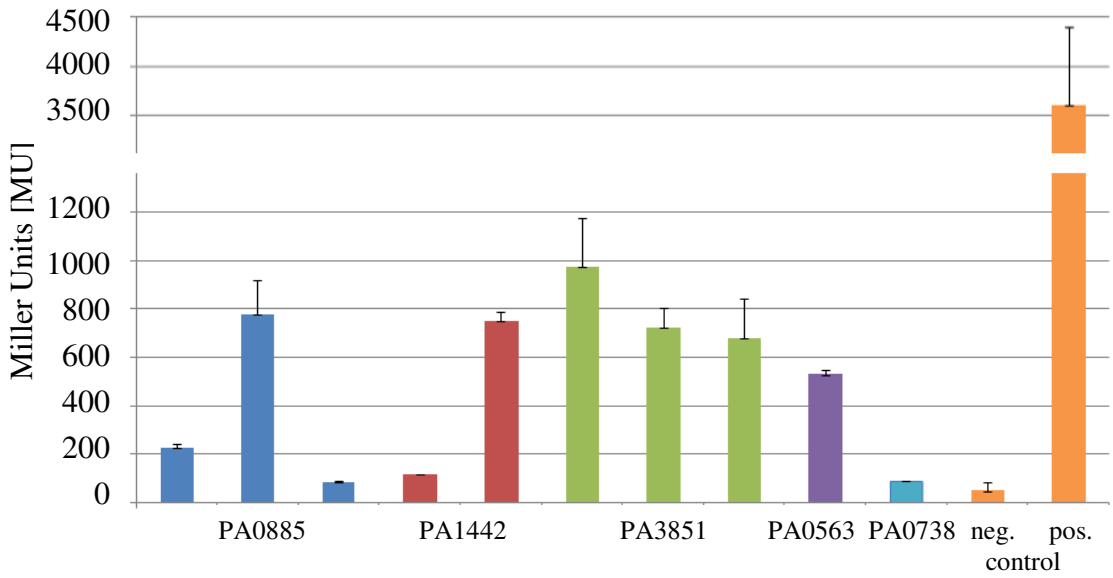

Fig. 27: Intensity of interaction for HemH and its newly found interaction partners.
Presented is the β-galactosidase activity in Miller Units [MU] resulting of the contact of HemH and its respective interaction partners PA0885, PA1442, PA3851, PA0563 and PA0738 (see table 12). As controls pKT25-zip and pUT18C-zip (positive control) as well as pKT25 and pUT18C (negative control) were measured. The bar of the positive control is truncated; the actual value is 3606.54 ± 795.55 MU.
■ PA0885, ■ PA1442, ■ PA3851, ■ PA0563, ■ PA0738 and ■ controls.

As positive control pKT25-zip und pUT18C-zip were employed, the empty vectors pKT25 and pUT18C were included as negative control. Overall, PA3851, which was detected several times as interaction partner of HemH, mediated an increased and consistent β-galactosidase activity. In figure 27, β-galactosidase activity mediated by the HemH-PA3851 contact is depicted in green (■) and was measured an average of 789 MU. PA0885 and PA1442 interaction lead to inconsistent β-galactosidase activity. PA0885 depicted in blue (■) mediated low β-galactosidase activity for two clones, with an average of 154 MU, while one clone showed an elevated activity with 776 MU. The red bars (■) represent the results obtained for HemH-PA1442 interaction. The two clones lead to an average β-galactosidase activity of 118 Mu and 751 MU, respectively. From the nonrecurring interaction partners the β-galactosidase activity from PA0563-HemH interaction shown in purple (■), was increased with 529 MU, while PA0738 (■) lead to very low activity with an average of 88 MU. As mentioned above PA056 was described as a so far uncharacterized protein of unknown function.

PA3851 is a membrane protein with homology to iron and manganese transporters. HemH is responsible for iron inserting in protoporphyrin IX, thus mediating the formation of heme. In considerations of these facts PA3851 could be an iron transporter responsible for channeling iron to HemH. To verify this hypothesis, a *P. aeruginosa* PA3851 knock-out mutant was constructed and characterized.

3.1.4 Gene Deletion of the chromosomal copy *Pseudomonas aeruginosa* gene PA3851 – a potential iron transport protein

A *P. aeruginosa* ΔPA3851 knock-out mutant was constructed as described in MATERIALS AND METHODS (2.5.10). The method developed by Schweizer and coworkers in 1998, is based on the replacement of the target gene by a gentamycin resistance gene next to a green fluorescent protein (GFP) gene. Both markers are flanked by FLP recombinase target sites, to allow subsequent generation of an unmarked ΔPA3851 mutant (Fig. 28).

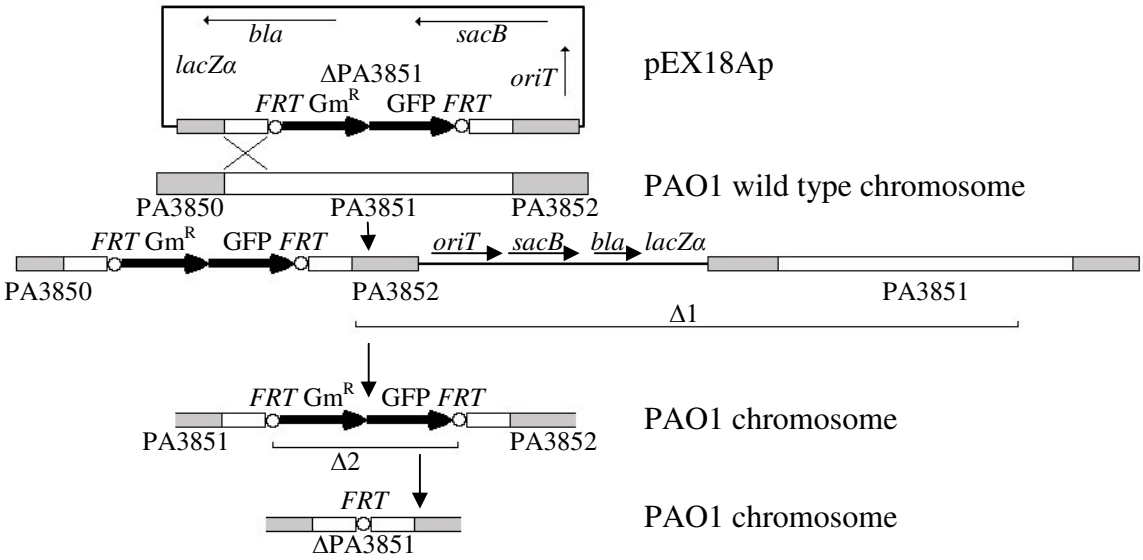

Fig. 28: Strategy for construction of the *P. aeruginosa* ΔPA3851 mutation. (Hoang *et al*., 1998)
A gentamicin cassette and the GFP gene were cloned interjacent of two DNA fragments homologous to the up- and downstream regions of the target gene PA3851 into the MCS of the suicide vector pEX18Ap. The vector was transferred into *P. aeruginosa* PAO1 per diparental mating. Selection followed by plating the cells on LB plates containing gentamicin. The gentamicin cassette is integrated into the genome through homologous recombination between upstream and downstream region of the target gene. A single crossover event leads to integration of the plasmid (Δ1). To ensure that the strain carries the required double crossover (Δ2) the cells were plated on agar plates containing 5 % (w/v) sucrose and gentamicin. The *sacB* gene encoding for levansucrase on vector pEX18Ap produces a toxic polysaccharide from sucrose which allows for selection. Afterwards, the Gm^R-GFP integrant was removed by FLP catalyzed excision.

The FLP-Gm^R-GFP-FLP construct was excised from the plasmid pPS858. It was placed into the suicide vector pEX18Ap, between chromosomal regions flanking PA3851 on the *P. aeruginosa* PAO1 chromosome. The flanking regions were amplified using the primers KOPA3850for and KOPA3851rev amplifying 550 bp upstream of PA3850, and the primers KOPA3852for and KOPA3852rev amplifying 480 bp downstream of

PA3851. The products were digested (2.5.8.1) and purified (2.5.7.3) as described in MATERIAL AND METHODS.

Plasmid pEX18Ap (Fig. 28) contains the gene *sacB* encoding for a levansucrase. Addition of sucrose to the growth medium leads to a toxic synthesis product, which allows for elimination of the plasmid. Furthermore, pEX18Ap contains the *lacZα* allel, allowing for blue-white screening on X-Gal containing medium, the *bla* gene encoding the TEM-1 β-lactamase, an ampicillin resistance marker and an *oriT* for conjugation-mediated plasmid transfer. *E. coli* ST18 was transformed with pEX18AP containing the desired construct. *E. coli* ST18 is 5-aminolevulinic acid deficient and thus can only grow with the addition of ALA to the medium. After selection for ampicillin resistance diparental mating with *P. aeruginosa* PAO1 took place. Successful transformation of pEX18Ap into *P. aeruginosa* PAO1 lead to gentamycin resistance and a single crossover event (Fig. 28). Loss of *E. coli* ST18 was promoted by the omission of ALA from the medium. The addition of sucrose to the medium should lead to the elimination of the helper plasmid pEX18Ap and select for cells having undergone a double crossover. The target gene PA3851 should be replaced by the FLP-GM^R-GFP-FLP construct. Confirmation of this step was conducted by PCR amplification of the chromosomal region. To excise the GM^R-GFP markers, the plasmid pFLP2 was transferred into *P. aeruginosa* PAO1 ΔPA3851 *via* mating. Plasmid pFLP2 contained a FLP-expressing cassette and a *sacB* marker. After excision of the GM^R-GFP markers the plasmid was curable from its host by $sucrose^R$ selection. Final investigations indicated the presence of a single crossover event despite various trials and modifications of the protocol. Nevertheless, it was investigated whether this *P. aeruginosa* PA3851 mutant showed growth defects in respect of iron conditions.

P. aeruginosa possesses a series of iron transporters like the two siderophores, pyochelin and pyoverdine, as well as a number of heterologous siderophores of fungal and bacterial origin and its genome is rich with homologues of iron-siderophore receptor genes (Poole and McKaye, 2003). It is plausible that the shortfall of one transporter is counterbalanced by another transporter, acting as back-up system. Therefore, it was important to choose conditions to limit the active iron transport systems in *P. aeruginosa*.

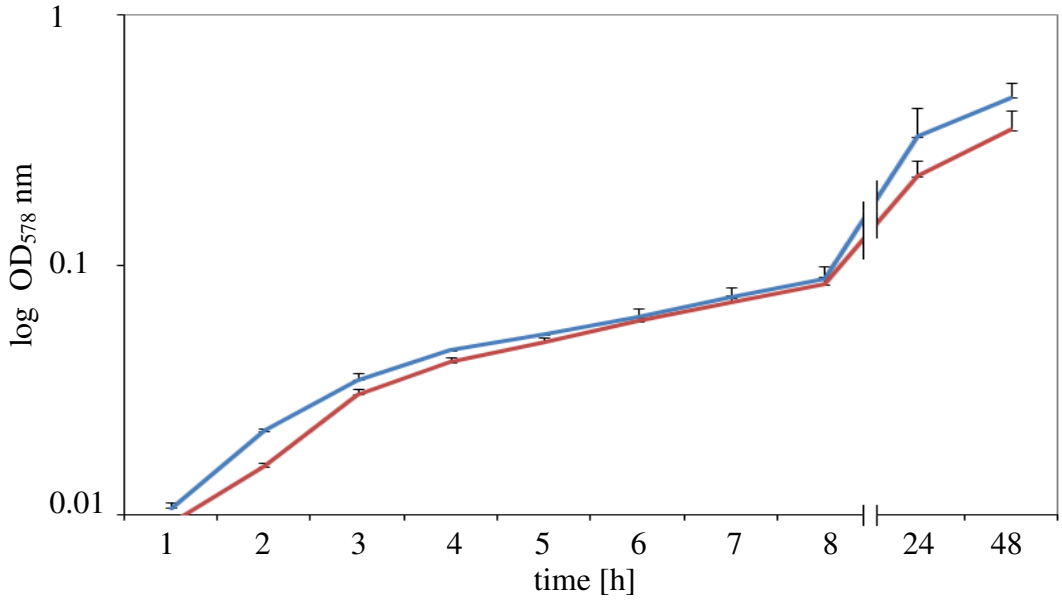

Fig. 29: Comparison of the growth under aerobic conditions at 42 °C of *P. aeruginosa* wild type and the PA3851 mutant.
Cells were grown at 42 °C in M9 medium containing 1.8 µM $FeSO_4$ and no antibiotics. Values for each strain are averages of three parallel cultures. — wild type *P. aeruginosa* PA01, — *P. aeruginosa* PA3851 mutant.

Comparative growth experiments were performed at 42 °C in M63 medium (2.3.1) supplemented with iron. *P. aeruginosa* was reported to fail pyoverdine synthesis at this temperature (Poole *et al.*, 1991), which means one main siderophore is inactive. Wild type *P. aeruginosa* PA01 and the PA3851 mutant showed no significant growth differences (Fig. 29). The same was true for growth experiments that differed in temperature and growth media (shown in figures 30 to 35).

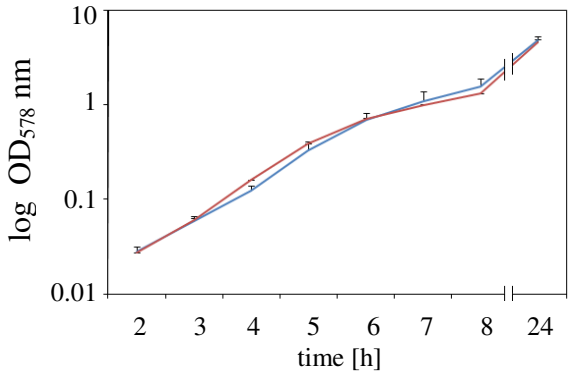

Fig. 30: Comparison of the growth under aerobic conditions at 30 °C of *P. aeruginosa* wild type and the PA3851 mutant in LB medium.
Cells were grown at 30 °C in LB medium containing no antibiotics. Values for each strain are averages of three parallel cultures. — wild type *P. aeruginosa* PA01, — *P. aeruginosa* PA3851 mutant.

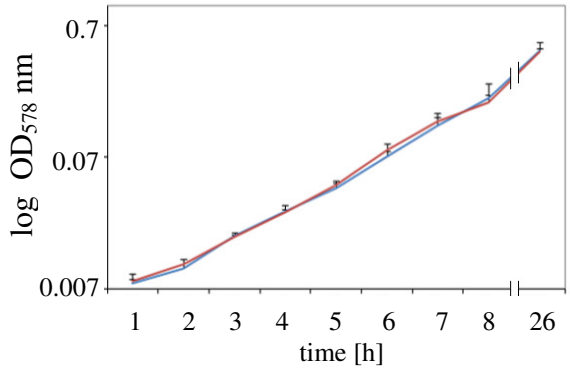

Fig. 31: Comparison of the growth under aerobic conditions at 30 °C of *P. aeruginosa* wild type and the PA3851 mutant in M9 medium.
Cells were grown at 30 °C in M9 medium containing no antibiotics. Values for each strain are averages of three parallel cultures. — wild type *P. aeruginosa* PA01, — *P. aeruginosa* PA3851 mutant.

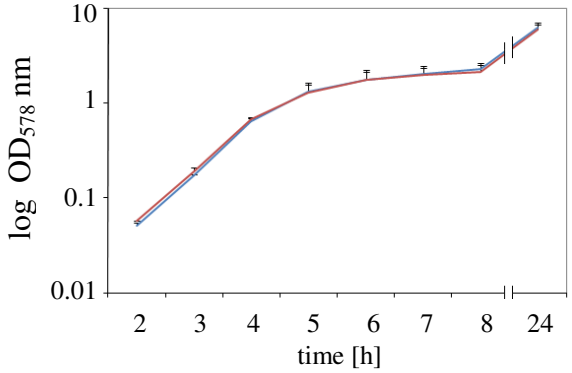

Fig. 32: Comparison of the growth under aerobic conditions at 37 °C of *P. aeruginosa* wild type and the PA3851 mutant in LB medium.
Cells were grown at 37 °C in LB medium containing no antibiotics. Values for each strain are averages of three parallel cultures. — wild type *P. aeruginosa* PA01, — *P. aeruginosa* PA3851 mutant.

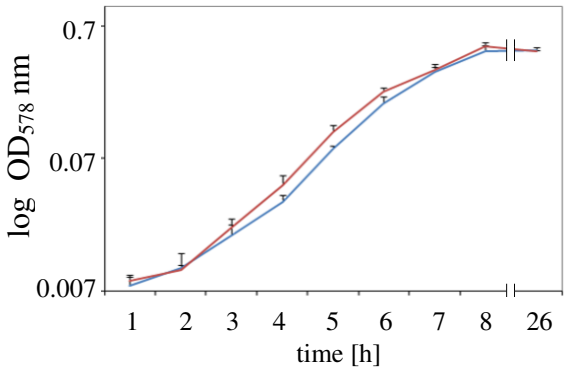

Fig. 33: Comparison of the growth under aerobic conditions at 37 °C of *P. aeruginosa* wild type and the PA3851 mutant in M9 medium.
Cells were grown at 37 °C in M9 medium containing no antibiotics. Values for each strain are averages of three parallel cultures. — wild type *P. aeruginosa* PA01, — *P. aeruginosa* PA3851 mutant.

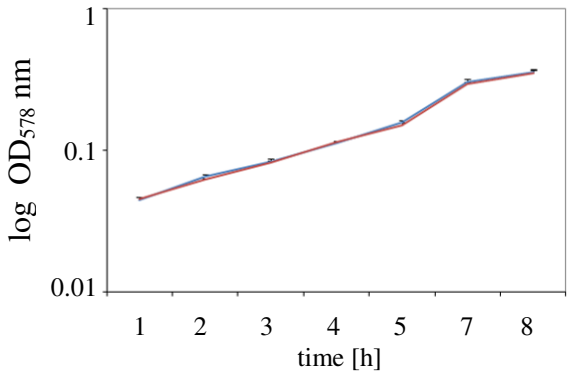

Fig. 34: Comparison of the growth under aerobic conditions at 42 °C of *P. aeruginosa* wild type and the PA3851 mutant in LB medium.
Cells were grown at 42 °C in LB medium containing no antibiotics. Values for each strain are averages of three parallel cultures. — wild type *P. aeruginosa* PA01, — *P. aeruginosa* PA3851 mutant.

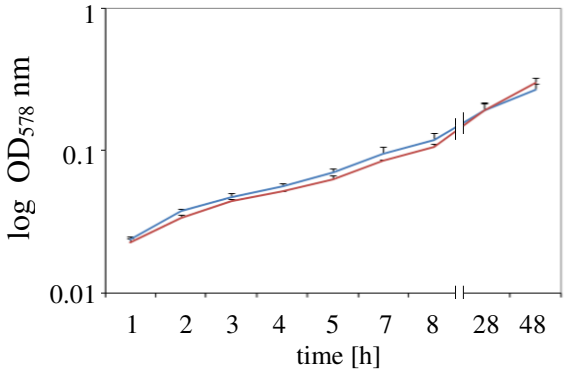

Fig. 35: Comparison of the growth under aerobic conditions at 42 °C of *P. aeruginosa* wild type and the PA3851 mutant in M9 medium.
Cells were grown at 42 °C in M9 medium containing no antibiotics. Values for each strain are averages of three parallel cultures. — wild type *P. aeruginosa* PA01, — *P. aeruginosa* PA3851 mutant.

No significant growth difference was observed in nutritionally rich LB medium at temperatures of 30 °C (Fig. 30), 37 °C (Fig. 32) and 42 °C (Fig. 34) between wild type *P. aeruginosa* PA01 and the PA3851 mutant. The same was true for cultures grown in minimal medium M9 at 30 °C (Fig. 31), 37 °C (Fig. 33) and 42 °C (Fig. 35). The reasons for this could be the mutant itself, as it is only a single crossover mutant. Another reason could be that *P. aeruginosa* most likely has at least one if not more iron transporter covering the deficiency.

3.1.5 Conclusion of the protein-protein interaction studies

The original working hypothesis for the search of unknown heme chaperones in bacteria relied on the search for interaction partners of the last enzyme of heme biosynthesis, the ferrochelatase HemH. Moreover, proteins contacting the heme *b* containing target enzyme catalase A KatA were searched. One potential candidate was the heme binding bacterioferritin BfrA. None of the outlined proteins were found interacting with each other in a bacterial two hybrid system. The gene library screen for interaction partners of the three proteins revealed various membrane proteins with potential transport functions interacting with HemH. These novel candidates require further characterization to unravel their physiological function.

3.2 The *Escherichia coli* Heme Chaperone HemW

The aim of this work was to biochemically characterize the *E. coli* heme chaperone HemW. *E. coli* HemW was chosen because preliminary tests by the Solioz and our group (Abicht *et al*., 2012) showed that the *L. lactis* HemW might be a heme chaperone (see 1.1.4). In studies concerning the maturation of cytochrome *bd* in *L. lactis* it was found that HemW (previously annotated as coproporphyrinogen III dehydrogenase – HemN) is involved in heme transport. First, the potential role of HemW as coproporphyrinogen III dehydrogenase was analyzed. Abbicht *et al.* showed that *L. lactis* HemW was not able to functionally complement an *E. coli* Δ*hemN* mutant. On the other hand it was possible to functionally complement a *L. lactis* Δ*hemW* mutant with *E. coli* HemW. They could show that a *L. lactis* Δ*hemW* mutant was unable to respire upon heme supplementation. The added heme accumulated as free heme in the membranes, the place where cytochrome *bd* maturation normally would occur. The presence of an iron-sulfur cluster in *L. lactis* HemW was initially observed, as well as the binding of heme to HemW *in vitro* and *in vivo*. While the iron-sulfur cluster was not required for heme binding, it was reported to be required for dimerization. Finally, in a NADH-dependent process, the transfer of heme from *L. lactis* HemW to a membrane localized target could be shown. Together these results support the presumption of HemW being a heme transporter, incorporating heme in cytochrome *bd*.

Dr. Katrin Grage from our Institute studied the role of *E. coli* HemW as potential CPDH in more detail (Grage, 2005). She tested *E. coli* HemW as well as *B. subtilis* HemW1 and HemW2 (in her work all referred to as HemN and HemZ), with regard to their CPDH activity. She could exclude *in vitro* CPDH enzyme activity for the tested recombinant and purified HemWs. None of the genes complemented an *E. coli* Δ*hemN* mutant or *S. typhimurium hemN/hemF* double mutant. This further supports the hypothesis that *E. coli* HemW is no CPDH and might be involved in heme transfer.

3.2.1 Purification of *Escherichia coli* HemW

The *E. coli hemW* gene consists of 1134 bp and was cloned into the pGEX-6p-1 high-level expression vector, resulting in the plasmid pGEX-*hemW* (Grage, 2005). The protein was produced in *E. coli* BL21(DE3) and purified to apparent homogeneity under anaerobic conditions. Purification was achieved in a single chromatographic step using Glutathione-Sepharose chromatography. The fusion protein consisting of HemW and the N-terminal GST-tag was isolated. After PreScission™ Protease cleavage of the HemW fusion protein, recombinant HemW was separated from the still bound GST-tag and the GSTtagged protease. Fig. 36 provides documentation of the purification procedure.

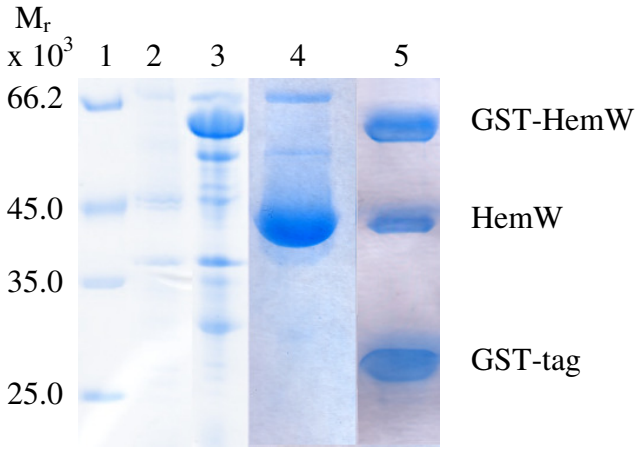

Fig. 36: **Production and purification of recombinant *E. coli* HemW.**
Proteins were separated by 12 % SDS PAGE and visualized by staining with Instant*Blue*™. Lane 1: molecular weight marker, lane 2 and 3: *E. coli* BL21(DE3) cell carrying pGEX-*hemW* before (lane 2) and after (lane 3) induction with 0.5 mM IPTG, lane 4: pure recombinant HemW, lane 5: eluate from the Glutathion Sepharose column with cleaved GST-tag.

SDS PAGE analysis of the purified protein (lane 4 in Fig. 36) revealed a major band corresponding to a protein with a relative molecular mass of about 40,000, which is in good agreement with the calculated molecular mass of 42.584 kDa. About 15 mg of purified recombinant HemW were obtained per liter cell culture.

3.2.2 Exchange of the N-terminal region and introduction of cysteine 25 do not convert *E. coli* HemW into a coproporphyrinogen III dehydrogenase (HemN)

E. coli HemN and HemW differ in two main points (Fig. 37). One are the extra N-terminal residues of HemN. These residues were proposed to be crucial for substrate binding (Layer *et al*., 2003). Even though lacking the 46 extra residues of the N-terminus, HemW still possesses the conserved cysteine motive CxxxCxxC, however very close to the N-terminus.

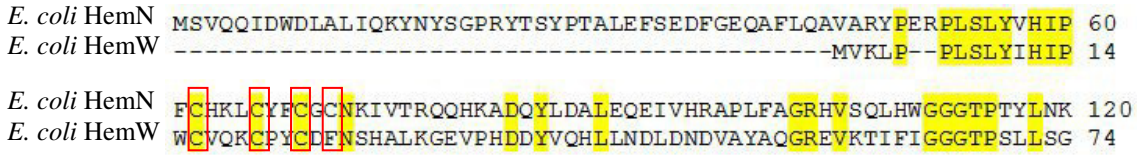

Fig. 37: Alignment of the N-terminus of *E. coli* HemN and HemW.
Boxed in red are the conserved CxxxCxxCxC motive in HemN and CxxxCxxCxF motive in HemW. Numbers on the right indicate amino acid positions of the individual sequences. The alignment was generated with the program ClustalW2 by EMBL-EBI, using the clustalW method.

This cysteine motive is the second difference. HemN contains a CxxxCxxCxC motive, the first three cysteines involved in iron-sulfur cluster coordination (Layer *et al*., 2003), and the fourth cysteine being essential for enzyme function (Layer *et al*, 2002). In place of the fourth cysteine HemW contains a phenylalanine. In order to investigate HemW evolution a conversion of HemW into a functional CPDH was systematically tried. The additional 46 N-terminal amino acids of *E. coli* HemN were fused to *E. coli* HemW F25C, a mutant with the typical fourth cysteine in position 25 (Grage, 2005). Both artificial *hemW* derivative genes were tested in *in vivo* complementation assays using an *E. coli* Δ*hemN* mutant.

E. coli hemN (pET-3a-hemN) was included as positive control, *E. coli* Δ*hemN* mutant without plasmid as negative control. As shown in Fig. 38, no complementation of the *E. coli hemN* mutant by both artificial *hemW* constructs (*hemW*F25C and

*hemW*F25C+46N-term.) was detected. Notwithstanding its high homology to other O_2-independent CPDHs, *E. coli* HemW does not seem to have any CPDH activity.

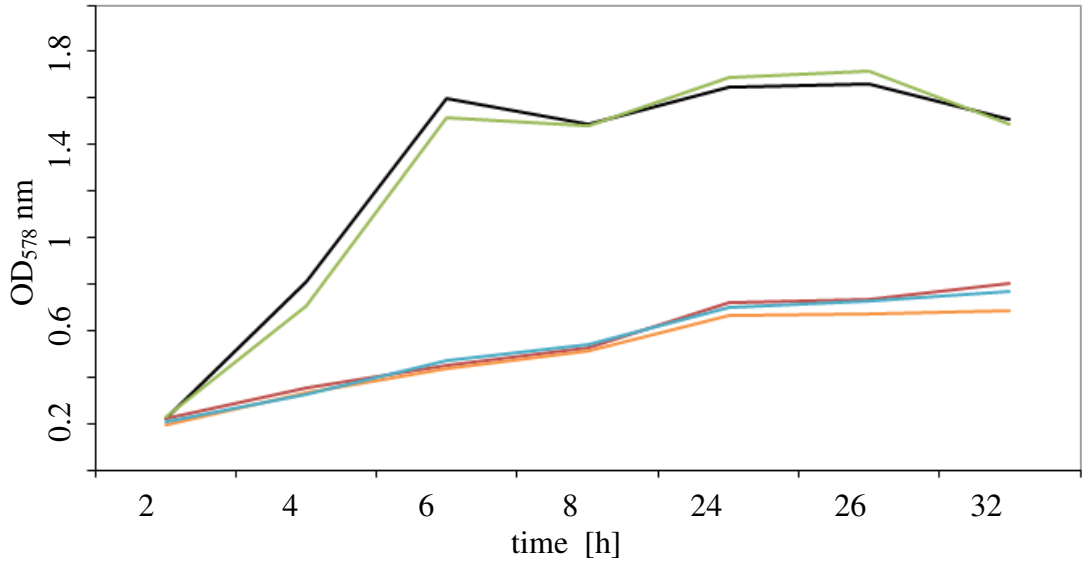

Fig. 38: Complemtation of an *E. coli* Δ*hemN* mutant by artificial *hemW* genes mutated towards *hemN* structure.
Cells were grown at 37 °C in LB medium containing 10 mM $NaNO_3$ and no antibiotics in tightly sealed anaerobic flasks. Values for each strain are averages of three parallel cultures. ▬ wild type *E. coli* BW25113, ▬ *E. coli* Δ*hemN*, ▬ Δ*hemN* with pET-3a-*hemN* (*E. coli hemN*), ▬ Δ*hemN* with pGEX-*hemW*F25C+46N-term, ▬ Δ*hemN* with pGEX-*hemW*F25C.

Both artificial HemW constructs, heavily mutated towards the HemN protein, failed to sustain CPDH activity *in vivo*. Obviously, there is more to the CPDH enzyme as the typical N-terminus of the HemN protein.

3.3 Covalent binding of heme by *Escherichia coli* HemW

E. coli HemW has clearly no CPDH activity. From the studies with the homologous *L. lactis* HemW protein a role of *E. coli* HemW as heme binding protein was predictable. Consequently we investigated the heme binding capacity and the structural consequences of heme binding by *E. coli* HemW.

3.3.1 Analysis of covalent HemW-heme binding *via* SDS-Page and heme stain

To verify heme binding by *E. coli* HemW a heme stain of recombinant purified HemW incubated with heme was performed as described in MATERIALS AND METHODS (2.7.9). During this analysis the HemW-heme complex was assayed *via* denaturing SDS PAGE and subsequent heme detection through a gel based on peroxidase activity (Fig. 39). A positive heme stain would indicate stable, most likely covalent heme binding by *E. coli* HemW. Ten µM cytochrome *c* was included as positive control for a heme binding protein and *E. coli* BL21 (DE3) cell free extract to check for potential background.

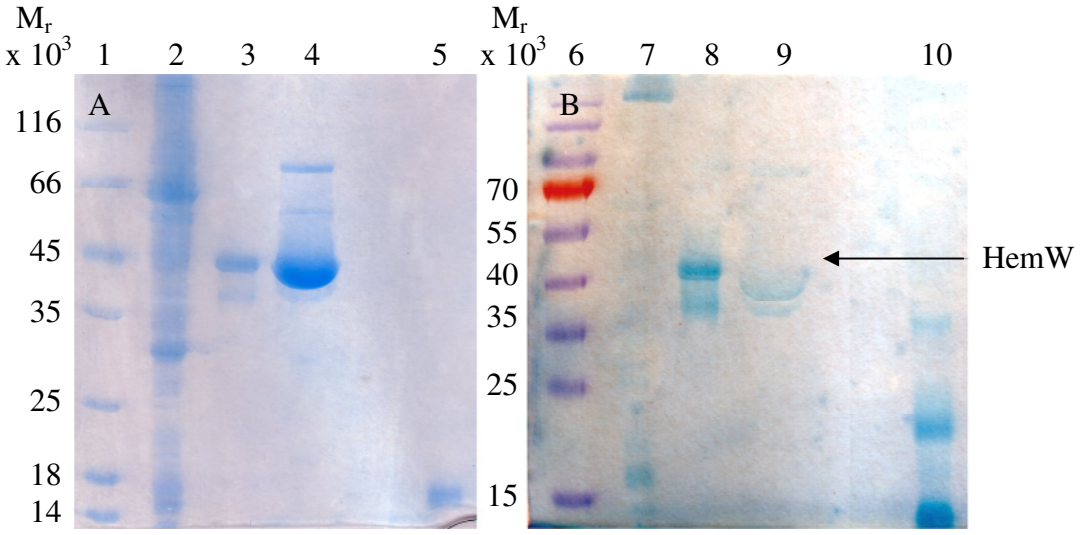

Fig. 39: Heme stain of *E. coli* HemW with and without heme supplementation.
Proteins were separated by 12 % SDS PAGE and visualized by staining with A: Instant*Blue*™ and B: heme stain solution. Lane 1: unstained protein molecular weight marker, lane 6: PageRuler prestained protein ladder, lane 2 and 7: *E. coli* BL21 (DE3) cells, lane 3 and 8: 10 µM *E. coli* HemW + 10 µM heme, lane 4 and 9: *E. coli* HemW, lane 5 and 10: 10 µM cytochrome *c*.

HemW incubated with heme is shown Coomassie stained in lane 3, and heme stained in lane 8 of figure 39. The stained bands in both lanes correspond to the same relative molecular mass of about 40,000 and show about the same intensity. HemW incubated with heme is almost as strongly stained as cytochrome *c* (lane 10), which is known to possess a covalently bound heme *c* group. Comparison of lane 4 and lane 9 show that pure *E. coli* HemW (lane 4) has bound heme (lane 9), indicating a low amount of naturally bound heme. An unspecific staining of HemW is unlikely, since *E. coli* cell free extract in lane 7 shows no arbitrary heme staining compared to the protein stain of

lane 2. Together these results suggest that *E. coli* HemW contains a covalently bound heme cofactor.

3.3.2 Analysis of HemW-heme binding *via* UV/Vis spectroscopy

In order to support the findings of covalent heme binding by *E. coli* HemW with *in vitro* experiments in solution, UV-visible light absorption spectra of HemW supplemented with heme were recorded under anaerobic conditions.

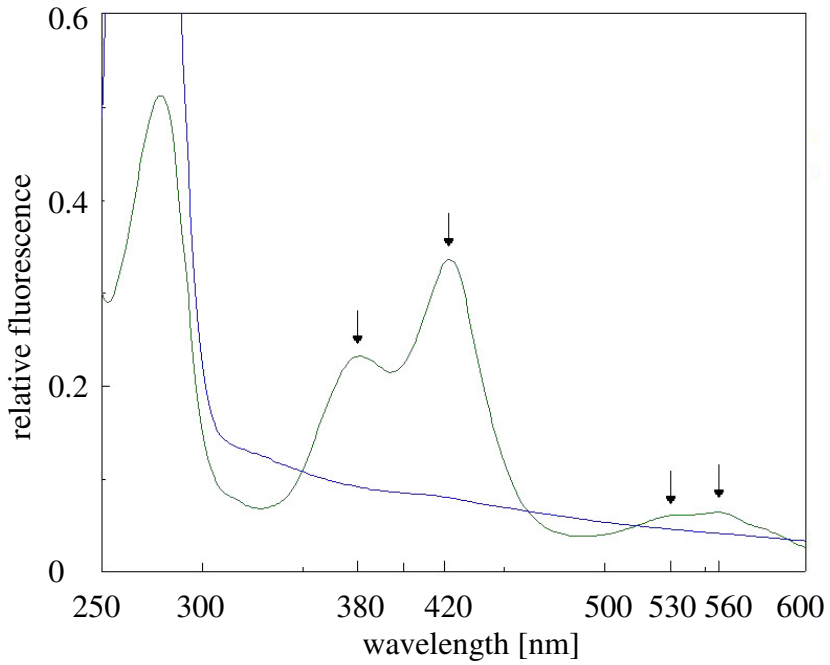

Fig. 40: UV/Vis spectrum from purified *E. coli* HemW with and without heme supplementation. Comparison between *E. coli* HemW and HemW supplemented with heme. Spectra were recorded from 250 – 600 nm and the relative fluorescence was measured. A peak at 280 nm indicates the protein concentration and a peak at 420 nm the presence of an iron-sulfur cluster and bound heme respectively. Peaks at 530 nm and 560 nm are typical Q bands of heme. — *E. coli* HemW, showing a weak signal for an iron sulfur-cluster; — *E. coli* HemW supplemented with heme, showing a strong signal for bound heme.

The absorption from pure *E. coli* HemW (blue line) at 420 nm was nearly nonexistent in comparison with the protein concentration measured at 280 nm, the HemW-heme mixture (green line) showed a peak at 380 nm and at 420 nm about half the size of the peak at 280 nm. Additional peaks were observed at 530 nm and 560 nm, typical of the Q bands of heme. Clearly, HemW binds heme covalently and quantitatively.

3.3.3 *Escherichia coli* HemW binds heme with high specificity

The next question was which part of the heme molecule is recognized during the binding process. Therefore, HemW was incubated with a number of heme analogues (table 13) and UV-visible light absorption spectra were recorded as stated above.

Tab. 13: Heme analoga employed for HemW-heme binding assays.
Shown are the different heme analogues and their molecular characteristics.

	porphyrin	R	R'	R''
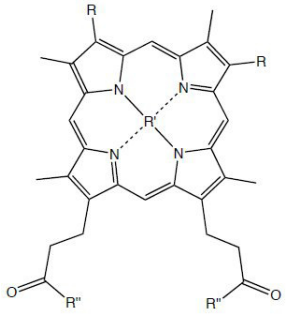	PPIX	vinyl	-	OH
	PPIX dimethyl ester	vinyl	-	O-CH3
	PPIX disodium salt	vinyl	-	ONa

None of the employed heme analogues achieved the same result as heme, as documentated in figure 41.

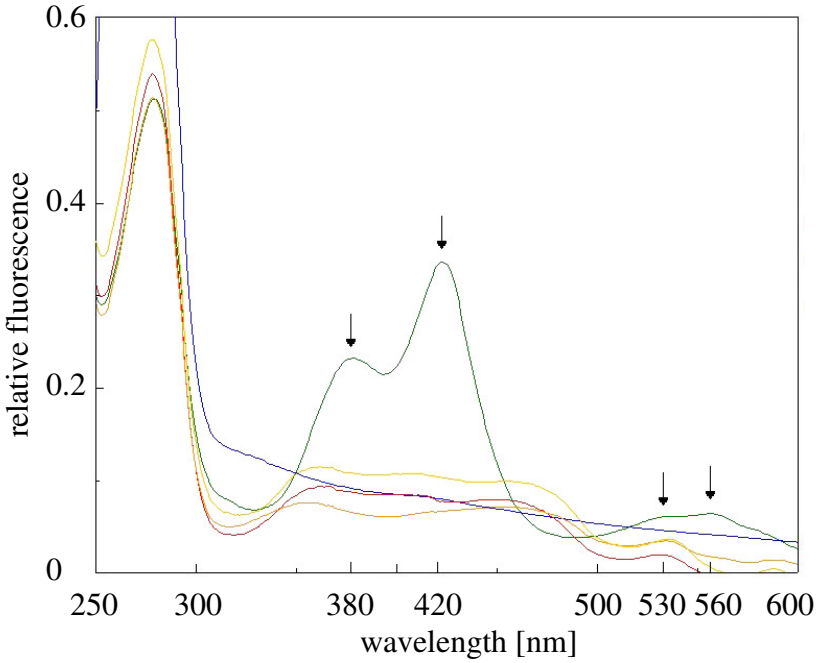

Fig. 41: UV/Vis spectrum from purified *E. coli* HemW with different heme analogues.
Comparison of the absorption spectrum between native *E. coli* HemW and HemW supplemented with different heme analoga. Spectra were recorded from 250 – 600 nm and the relative fluorescence was measured. A peak at 280 nm indicates the protein concentration and a peak at 420 nm the presence of bound heme. Peaks at 530 nm and 560 nm are typical Q bands of heme. — *E. coli* HemW, — *E. coli* HemW supplemented with heme, — *E. coli* HemW supplemented with PPIX, — *E. coli* HemW supplemented with PPIX dimethylester, — *E. coli* HemW supplemented with PPIX disodium salt.

The green line shows the spectrum recorded for HemW supplemented with heme, with its typical peaks at 380 nm, 420 nm, 530 nm and 560 nm. For the other heme analogues, PPIX (red line), PPIX dimethylester (orange line) and PPIX disodium salt (yellow line) no significant peaks were detected, comparable to HemW without additive (blue line).
It was shown for cytochrome *c* that attachment of heme to the protein is established by two thioether bonds formed between the heme vinyl groups and cysteine residues of cytochrome *c* (Pettigrew and Moore, 1987), while the heme iron is typically ligated by two amino acid side chains from the protein. The same could hold true for *E. coli* HemW. While all heme analogs possessed the vinyl groups necessary for ligation, none contained the central metal atom. The central atom of *E. coli* HemW plays a vital role for HemW-heme interaction.

3.3.4 Determination of the oligomerization state of recombinantly produced and purified *Escherichia coli* HemW in the absence of heme

To further characterize HemW in terms of its oligomerization state, a gel permeation chromatography (GPC) under strict anaerobic conditions (2.7.7) was performed.

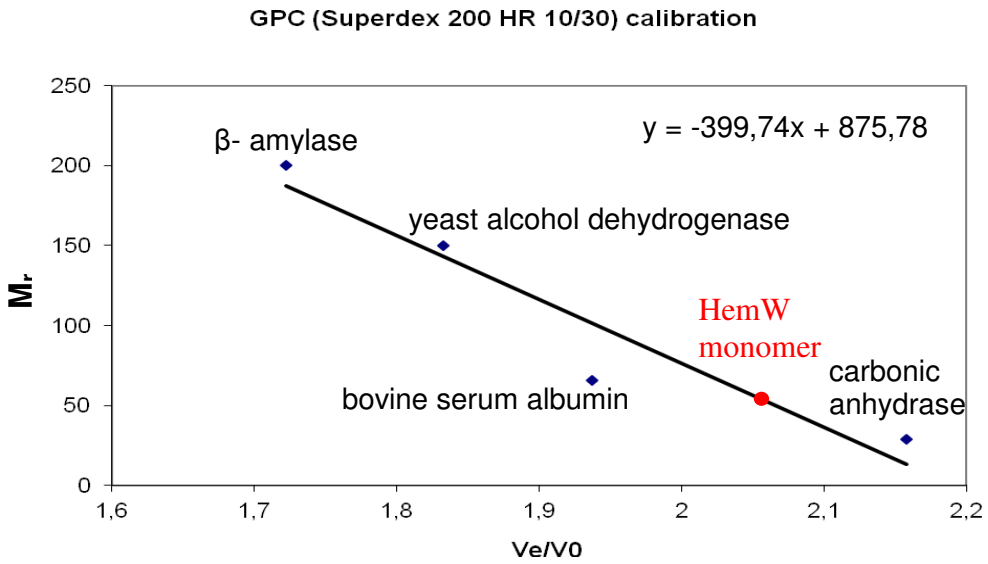

Fig. 42: Determination of the oligomerization state of *E. coli* HemW.
The relative molecular mass (M_r) of the marker proteins was plotted against their elution volume (Ve) divided with the 'dead volume' (V0) of the column. Molecular masses of approximately 45,000 and 117,000 were determined for HemW matching with the calculated molecular mass of 42,600 of the monomer and the dimer respectively. The column was calibrated using carbonic anhydrase (M_r = 29,000), bovine serum albumin (M_r = 66,000), yeast alcohol dehydrogenase (M_r = 150,000) and β- amylase (M_r = 200,000) as marker proteins.

Purified protein of a concentration of 1 mg/ml was chromatographed at a flow rate of 0.25 ml/min. With a calibration curve (Fig. 42) the relative molecular mass of HemW was determined. The GPC showed two different molecular masses for HemW. The value of approximately 45,000 was in good agreement with the calculated relative molecular mass of 42,600 of the HemW monomer. The second minor peak of about 117,000 correlates to the relative molecular mass of the HemW homodimer.

3.3.5 Heme binding to HemW induces dimerization of the protein

Gel permeation chromatography (GPC) was performed as described in MATERIAL AND METHODS (2.7.7) Protein concentration was determined by measuring the absorbance at 280 nm. Heme binding was detected by 420 nm absorbance. Both HemW and HemW supplemented with heme were assayed *via* GPC. Resulting protein solutions were fractionated and analyzed by SDS PAGE. Subsequently, the gels were tested for protein by Coomassie Blue staining and for the presence of heme by peroxidase activity testing. The combined results are displayed in figure 43. The chromatogramme of HemW without heme showed a prominent peak indicating the monomeric state with a little shoulder (blue line), representing the dimeric state as seen in figure 43 A.1. In addition, there was little to no absorbance at 420 nm (purple line), just a very low increase within the range of the dimer-shoulder. Fractions stained with Coomassie Blue showed an increased protein concentration from fraction 10 to 14 (A.2), in agreement with the shown chromatogramme. The heme stain depicted in figure A.3 showed no peroxidase activity and thus no presence of heme, again in agreement with the measured absorbances.

Figures 43 B.1 to B.3 show the results for the analyses of HemW supplemented with heme. The chromatogramme (B.1) showed the same monomeric protein peak as HemW without heme. But in the presence of heme the dimeric peak was much more pronounced. The same was true for the presence of heme. The absorbance at 420 nm (purple line) was dramatically increased in the range of the dimeric peak, while it decreased almost to the detection limit in the range of the peak for the monomeric HemW.

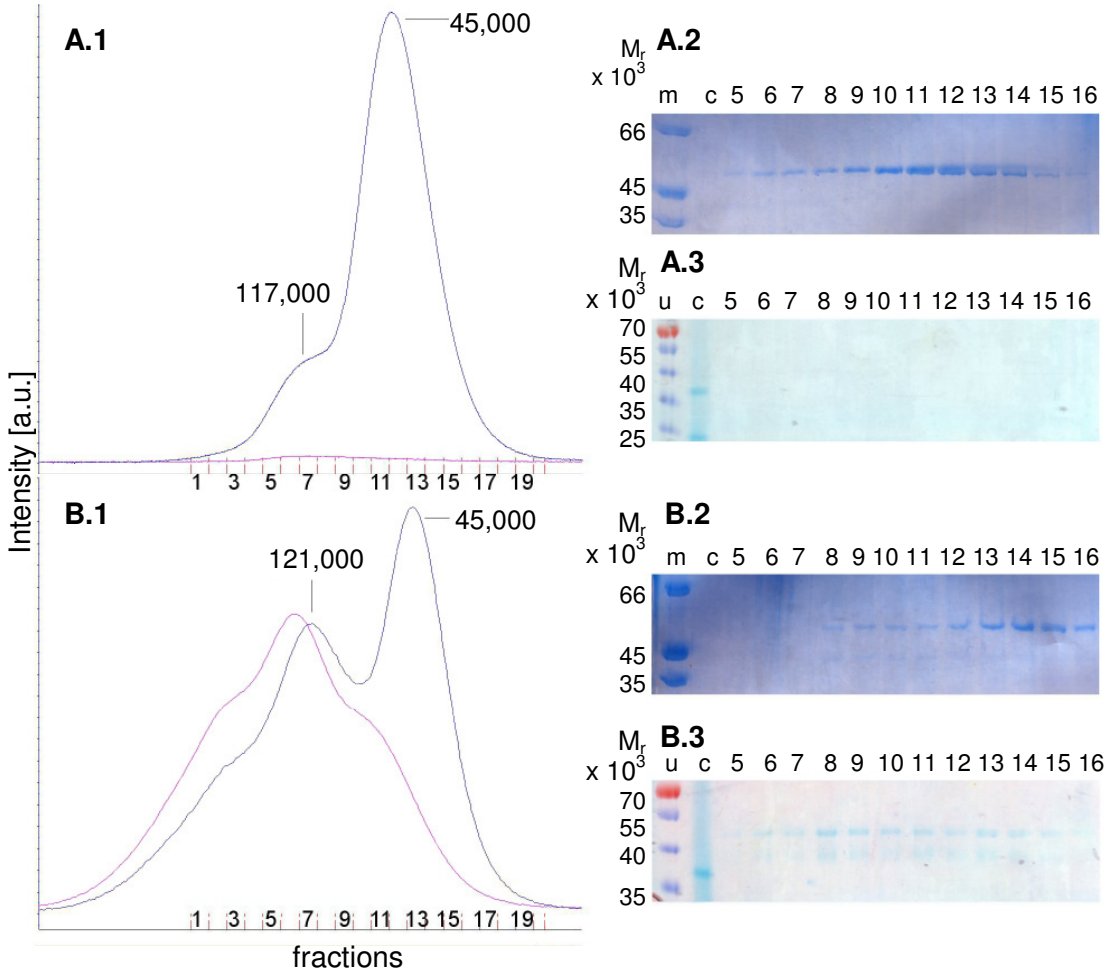

Fig. 43: Heme induced dimerization of *E. coli* HemW analyzed by GPC, subsequent SDS-PAGE and protein as well as heme staining.
Figures A show the results for *E. coli* HemW, figures B the results for HemW supplemented with heme. A.1: GPC chromatogram of *E. coli* HemW. Monomer and dimer with their respective calculated relative molecular masses are indicated. A.2: protein stain of *E. coli* HemW fractions with Instant*Blue*™, A.3: heme stain of *E. coli* HemW fractions with heme stain solution, B.1: GPC chromatogram of *E. coli* HemW supplemented with heme. Monomer and dimer with their respective calculated relative molecular masses are indicated. B.2: protein stain of *E. coli* HemW supplemented with heme fractions with Instant*Blue*™, B.3: heme stain of *E. coli* HemW supplemented with heme fractions with heme stain solution. — 280 nm wavelength, — 420 nm wavelength. 1-16: labeling of fractions, m: unstained protein molecular weight markers (M_r x 10^3), u: PageRuler prestained protein ladder, c: cytochrome *c*.

The Protein stain with Coomassie Blue (B.2) confirmed these results, in that protein concentration in fractions with dimeric HemW increased in comparison to the fractions with monomeric HemW. The heme stain in figure B.3 shows an increased peroxidase activity in the fractions of the dimeric state of HemW supplemented with heme, again supporting the results of the GPC.

The results indicate that the addition of heme to *E. coli* HemW leads to covalent binding of heme. Heme itself seems to be necessary for dimer formation.

A similar process is known for other proteins like ChaN, an iron-regulated lipoprotein from *Campylobacter jejuni*. Apo-ChaN is predominantly monomeric and dimerization occurs upon coordination of two cofacial heme molecules (Chan *et al*., 2006). This was established by resolving the corresponding crystal structure.

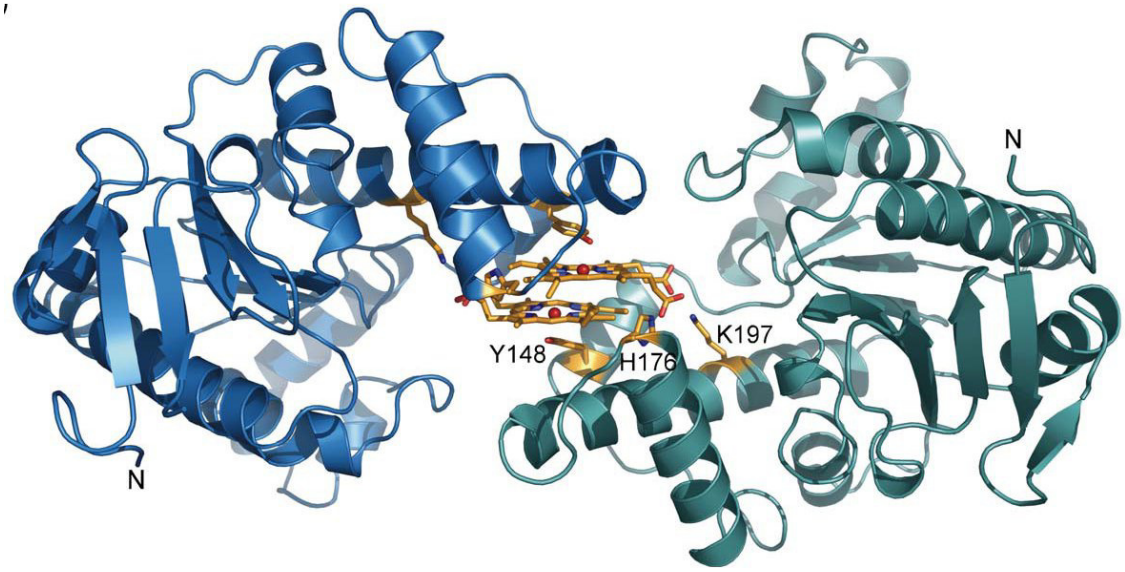

Fig. 44: The crystal structure of heme-bound ChaN. (Chan *et al*., 2006)
Dimeric holo-ChaN enclosing two cofacial heme molecules. The two ChaN monomers are indicated in blue and teal. The heme and heme ligands are depicted as ball-and-stick representations and are colored in orange. The coordination dependent residues Tyr148, His176 and Lys197 are indicated.

In this structure, heme is not found in the interdomain cleft but is bound at the surface. The two ChaN monomers form a pocket, which encloses the cofacial hemes (Fig. 44). In this pocket heme is coordinated by Tyr148, His176 and Lys197, amongst other residues. Both Lys197 and His176 are derived from the symmetry related monomer. Thus, the heme dimer serves as a bridge linking the ChaN monomers (Chan *et al*., 2006). Interestingly, ChaN is proposed to play a role in heme uptake. A knockout mutation of the ChaN homologue PhuW in *P. aeruginosa* exhibited decreased growth compared to the wild type *P. aeruginosa* PAO1 using heme as the sole iron source (Ochsner, 2000).

3.3.6 Drastic conformational changes of *Escherichia coli* HemW upon heme supplementation

Heme induced dimerization was investigated for the accompanying structural changes by CD-spectroscopy in the far and near UV region (Fig. 45). The samples contained 11.74 µM HemW and equimolar heme in PBS buffer.

The near UV spectrum from 260 to 300 nm showed that HemW (blue line) and HemW supplemented with heme (green line) have very similar tertiary structures. The far UV spectrum in the range from 200 to 260 nm showed significant changes at about 220 to 230 nm.

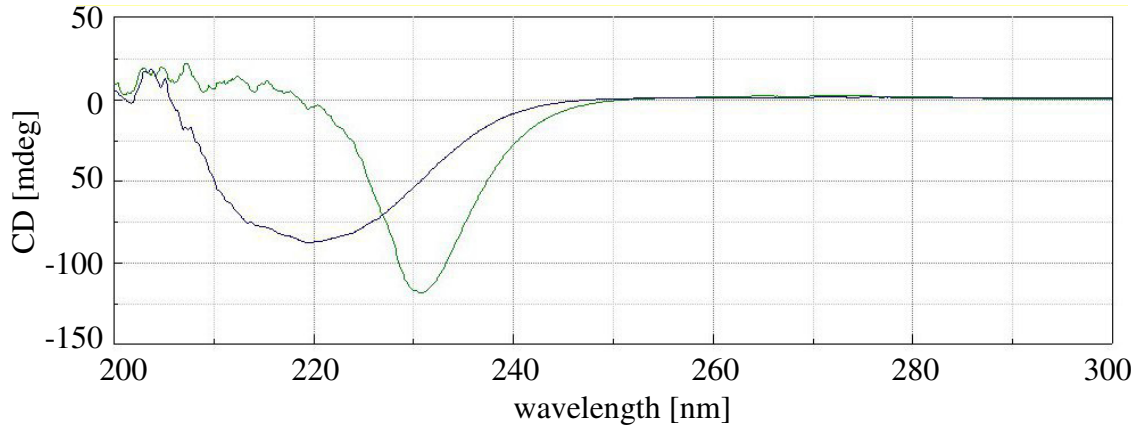

Fig. 45: CD spectra of *E. coli* HemW and HemW supplemented with heme.
The far UV spectrum (200 – 260 nm) shows that — HemW and — HemW supplemented with heme have different secondary structures (Sreerama and Woody, 2000 and 2004).

Clearly, HemW and HemW supplemented with heme have different secondary structures, supporting the hypothesis that dimerization upon heme binding is accompanied by significant structural changes. Complete analysis is given in table 14. The most consistent difference is the increase of unordered structures and decrease of β-sheet structures in HemW supplemented with heme. CONTILL and CDSSTR method computed that in HemW a mean of 26.77 % represents unordered structures, while for HemW supplemented with heme an average of 36.39 % unordered structures was calculated. The percentage of β-sheet structures in HemW is about 44.21 % and therefore higher than in HemW supplemented with heme, which is composed of averaged 36.5 % β-sheet structures.

Tab. 14: Far ultraviolet circular dichroism analysis of HemW and HemW supplemented with heme
Estimation of secondary structure parameters was performed using CDPro program CONTINLL and CDSSTR method. H(r) = helix regular, H(d) = helix distorted, S(r) = sheet regular, S(d) = sheet distorted, NRMSD = normalized root of mean square devia

method	α-helix (%)			β-sheet (%)			turns	unordered	NRMSD
	H(r)	H(d)	total	S(r)	S(d)	total			
HemW									
CONTINLL	1.10	3.80	4.9	37.24	16.42	53.66	20.12	21.32	0.196
CDSSTR	1.22	3.55	4.77	21.68	13.07	34.75	28.27	32.22	0.286
HemW + heme									
CONTINLL	1.10	4.10	5.20	23.18	12.79	35.97	21.98	36.86	0.059
CDSSTR	-0.61	3.87	3.26	23.80	13.22	37.02	23.80	35.91	0.122

The CD spectroscopy of *E. coli* HemW in comparison with HemW supplemented with heme showed drastic differences in respective secondary structures. Unusual is the wavelength shift from 220 nm of HemW to 230 nm of HemW supplemented with heme. These drastic differences are caused by the heme-dependent dimerization of *E. coli* HemW.

3.3.7 *Escherichia coli* HemW contains an iron-sulfur cluster

To investigate whether *E. coli* HemW contains an iron-sulfur cluster the protein iron content was determined, as described in MATERIAL AND METHODS (2.7.4), colorimetrically with bathophenanthroline after acid denaturation of HemW. With a calibration curve the iron content was as determined to be about 0.25 mol iron per mol protein. This is very low for a protein expected to have an iron-sulfur cluster, e.g. *E. coli* HemN, containing an [4Fe-4S] cluster, possess between 1.2 and 2.0 mol iron / mol protein. It is well known that iron incorporation into recombinant proteins is incomplete (Lazazzera *et al*., 1996), caused by the high level production. For example purified recombinant *E. coli* HemN was reported to contain maximal two of the predetermined four mol iron / mol protein (Layer *et al*., 2005). The characteristic yellow-brown color of iron containing proteins was present, but faint. UV-visible light absorption spectra recorded under anaerobic conditions revealed a slight peak at 420 nm (Fig. 46), indicating an iron- sulfur cluster.

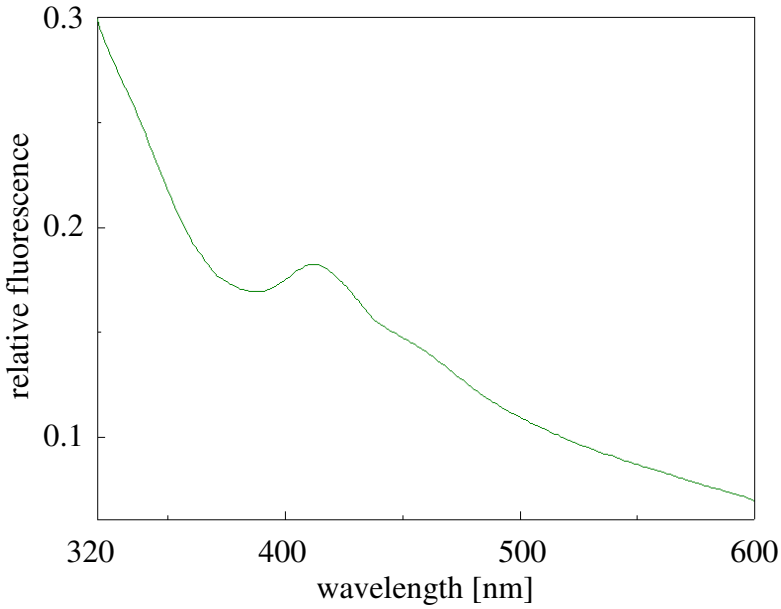

Fig. 46: UV/Vis spectrum from purified *E. coli* HemW.
Spectra were recorded from 250 – 600 nm and the relative fluorescence was measured. The peak at 420 nm indicates the presence of an iron-sulfur cluster.

3.3.8 *Escherichia coli* HemW transfers electrons from its iron-sulfur cluster upon heme binding

Until now, strong evidence was provided that *E. coli* HemW dimerizes upon heme supplementation. Since HemW also contains an [Fe-S] cluster, the next step was to investigate the function of the cluster during and after the dimerization process. Therefore, HemW and HemW supplemented with heme were subjected to EPR spectroscopy. Required for this technique is the presence of at least one unpaired electron. Determination of the *g*-value gives information about symmetry and electronic structure of transition metal complexes.

Due to their different composition and different oxidation states, different [Fe-S] clusters give rise to different EPR spectra (Fig. 47). The $[2Fe\text{-}2S]^{1+}$ clusters (Fig. 47A) have a spin of S = ½, with signals of *g*-values 2.01, 1.94 and 1.89 (Hill, 1981). The $[3Fe\text{-}4S]^{1+}$ cluster (Fig. 47B) is oxidized and contains three Fe^{3+}-ions. It has a spin of S = ½ and gives an almost isotropic signal at a *g*-value of 2.02 (Huynh *et al.*, 1980). The $[4Fe\text{-}4S]^{1+}$ cluster (Fig. 47C) contains three Fe^{2+}-ions and one Fe^{3+}-ion. It has a spin of S = ½ and its spectrum shows a rhombic signal with two *g*- values below 2.0023 (Sweeney and Rabinowitz, 1980). $[4Fe\text{-}4S]^{3+}$ clusters (Fig. 47D) are oxidized and

contain three Fe^{3+} -ions and one Fe^{2+} -ion. An EPR signal is detectable around g = 2.02 (Hoff, 1989).

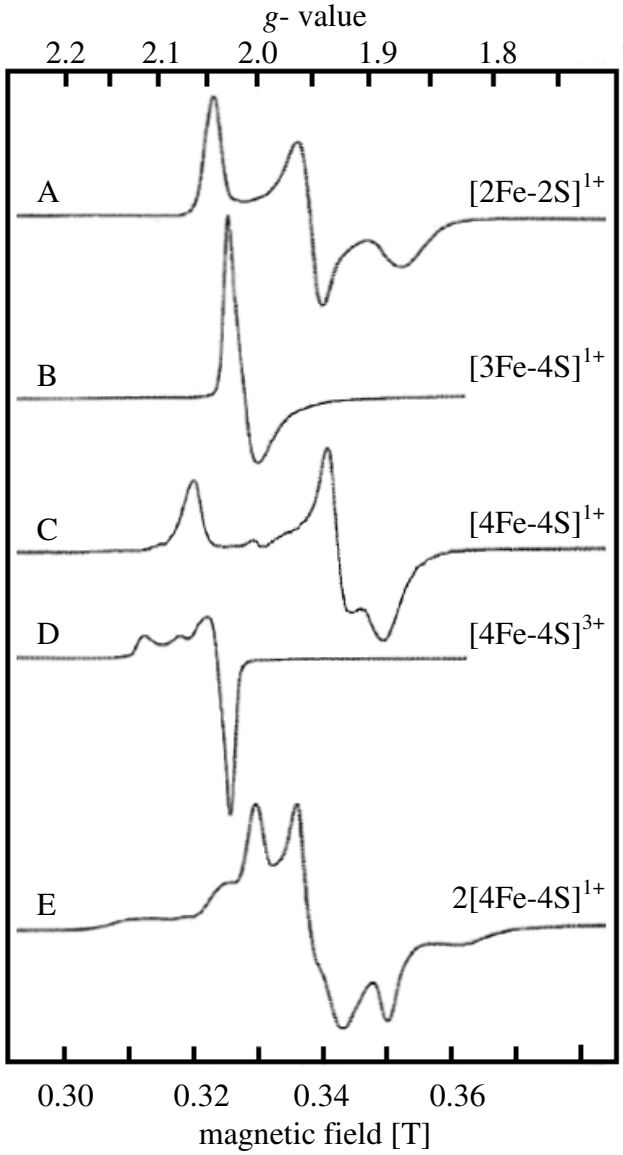

Fig. 47: EPR spectra of Fe-S clusters in ferredoxins.
Shown are the EPR spectra of reduced Fe-S clusters from A: *Mastigocladus laminosus*, B: *Desulfovibrio gigas*, C: *Bacillus stearothermophilus*, D*: Chromatium vinosum* high potential iron-sulphur protein (HiPIP), E: *Clostridium pasteurianum* 8Fe ferredoxin.

The incubation of 150 µM HemW with equimolar heme, as well as 80 µM HemW with equimolar Fe^{3+} corrole (kindly provided by Prof. Dr. Bröring, Institute of Inorganic Chemistry, TU-Braunschweig) was carried out overnight under strict anaerobic conditions. In neither case the HemW was reduced by dithionate prior to the incubation or the EPR recordings. The samples were transferred into 4 mm EPR tubes, cooled to 4 K and measured by a frequence of 9.2399 GHz using a Bruker Spin R ESP 300 E

instrument. The measurements were performed by Dr. O. Burghaus from the Faculty of Chemistry at the Phillips University Marburg.

EPR spectra were recorded for *E. coli* HemW with bound heme and a bound Fe^{3+} corrole, respectively. The core macrocyclic structure of the iron corrole mimics much of the natural heme moiety (Fig. 48), however, it is truncated by one *meso*-situated carbon atom. As a consequence, binding of this ligand to the central iron atom occurs in a slightly different fashion. First, the corrole core is trinegative (protoporphyrin is dinegative in heme) and thus stabilizes the iron atom in an unusual oxidation state one above the naturally found one. Second, iron atoms in corrole ligand sets have only four accessible 3*d* orbitals and usually show special spin states. Particularly prominent is the intermediate spin (S = 3/2) state for Fe^{3+} in pseudo-ferrous iron corrole (Ye *et al.* 2008; Hocking *et al.* 2009). Iron in this state is EPR active.

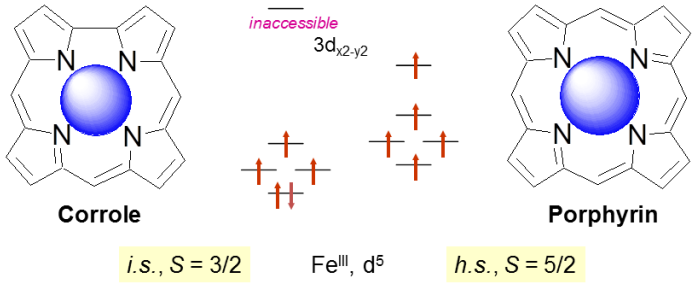

Fig. 48: Schematic drawing of iron(III) corrole and porphyrin basic structures, with ligand field splittings.
Displayed are the structures of an iron corrole (left) and porphyrin (right), with their respective spin states. The central iron atom is shown in blue. *i.s.* = intermediate spin, *h.s.* = high spin.

Heme is EPR silent and should give no signal, while the iron corrole is detectable due to its described spectroscopic features. Images of the spectra are seen below in figure 49.

The top trace in figure 49 shows the EPR spectrum of HemW with bound heme. The signal of g = 2.04 represents a $[4Fe\text{-}4S]^{3+}$ cluster. The initial natural state of this Fe-S clusters is probably $[4Fe\text{-}4S]^{2+}$ containing two Fe^{3+} -ions and Fe^{2+} -ions respectively. This cluster has a spin of S = 0 and gives no EPR signal. Once heme was bound a change of potential occurred which allowed heme to oxidize the cluster by removing one electron. Now the cluster contained three Fe^{3+} -ions and one Fe^{2+} -ion, leading to a $[4Fe\text{-}4S]^{3+}$ cluster, as detected in the EPR analysis.

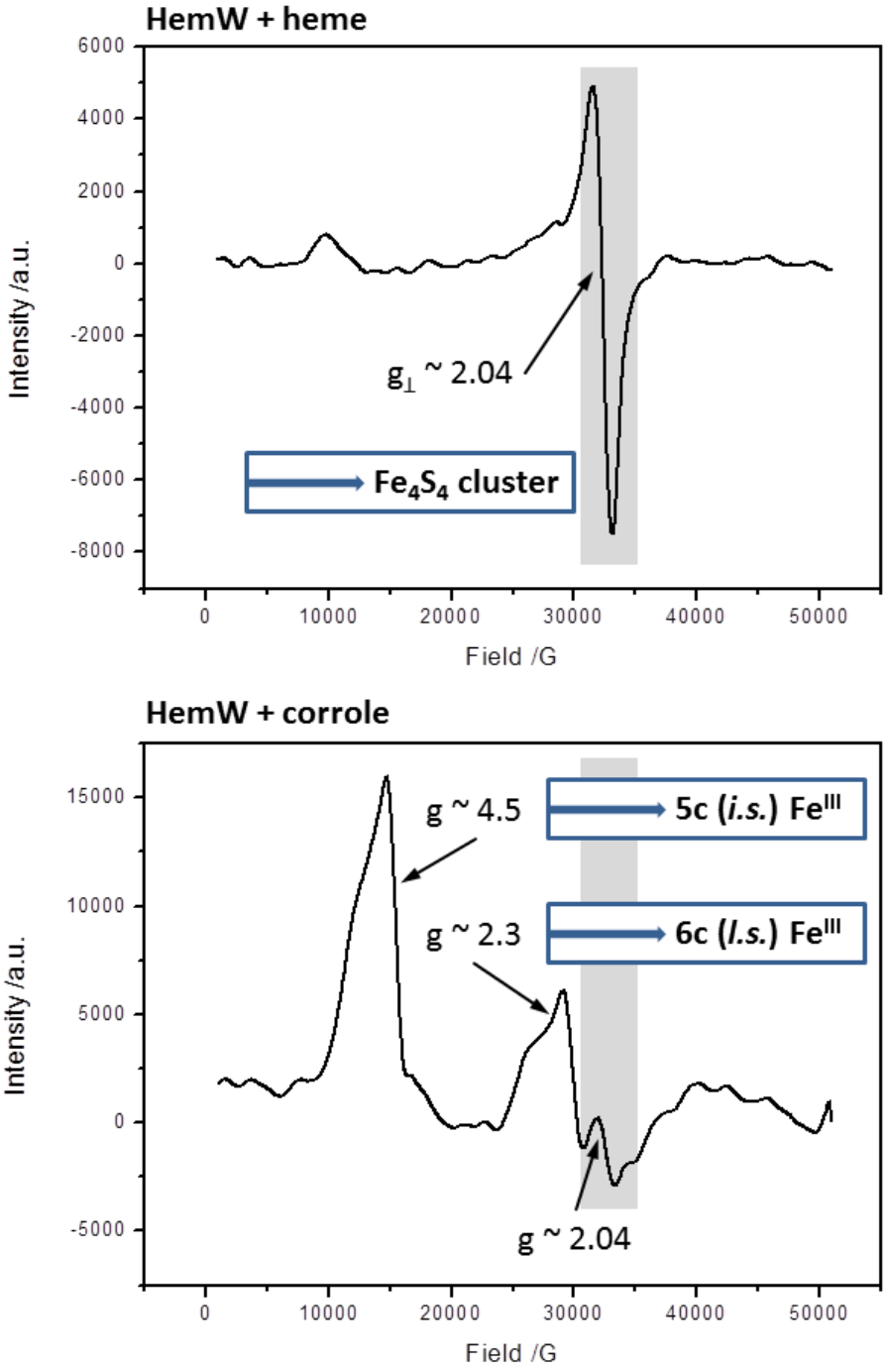

Fig. 49: EPR spectra of HemW with bound heme and with a bound iron corrole.
X band EPR spectra (9.2399 GHz, 4 K) of HemW with bound heme (top trace; 150 µM in PBS buffer) and with a bound Fe^{3+} corrole (bottom trace, 80 µM in PBS buffer). Spectra are corrected for base line drifts and smoothed with the moving average method.

Since heme itself is EPR silent information about the coordination was obtained with the bound Fe^{3+} corrole, as seen in the bottom trace of figure 49. Three significant EPR signals are visible. At g = 2.04 the $[4Fe\text{-}4S]^{3+}$ cluster is represented again. An intermediate spin (S = 3/2) at g = 4.5 shows a 5-times coordination of the iron center.

This is the typical state of protein coordinated heme, as found in hemoglobin, myoglobin, cytochrome *c* and nitric oxide synthase for example (Perutz, 1979; Kendrew *et al*., 1958; Moore and Pettigrew, 1990; Wang *et al*., 1993). There is also a low spin (S = ½) visible at g = 2.3, indicating a 6-times coordination of the iron. Normally this coordination is only adopted upon necessity. Neuroglobin and cytoglobin as well as some plant and bacterial globins contain hexacoordinated hemes (Dewilde *et al*., 2001; Pesce *et al*., 2004; de Sanctis *et al*., 2004; Hargrove *et al*., 2001). It could be explained as a mechanism for O_2 protection, since in this state the heme is shielded from external influences. Additionally, in our experiments HemW with bound heme was stable over at least two days under aerobic conditions. It was also proposed that hexacoordination facilitates electron transfer, while pentacoordination is preferred for ligand binding and releasing (Kakar *et al*., 2010).

The here performed analysis of *E. coli* HemW have revealed an unusual heme-binding, [Fe-S] cluster containing protein. Future experiments will hopefully verify HemW as a true heme chaperone.

3.4 Crystallization of *Escherichia coli* HemW

Crystallization of *E. coli* HemW would give undisputable information about its structure. As of today there are no crystal structures of HemW-like proteins. However, a crystal structure of the structurally related *E. coli* CPDH (HemN) exists (Fig. 11; Layer e*t al*., 2003)

Crystallization trials were performed using buffers and salts provided by the Qiagen Cryos Suite under strict anaerobic conditions at 17 °C. The protein concentration was varied between 5 mg/ml and 10 mg/ml. After four to five weeks the most promising crystal formation was observed under following condition: 85 mM Hepes pH 7.5, 17 % (v/v) Jeffamine M-600 and 15 % (v/v) glycerol (Qiagen Cryos Suite E8). The crystal was fished and immediately frozen in liquid nitrogen. X-ray diffraction was performed at the HZI structural biology unit (Helmholzzentrum für Infektionsforschung, Braunschweig, Germany). Regrettably, the analyzed crystal (Fig. 50) turned out to be to low in dimension and defracted poorly.

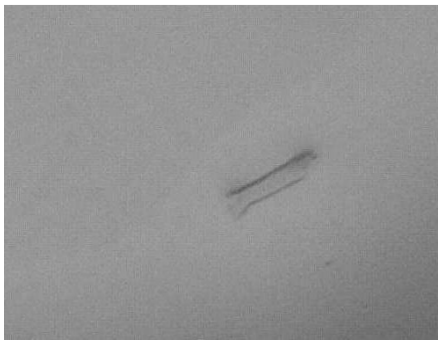

Fig. 50: *E. coli* HemW crystal.
E. coli HemW crystals were obtained using the E8 Cryos Suite (Qiagen) after approximately four to five weeks ander anaerobic conditions at 17 °C. X-ray diffraction revealed poor diffraction.

Experiments to obtain suitable crystals for x-ray analysis are still going on.

4 SUMMARY

At the beginning of this thesis bacterial heme chaperones for the transport and insertion of hemes into target proteins were unknown with the exception of cytochrome *c* maturation. Our initial working hypothesis proposed a transfer of heme *b* from the last enzyme of heme biosynthesis ferrochelatase (HemH) to target enzymes like catalase (KatA) with the potential involvement of heme binding bacterioferritin (BfrA). However, a *Pseudomonas aeruginosa* based bacterial two hybrid system analysis excluded direct interaction of these proteins. Screening of a *P. aeruginosa* genomic library for interaction partners of these proteins identified over 20 potential candidates, including various membrane localized transport proteins. Gene PA3851 might encode a potential iron transporter interacting with iron-inserting ferrochelatase.

In the second part of this thesis the potential *E. coli* heme chaperone HemW, which was originally described in *Lactococcus lactis*, was recombinantly produced and subjected to an initial biochemical characterization. The protein was highly homologous to coproporphyrinogen III dehydrogenase (HemN), however without the corresponding enzyme activity *in vitro* and *in vivo*. Introduction of typical HemN elements into HemW did not restore enzyme activity. The protein carries an [4Fe-4S] cluster. It binds heme covalently with high specificity. Upon heme binding the originally monomeric protein forms quantitatively a dimer. Moreover, electron transfer from the [4Fe-4S] cluster to the bound heme was observed *via* EPR spectroscopy. Initial crystallization trials yielded crystals with low defraction. Overall, this thesis provides basis for the biochemical understanding of a central heme chaperone found in bacteria, animals and plants.

5 OUTLOOK

Escherichia coli HemW

Our new working hypothesis (Fig. 51) says that in *E. coli* heme is formed *via* heme biosynthesis or in the case of *L. lactis* taken up from the environment. In the cytoplasm heme is bound by monomeric HemW (dark green). The binding of heme leads to dimerization of HemW and electron transfer from the [4Fe-4S] cluster to heme. Subsequently, HemW is directed to the cytoplasmic membrane where heme is supplied to membrane localized cytochromes (light green) in a NADH-dependent fashion (Abicht *et al.*, 2012).

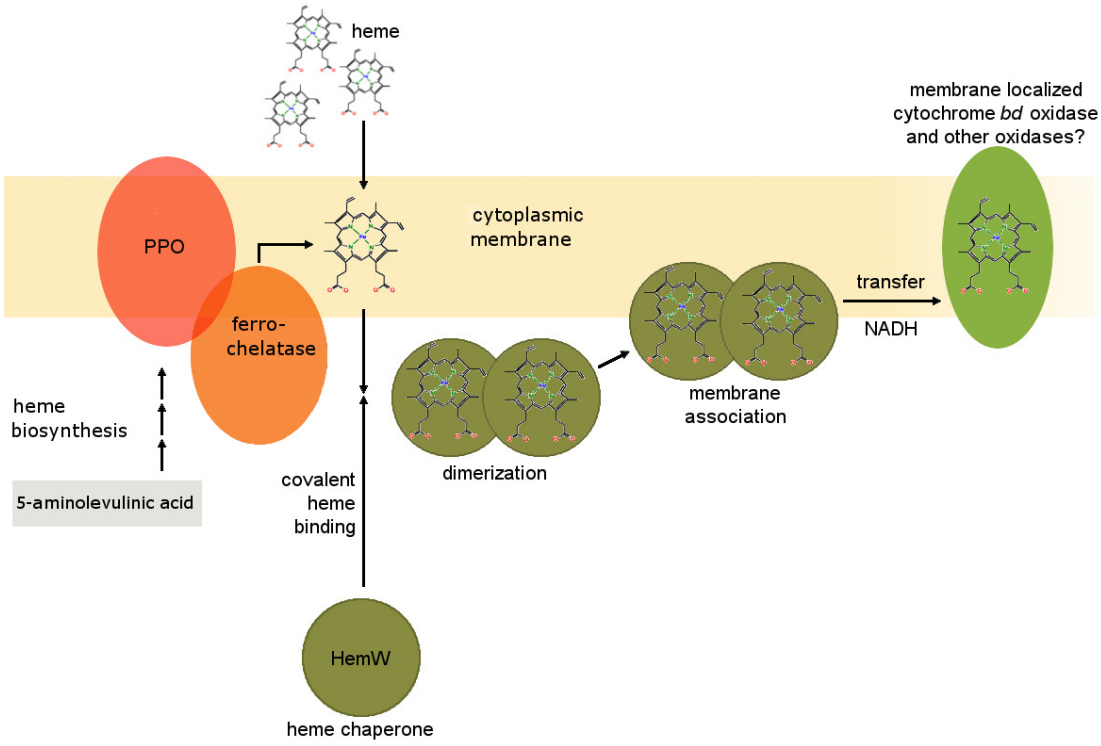

Fig. 51: Working hypothesis for the function of the heme chaperone HemW in *L. lactis* and *E. coli*. Heme is formed from 5-aminolevulinic acid. The last two enzymes of the heme biosynthetic pathway protoporphyrinogen IX oxidase (PPO, shown in red) and ferrochelatase (shown in orange) are forming a complex (Masoumi *et al.*, 2008). Alternatively, heme is taken up from the environment. Subsequently, heme is bound by monomeric HemW (shown in dark green) inducing dimer formation by restructuring of the protein. Electron transfer from the bound [4Fe-4S] cluster to heme follows. In the end, HemW is directed to the cytoplasmic membrane to supply heme in a NADH-dependent reaction to membrane-localized cytochromes (shown in light green).

To prove that *E. coli* HemW is involved in heme transport an activity test should be established, where the transfer of heme from HemW to a target protein is traceable.

Since a number of heme binding proteins like cytochrome *bo* and nitrate reductase are known, attempts should be made in isolation of heme-free variants of these proteins. Subsequently, these heme-free proteins should be supplemented with monomeric and dimeric HemW. The transfer of heme could be verified *via* heme stain. Determination of kinetic parameters and pH dependence would be advisable. To further determine the structural features of HemW crystallization should be attempted, if possible also with bound heme. Additionally, Mössbauer spectroscopy would give a clearer insight in the structural environment of the [Fe-S] cluster. Finally, homologous proteins of other organisms should be analyzed for the same characteristics as displayed by *E. coli* HemW.

Pseudomonas aeruginosa PA3851

From the results above it is not sure whether or not *P. aeruginosa* PA3851 actually plays a role in the transport of iron to ferrochelatase. For clearer understanding an unmarked knock-out mutant should be created, containing neither the target gene nor the resistance cassette replacement. Further interaction studies with PA3851 could be performed, with subsequent purification and characterization of the involved proteins.

6 REFERENCES

Abicht H. K., Martinez J., Layer G., Jahn D. and Solioz M. HemW is a novel heme chaperone required for cytochrome *bd* maturation. Under revision.

Ahuja U., Kjelgaard P., Schulz B. L., Thony-Meyer L. and Hederstedt L. (2009) Haem-delivery proteins in cytochrome *c* maturation system II. Mol. Microbiol. 73:1058-1071.

Akhtar M. (1991) Mechanism and stereochemistry of the enzymes involved in the conversion of uroporphyrinogen III into haem. Elsevier, Amsterdam.

Astner I., Schulze J. O., van den Heuvel J., Jahn D., Schubert W.-D. and Heinz D. W. (2005) Crystal structure of 5-aminolevulinate synthetase, the first enzyme of heme biosynthesis, and its link to XLSA in humans. EMBO J. 24:3166-3177.

Attmannspacher U., Scharf B. E. and Harshey R. M. (2008) FliL is essential for swarming: motor rotation in absence of FliL fractures the flagellar rod in swarmer cells of *Salmonella enterica*. Mol. Microbiol. 68:328–341.

Ausubel F. M., Brent R., Kingston R. E., Moore D. D., Seidman J. G., Smith J. A., Struhl K. (ed.). (1994) Current Protocols in Molecular Biology. 1st ed., vol. 1. Current Protocols. New York, N.Y.

Banerjee R. and Ragsdale S. W. (2003) The many faces of vitamin B12: catalysis by cobalamin-dependent enzymes. Annu. Rev. Biochem. 72:209-247.

Battersby A. R. (2000) Tetrapyrroles: the pigments of life. Nat. Prod. Rep. 17:507-526.

Beale S. I. and Castelfranco P. A. (1973) 14C incorporation from exogeneous compounds into δ-aminolevulinic acid by green cucumber cotyledons. Biochem. Biophys. Res. Commun. 52:143-149.

Beale S. I. (1993) Biosynthesis of phycobilins. Chem. Rev. 93:785-802.

Beale S. I. and Yeh J. I. (1999) Deconstructing heme. Nature Struct. Biol. 6:903-905.

Beale S. I. (1999) Enzymes of Chlorophyll biosynthesis. Photosynthesis Research 60:43-73.

Beckman D. L., Trawick D. R., Kranz R. G. (1992) Bacterial cytochromes *c* biogenesis. Genes Devel. 6:268-283.

Bhakta M. N. and Wilks A. (2006) The mechanism of heme transfer from the cytoplasmic heme binding protein PhuS to the delta-regioselective heme oxygenase of *Pseudomonas aeruginosa*. Biochemistry, 45:11642–11649.

Bollivar D. W., Clauson C., Lighthall R., Forbes S., Kokona B., Fairman R., Kundrat L. and Jaffe E.K. (2004) *Rhodobacter capsulatus* porphobilinogen synthase, a high activity metal ion independent hexamer. BMC Biochem. 5:17.

Bolotin A., Wincker P., Mauger S., Jaillon O., Malarme K., Weissenbach J., Ehrlich S. D. and Sorokin A. (2001) The complete genome sequence of the lactic acid bacterium Lactococcus lactis ssp. lactis IL1403. Genome Res. 11:731-753.

Bonnard G., Corvest V., Meyer E. H. and Hamel P. P. (2010) Redox processes controlling the biogenesis of *c*-type cytochromes. Antioxid Redox Signal 13:1385-1401.

Braun V. (1995). Energy-coupled transport and signal transduction through the gram-negative outer membrane via TonB-ExbB-ExbD-dependent receptor proteins. FEMS Microbiol.Rev. 16:295-307.

Braun V, Killmann H. (1999) Bacterial solutions to the iron-supply problem. Trends Biochem Sci. 24(3):104-109.

Brown S. M., Howell M. L., Vasil M. L., Anderson A. and Hassett D. J. (1995) Cloning and characterization of the *katB* gene of *Pseudomonas aeruginosa* encoding a hydrogen peroxide-inducible catalase: purification of KatB, cellular localization, and demonstration that it is essential for optimal resistance to hydrogen peroxide. J. Bacteriol. 177:6536–6544.

Chan A. C., Lelj-Garolla B., Rosell I. F., Pedersen K. A., Mauk A. G., Murphy M. E. (2006) Cofacial heme binding is linked to dimerization by a bacterial heme transport protein. J. Mol. Biol. 362:1108–1119.

Chang C. K., Chadwick D. J. (ed.) and Ackrill K. (ed.) (1994) Haem d1 and other haem cofactors from bacteria. In The biosynthesis of tetrapyrrole pigments; Ciba Foundation Symposium 180. Wiley, Chichester, pp. 228-246.

Clowes R.C., and Hayes W., ed. (1968) Experiments in Microbial Genetics New York, 187.

Condon S. (1987) Responses of lactic acid bacteria to oxygen. FEMS Microbiol. Rev. 46:269–280.

Corradi H. R., Corrigall A. V., Boix E., Mohan C. G., Sturrock E. D., Meissner P. N., Acharya K. R. (2006) Crystal structure of protoporphyrinogen oxidase from *Myxococcus xanthus* and its complex with the inhibitor acifluorfen. J. Biol. Chem. 281:38625-38633.

Cotter P. A., Chepuri V., Gennis R. B., and Gunsalus R. P.(1990) Cytochrome *o* (*cyo*ABCDE) and *d* (*cyd*AB) oxidase gene expression in *Escherichia coli* is regulated by oxygen, pH, and the fnr gene product. J. Bacteriol. 172:6333–6338.

Dailey H. A. and Fleming J. E. (1983) Bovine ferrochelatase. Kinetic analysis of inhibition by N-methylprotoporphyrin, manganese, and heme. J. Biol. Chem. 258:11453-11459.

Dailey H. A. and Dailey T. A. (1996) Protoporphyrinogen oxidase of *Myxococcus xanthus*. Expression, purification, and characterization of the cloned enzyme. J. Biol. Chem. 271:8714-8718.

Dailey H. A., Finnegan M. G., Johnson M. K. (1994) Human ferrochelatase is an iron-sulfur protein. Biochemistry. 33:403-407.

Dailey H. A. (2002) Terminal steps of haem biosynthesis. Biochem. Soc. Trans. 30:590-595.

Dailey T. A., Dailey H. A. (2002) Identification of [2Fe-2S] clusters in microbial ferrochelatases. J. Bacteriol. 184:2460-2464.

Day A. L., Parsons B. M., Dailey H. A. (1998) Cloning and characterization of Gallus and Xenopus ferrochelatases: presence of the [2Fe-2S] cluster in nonmammalian ferrochelatase. Arch. Biochem. Biophys. 359:160-169.

de Sanctis D., Dewilde S., Pesce A., Moens L., Ascenzi P., Hankel T., Burmester T. and Bolognesi M. (2004) Crystal structure of cytoglobin: the fourth globin type discovered in man displays heme hexa-coordination. J. Mol. Biol. 336:917-927.

Dewilde S, Kiger L, Burmester T, Hankeln T, Baudin-Creuza V, Aerts T, Marden MC, Caubergs R, Moens L. (2001) Biochemical characterization and ligand binding properties of neuroglobin, a novel member of the globin family. J. Biol. Chem. 276:38949-38955.

Duwat P., Ehrlich S. D. and Gruss A. (1995) The *recA* gene of *Lactococcus lactis*: characterization and involvement in oxidative and thermal stress. Mol. Microbiol. 17:1121–1131.

Duwat P., Sourice S., Cesselin B., Lamberet G., Vido K., Gaudu P., Le Loir Y., Violet F., Loubiere P. and Gruss A. (2001) Respiration capacity of the fermenting bacterium *Lactococcus lactis* and its positive effects on growth and survival. J. Bacteriol. 183:4509–4516.

Frankenberg N., Erskine P. T., Cooper J. B., Shoolingin-Jordan P. M., Jahn D. and Heinz D. W. (1999) High resolution crystal structure of a Mg2+-dependent porphobilinogen synthase. J. Mol. Biol. 289:591-602.

Frankenberg N., Heinz D. W. and Jahn D. (1999) Production, purification, and characterization of a Mg2+-responsive porphobilinogen synthase from *Pseudomonas aeruginosa*. Biochemistry 38:13968-13975.

Frankenberg N. and Lagarias, J. C. (2003) Phycocyanobilin:ferredoxin oxidoreductase of Anabaena sp. PCC 7120. Biochemical and spectroscopic. J. Biol. Chem. 278:9219-9226.

Frankenberg N., Moser J., and Jahn D. (2003) Bacterial heme biosynthesis and its biotechnological application. Appl. Microbiol. Biotechnol. 63:115-127.

Friedmann H. C. and Thauer R. T. (1992) Encyclopedia of Microbiology. Academic Press, New York. 3:1-19.

Genco C. A. and Dixon D. W. (2001) Emerging strategies in microbial haem capture. Mol Microbiol. 39:1-11.

Gennis R. B. and Stewart V. Respiration. (1996) In F. C. Neidhardt *et al*. (ed.), *Escherichia coli* and *Salmonella*: cellular and molecular biology, 2nd ed., vol. 1. ASM Press, Washington, D.C. 217–261.

Ghigo J.M., Létoffé S. and Wandersman C. (1997) A new type of hemophore-dependent heme acquisition system of *Serratia marcescens* reconstituted in Escherichia coli. J. Bacteriol. 179: 3572–3579.

Gibbs P. N., Chaudhry A. G. and Jordan P. M. (1985) Purification and properties of 5-aminolaevulinate dehydratase from human erythrocytes. Biochem. J. 230 (1):25-34.

Glaser P, Rusniok C, Buchrieser C, Chevalier F, Frangeul L, Msadek T, Zouine M, Couvé E, Lalioui L, Poyart C, Trieu-Cuot P, Kunst F. (2002) Genome sequence of Streptococcus agalactiae, a pathogen causing invasive neonatal disease. Mol Microbiol. 45:1499-1513.

Goldman B. S., Kranz R. G. (2001) ABC transporters associated with cytochrome *c* biogenesis. Res. Microbiol. 152:323-329.

Grage K. (2005) Oxygen-independent coproporphyrinogen III oxidase: characterization of *Escherichia coli* HemN and investigation of proposed functional analogs. Dissertation, TU Braunschweig.

Grzybowska E., Gora M., Plochocka D., Rytka J. (2002) *Saccharomyces cerevisiae* ferrochelatase forms a homodimer. Arch. Biochem. Biophys. 398:170-178.

Hännig A.-L. (2011) Aminolevulinic acid synthase of *Rhodobacter capsulatus*. Dissertation, TU Braunschweig.

Hambright P., SmithK. (ed.) (1975) Dynamic coordination chemistry of metalloporphyrins. In: Porphyrins and Metalloporphyrins. Elsevier, Amsterdam. pp. 233–278.

Hanahan D. (1983): Studies on transformation of *Escherichia coli* with plasmids. In: J. Mol. Biol. Bd. 166, 4:557-580.

Hansson M. and Hederstedt L. (1994) Purification and characterisation of a water-soluble ferrochelatase from *Bacillus subtilis*. Eur. J. Biochem. 220:201-208.

Hargrove M. S., Brucker E. A., Stec B., Sarath G., Arredondo-Peter R., Klucas R. V., Olson J. S., Phillips G. N. Jr. (2000) Crystal structure of a nonsymbiotic plant hemoglobin. Structure. 8:1005-1014.

Hassett D. J., Charniga L., Bean K. A., Ohman D. E. and Cohen M. S. (1992) Antioxidant defense mechanisms in *Pseudomonas aeruginosa*: resistance to the redox-active antibiotic pyocyanin and demonstration of a manganese- cofactored superoxide dismutase. Infect. Immun. 60:328–336.

Heinemann I. U., Diekmann N., Masoumi A., Koch M., Messerschmidt A., Jahn M., Jahn D. (2007) Functional definition of the tobacco protoporphyrinogen IX oxidase substratebinding site. Biochem. J. 402:575-580.

Heinemann I. U., Jahn M. and Jahn D. (2008) The biochemistry of heme biosynthesis. Arch. Biochem. Biophys. 474 (2):238-251.

Hill H. A. O. (ed.). (1981) Inorganic Biochemistry: Volume 2: A Review of Chemical Literature. Royal Society of Chemistry, London.

Hoang T. T., Karkhoff-Schweizer R. R., Kutchma A. j., Schweizer H. P. (1997) A broad-host-range Flp-*FRT* recombination system for site-specific excision of chromosomally-located DNA sequences: application for isolation of unmarked *Pseudomonas aeruginosa* mutants. Gene. 212:77-86.

Hocking R. K., DeBeer George S., Gross Z., Walker F. A., Hodgson K. O., Hedman B., Solomon E. I. (2009) Fe L- and K-edge XAS of low-spin ferric corrole: bonding and reactivity relative to low-spin ferric porphyrin. Inorg. Chem. 48:1678-1688.

Holt J. G., Krieg N. R., Sneath P. H. A., Staley J. T. and Williams S. T. (1994) Gram-positive cocci. Bergey's manual of determinative microbiology, 9th ed. Williams & Wilkins, Baltimore, 527–558.

Hoff A. J. (ed.). (1989) Advanced EPR. Applications in Biology and Biochemistry. Elsevier Science Ltd, Amsterdam, Oxford, New York.

Hrycay E. G. and O'Brien P. J. (1971) Cytochrome P-450 as a microsomal peroxidase utilizing a lipid peroxide substrate. Arch. Biochem. Biophys. 147:14-27.

Hrycay E. G. and O'Brien P. J. (1971) The peroxidase nature of cytochrome P-420 utilizing a lipid peroxide substrate. Arch. Biochem. Biophys. 147:28-35.

Hunter G. A., Ferreira G. C. (2009) 5-aminolevulinate synthase: catalysis of the first step of heme biosynthesis. Cell. Mol. Biol. (Noisy-le-grand). 55:102-110.

Huynh B. H., Moura J. J. G., Moura I., Kent T. A., LeGall J., Xavier A. V., Munck E. (1980) Evidence for a three-iron center in a ferredoxin from *Desulfovibrio gigas*. Moessbauer and EPR studies. J. Biol. Chem. 255:3242-3244.

Ilag L. L. and Jahn D. (1992) Activity and spectroscopic properties of the *Escherichia coli* glutamate 1-semialdehyde aminotransferase and the putative active site mutant K265R. Biochemistry. 31:7143-7151.

Izadi-Pruneyre N., Huché F., Lukat-Rodgers G. S., Lecroisey A., Gilli R., Rodgers K. R., Wandersman C., Delepelaire P. (2006) The heme transfer from the soluble HasA hemophore to its membrane-bound receptor HasR is driven by protein-protein interaction from a high to a lower affinity binding site. J. Biol. Chem. 281:25541-25550.

Jacobs N. J. and Jacobs J. M. (1976) Nitrate, fumarate, and oxygen as electron acceptorsfor a late step in microbial heme synthesis. Biochim. Biophys. Acta. 449:1-9.

Jahn D., Michelsen U. and Soll D. (1991) Two glutamyl-tRNA reductase activities in *Escherichia coli*. J. Biol. Chem. 266:2542-2548.

Jahn D., Hungerer C., and Troup B. (1996) Unusual pathways and environmentally regulated genes of bacterial heme biosynthesis. Naturwissenschaften 83:389-400.

Jordan P. M. (1994) Highlights in haem biosynthesis. Curr. Opin. Struct. Biol. 4:902-911.

Josephy P. D., Eling T. and Mason R. P. (1982) The horseradish peroxidase catalyzed oxidation of 3,5,3',5'-tetramethylbenzidine: free radical and charge-transfer complex intermediates. J. Biol. Chem. 257:3669-3675.

Kadir F. H. A. and Moore G. R. (1990) Bacterial ferritin contains 24 haem groups. FEBS Lett. 271:141–143.

Kakar S., Hoffman F. G., Storz J. F., Fabian M. and Hargrove M. S. (2010) Structure and Reactivity of Hexacoordinate Hemoglobins. Biophysical Chemistry. 152:1–14.

Kendrew J. C., Bodo G., Dintzis H. M., Parrish R. G., Wyckoff H. W., Phillips D. C. (1958) A three-dimensional model of the myoglobin molecule obtained by X-ray analysis. Nature. 181:662–666.

Kitagawa M., Ara T., Arifuzzaman M., Ioka-Nakamichi T., Inamoto E., Toyonaga H., and Mori H. (2005) Complete set of ORF clones of *Escherichia coli* ASKA library (A Complete Set of *E. coli* K-12 ORF Archive): Unique Resources for Biological Research. DNA Research. 12:291–299.

Klebba PE, Newton SM. (1998) Mechanisms of solute transport through outer membrane porins: Burning down the house. Curr. Opin. Microbiol. 1:238-247.

Koch M., Breithaupt C., Kiefersauer R., Freigang J., Huber R. and Messerschmidt A. (2004) Crystal structure of protoporphyrinogen IX oxidase: a key enzyme in haem and chlorophyll biosynthesis. EMBO J. 23:1720-1728.

Kranz R., *et al*. (1998) Molecular mechanisms of cytochrome *c* biogenesis: three distinct systems. Mol. Microbiol. 29:383–396.

Krishnamurthy G., Vikram R., Singh S. B., Patel N., Agarwal S., Mukhopadhyay G., Basu S. K. and Mukhopadhyay A. (2005) Hemoglobin receptor in *Leishmania* is a hexokinase located in the flagellar pocket. J. Biol. Chem. 280:5884-5891.

Kikuchi G., Kumar A. M., Tamlage P. and Shemin D. (1958) The enzymatic synthesis of δ-aminolevulinic acid. J. Biol. Chem. 233:1214-1219.

Laemmli U. K. (1970) Cleavage of structural proteins during the assembly of the head of bacteriophage T4. Nature. 227:680-685.

Lansky I. B., Lukat-Rodgers G. S., Block D., Rodgers K. R., Ratliff M., Wilks A. (2006) The cytoplasmic hemebinding protein (PhuS) from the heme uptake system of *Pseudomonas aeruginosa* is an intracellular heme-trafficking protein to the delta - regioselective heme oxygenase. J. Biol. Chem. 281:13652– 13662.

Layer G., Moser J., Heinz D. W., Jahn D. and Schubert W.-D. (2003) Crystal structure of coproporphyrinogen III oxidase reveals cofactor geometry of Radical SAM enzymes. EMBO J. 22:6214-6224.

Layer G., Grage K., Teschner T., Schünemann V., Breckau D., Masoumi A., Jahn M., Heathcote P., Trautwein A. X. and Jahn, D. (2005) Radical SAM enzyme coproporphyrinogen III oxidase HemN: functional features of the [4Fe-4S] cluster and the two bound *S*-adenosyl-L-methionines. J. Biol. Chem. 280:29038-29046.

Layer G., Reichelt J., Jahn D. and Heinz D. W. (2010) Structure and function of enzymes in heme biosynthesis. Protein science. 19:1137-1161.

Layer G., Jahn D., Deery E., Lawrence A. D. and Warren M. J. (2010) Biosynthesis of heme and vitamin B_{12}. in "Comprehensive natural products II Chemistry and Biology" Elsevier, Oxford. 7:445–499.

Lazazzera B. A., Beinert H., Khoroshilova N., Kennedy M. C., and Kiley P. J. (1996) DNA binding and dimerization of the Fe–S-containing FNR protein from *Escherichia coli* are regulated by oxygen. J. Biol. Chem. 271: 2762–2768.

Lezhneva L., Kuras R., Ephritikhine G. and de Vitry C. (2008) A novel pathway of cytochrome c biogenesis is involved in the assembly of the cytochrome b6f complex in arabidopsis chloroplasts. J. Biol. Chem. 283:24608-24616.

Létoffé S., Deniau C., Wolff N., Dassa E., Delepelaire P., Lecroisey A. and Wandersman C. (2001) Haemophoremediated bacterial haem transport: evidence for a common or overlapping site for haem-free and haem-loaded haemophore on its specific outer membrane receptor. Mo.l Microbiol. 41: 439–450.

Létoffe S., Debarbieux L., Izadi N., Delepelaire P. and Wandersman C. (2003) Ligand delivery by haem carrier proteins: the binding of *Serratia marcescens* haemophore to its outer membrane receptor is mediated by two distinct peptide regions. Mol. Microbiol. 50:77–89.

Létoffé S., Delepelaire P., Wandersman C. (2004) Free and hemophore-bound heme acquisitions through the outer membrane receptor HasR have different requirements for the TonB-ExbB-ExbD complex. J. Bacteriol. 186:4067-4074.

Letoffe S., Nato F., Goldberg M. E and Wandersman C. (1999) Interactions of HasA, a bacterial haemophore, with haemoglobin and with its outer membrane receptor HasR. Mol. Microbiol. 33:546-555.

Loeb M. R. (1995) Ferrochelatase activity and protoporphyrin IX utilization in *Haemophilus influenzae*. J. Bacteriol. 177:3613-3615.

Louie G. V., Brownlie P. D., Lambert R., Cooper J. B., Blundell T. L., Wood S. P., Malashkevich V. N., Hädener A., Warren M. J., Shoolingin-Jordan P.M. (1996) The three-dimensional structure of *Escherichia coli* porphobilinogen deaminase at 1.76-A resolution. Proteins. 25:48-78.

Ma J.-F., Ochsner U. A., Klotz M. G., Nanayakkara V. K., Howell M. L., Johnson Z., Posey J. E., Vasil M. L., Monaco J. J. and Hassett D. J. (1999) Bacterioferritin A Modulates Catalase A (KatA) Activity and Resistance to Hydrogen Peroxide in *Pseudomonas aeruginosa*. J.Bacteriol. 181:3730-3742.

Marchler-Bauer A. *et al*. (2011) CDD: a Conserved Domain Database for the functional annotation of proteins. Nucleic Acids Res. 39:225-229.

Masoumi A., Heinemann I. U., Rohde M., Koch M., Jahn M. and Jahn D. (2008) Complex formation between protoporphyrinogen IX oxidase and ferrochelatase during haem biosynthesis in *Thermosynechococcus elongatus*. Microbiology**.** 154: 3707-3714.

Medlock A. E., Swartz L., Dailey T. A., Dailey H. A., Lanzilotta W. N. (1996) Substrate interactions with human ferrochelatase. Proc. Natl. Acad. Sci. USA. 104:1789-1793.

Medlock A. E., Dailey T. A., Ross T. A., Dailey H. A., Lanzilotta W. N. (2007) A pi-helix switch selective for porphyrin deprotonation and product release in human ferrochelatase. J. Mol. Biol. 373:1006-1016.

Mitchell L.W. and Jaffe E.K. (1993) Porphobilinogen synthase from *Escherichia coli* is a Zn(II) metalloenzyme stimulated by Mg(II). Arch. Biochem. Biophys. 300 (1):169-77.

Mizohata E., Matsuura T., Sakai H. et al. (2005) Crystal structure of uroporphyrinogen III synthase from thermus thermophilus Hb8 (PDB codes 1WCW and 1WD7) protein data bank.

Moore G. R., Kadir F. H. A., Al-Massad F. K., Le Brun N. E., Thomson A. J., Greenwood C., Keen J. N. and Findlay J. B. C. (1994) Structural heterogeneity of *Pseudomonas aeruginosa* bacterioferritin. Biochem. J. 304:493–497.

Moore, G. R. and Pettigrew, G. W. (1990) Cytochromes *c*; Evolutionary, Structural and Physicochemical Aspects, Springer-Verlag, Berlin.

Moser J., Lorenz S., Hubschwerlen C., Rompf A. and Jahn D. (1999) *Methanopyrus kandleri* glutamyl-tRNA reductase. J. Biol. Chem. 274:30679-30685.

Moser J., Schubert W. D., Beier V., Bringemeier I., Jahn D. and Heinz D. W. (2001) Vshaped structure of glutamyl-tRNA reductase, the first enzyme of tRNA-dependent tetrapyrrole biosynthesis. EMBO J. 20:6583-6590.

Munro A. W., Girvan H. M., McLean K. J., Cheesman M. R., Leys D., Warren M. J. (ed.), Smith A. G. (ed.) (2009) Tetrapyrroles: birth, life and death. Landes Bioscience, Austin. Springer Science+Business Media, LLC, New York. 160-183.

Ochsner U. A., Johnson Z. and Vasil M. L. (2000) Genetics and regulation of two distinct haem-uptake systems, phu and has, in *Pseudomonas aeruginosa*. Microbiology. 146:185-198.

Page M. D., Sambongi Y., Ferguson S. J. (1998) Contrasting routes of c-type cytochrome assembly in mitochondria, chloroplasts and bacteria. Trends Biochem. Sci. 23:103-108.

Pesce A., Dewilde S., Nardini M., Moens L., Ascenzi P., Hankeln T., Burmester T., Bolognesi M. (2004) The human brain hexacoordinated neuroglobin three-dimensional structure. Micron. 35:63-65.

Pettigrew G. W., Moore G. R., Rich A. (ed.). (1987) Cytochromes *c*: biological aspects. 1st ed. Springer-Verlag, Berlin Heidelberg New York.

Phillips J. D., Whitby F. G., Warby C. A., Labbe P., Yang C., Pflugrath J. W., Ferrara J. D., Robinson H., Kushner J. P., Hill C. P. (2004) Crystal structure of the oxygen-dependant coproporphyrinogen oxidase (Hem13p) of *Saccharomyces cerevisiae*. J. Biol. Chem. 279:38960-38968.

Poole K., Neshat S., and Heinrichs D. (1991) Pyoverdinemediated iron transport in Pseudomonas aeruginosa: involvement of a high-molecular-mass outer membrane protein. FEMS Microbiol. Lett. 78:1-5.

Poole K. and McKay G. A. (2003) Iron acquisition and its control in *Pseudomonas aeruginosa*: Many roads lead to Rome. Frontiers in Bioscience. 8:661-686.

Ramseier T. M., Winteler H. V., Hennecke H. (1991) Discovery and sequence analysis of bacterial genes involved in the biogenesis of c-type cytochromes. J. Biol. Chem. 266:7793-7803.

Rees D. C., Johnson E., Lewinson O. (2009) ABC transporters: the power to change. Nat. Rev. Mol. Cell Biol. 10:218–227.

Righetti, P. G. (1990) Recent developments in electrophoretic methods. J. Chromatogr. 516:3-22.

Sambrook J., Fritsch E. F. and Maniatis T. (1989) Liquid media for *E. coli*. In Molecular cloning: a laboratory manual. 2nd ed., vol. 3, Cold Spring Harbor Laboratory Press, New York.

Sanders J. W., Leenhouts K. J., Haandrikman A. J., Venema G. and Kok J. (1995) Stress response in *Lactococcus lactis*: cloning, expression analysis, and mutation of the lactococcal superoxide dismutase gene. J. Bacteriol. 177**:**5254–5260.

Sanders C., Turkarslan S., Lee D. W. and Daldal F. (2010) Cytochrome *c* biogenesis: the Ccm system. Trends Microbiol. 18:266-274.

Sanger F., Nicklen S. and Coulson, A.R. (1977) DNA sequencing with chainterminating inhibitors. Biotechnology 24:104-108.

Schauer S. (2003) Die Glutamyl-tRNA Reduktase aus *Escherichia coli*: rekombinante Produktion, Enzymmechanismus und biochemische Charakterisierung. Dissertation, TU Braunschweig.

Schulz H., Hennecke H., Thöny-Meyer L. (1998) Prototype of a heme chaperone essential for cytochrome *c* maturation. Science. 281:1197-1200.

Schulze J. O., Schubert W.-D., Moser J., Jahn D. and Heinz D. W. (2006) Evolutionary Relationship between Initial Enzymes of Tetrapyrrole Biosynthesis. J. Mol. Biol. 358:1212-1220.

Scott A. I., Roessner C. A., Stolowich N. J., Spencer J. B., Min C., Ozaki S. I. (1993) Biosynthesis of vitamin B12. Discovery of the enzymes for oxidative ring contraction and insertion of the fourth methyl group. FEBS Lett. 331:105-108.

Senior N. M., Brocklehurst K., Cooper J. B., Wood S. P., Erskine P., Shoolingin-Jordan P. M., Thomas P. G., Warren M. J. (1996) Comparative studies on the 5-aminolaevulinic acid dehydratases from *Pisum sativum*, *Escherichia coli* and *Saccharomyces cerevisiae*. Biochem. J. 2:401-412.

Senior N. M., Siligardi G., Drake A., Thomas P. G., Warren, M. J. (1997) Structural studies on 5-aminolaevulinic acid dehydratase from *Saccharomyces cerevisiae* (yeast). Biochem. Soc. Trans. 25:78S.

Severance S. and Hamza I. (2009) Trafficking of heme and porphyrins in metazoa. Chem. Rev. 109:4596-4616.

Shemin D. and Russel C. S. (1953) Delta-aminolevulinic acid, its role in the biosynthesis of porphyrins and purins. J. Am. Chem. Soc. 75:4873-4875.

Shepherd M., Dailey T. A., Dailey, H. A. (2006) A new class of [2Fe-2S]-cluster-containing protoporphyrin (IX) ferrochelatases. Biochem. J. 397:47-52.

Sigfridsson E. and Ryde U. (2003) The importance of porphyrin distortions for the ferrochelatase reaction. J. Biol. Inorg. Chem. 8:273-282.

Sijpesteijn A. K. (1970) Induction of cytochrome formation and stimulation of oxidative dissimilation by hemin in *Streptococcus lactis* and *Leuconostoc mesenteroides*. Antonie Leeuwenhoek, 36:335–348.

Smith, F.G. *et al*. (1952) Bathophenanthroline (4,7-Diphenyl-1,10-Phenanthroline) for use in iron determination. Analyst 77:418.

Sreerama N., Woody R. W. (2000) Estimation of protein secondary structure from circular dichroism spectra: comparison of CONTIN, SELCON, and CDSSTR methods with an expanded reference set. Anal. Biochem. 287:252–260.

Sreerama N., Woody R. W. (2004) Computation and analysis of protein circular dichroism spectra. Methods Enzymol. 383:318-351.

Stevens J. M., Daltrop O., Higham C. W., Ferguson S. J. (2003) Interaction of heme with variants of the heme chaperone CcmE carrying active site mutations and a cleavable N-terminal His tag. J. Biol. Chem. 278:20500-20506.

Stojiljkovic I., Perkins-Balding D. (2002) Processing of heme and heme-containing proteins by bacteria. DNA Cell Biol. 21:281-295.

Suaste-Olmos F., Domenzain C., Mireles-Rodríguez J. C., Poggio S., Osorio A., Dreyfus G., Camarena L. (2010) The flagellar protein FliL is essential for swimming in *Rhodobacter sphaeroides*. J. Bacteriol. 192:6230-6239.

Sweeney W. V., Rabinowitz J. C. (1980) Proteins containing 4Fe-4S clusters: an overview. Annu. Rev. Biochem. 49:139-161.

Switala J., Loewen P. C. (2002) Diversity of properties among catalases. Arch. Biochem. Biophys. 401:145-154.

Takeda J., Ohya T. and Sato M. (1992) Ferrochelatase transition-state model: rapid incorporation of copper (II) into nonplanar dodecaphenylporphyrin. Inorg. Chem. 31: 2877-2880.

Thauer R. K. and Bonacker L. G. (1994) Biosynthesis of coenzyme F430, a nickel porphinoid involved in methanogenesis. Ciba Found. Symp. 180:210-22; discussion 222-7.

Thöny-Meyer L. (1997) Biogenesis of respiratory cytochromes in bacteria. Microbiol. Mol. Biol. Rev. 61:337-376.

Thomas P. E., Ryan D. and Levin W. (1976) An Improved Staining Procedure for the Detection of the Peroxidase Activity of Cytochrome P-450 on Sodium Dodecyl Sulfate Polyacrylamide Gels. Anal. Biochem. 75:168-176.

Vavilin D. V. and Vermaas W.F. (2002) Regulation of the tetrapyrrole biosynthetic pathway leading to heme and chlorophyll in plants and cyanobacteria. Physiol. Plant. 115 (1):9-24.

Vincent S. H., Gradi R. W., Shaklai N. *et al*. (1988) The influence of heme-binding proteins in heme-catalyzed oxidations. Arch. Biochem. Biophys. 265:539-550.

Warren M. J., Roessner C. A., Ozaki S., Stolowich N. J., Santander P. J., Scott A. I. (1992) Enzymatic synthesis and structure of precorrin-3, a trimethyldipyrrocorphin intermediate in vitamin B12 biosynthesis. Biochemistry. 31:603-609.

Warren M. J., Smith A. G., (2009) Tetrapyrroles : birth, life, and death. Landes Bioscience, Austin. Springer Science+Business Media, LLC, New York.

Wandersman C., Stojiljkovic I. (2000) Bacterial heme sources: The role of heme, hemoprotein receptors and hemophores. Curr. Opin. Microbiol. 3:215-220.

Wang J., Stuehr D. J., Ikeda-Saito M., Rousseau D. L. (1993) Heme coordination and structure of the catalytic site in nitric oxide synthase. J. Biol. Chem. 268:22255-22258.

Wang K. F., Dailey T. A., Dailey H. A. (2001) Expression and characterization of the terminal heme synthetic enzymes from the hyperthermophile *Aquifex aeolicus*. FEMS Microbiol. Lett. 202:115-119.

Wesche A. (2008) Etablierung eines bakteriellen Two Hybrid Systems für Pseudomonas aeruginosa. Diplomarbeit, TU Braunschweig.

Whitby F. G., Phillips J. D., Kushner J. P. and Hill C. P. (1998) Crystal structure of human uroporphyrinogen decarboxylase. EMBO J. 17:2463-2471.

Wilks A. (2001) The ShuS protein of *Shigella dysenteriae* is a heme-sequestering protein that also binds DNA. Arch. Biochem. Biophys. 387:137-142.

Wu C. K., Dailey H. A., Rose J. P., Burden A., Sellers V. M., Wang B. C. (2001) The 2.0 A structure of human ferrochelatase, the terminal enzyme of heme biosynthesis. Nat. Struct. Biol. 8:156-160.

Ye S., Tuttle T., Bill E., Simkhovich L., Gross Z., Thiel W., Neese F. (2008) The electronic structure of iron corroles: a combined experimental and quantum chemical study. Chemistry. 14:10839-10851.

7 DANKSAGUNG

Mein besonderer Dank gilt Prof. Dr. Dieter Jahn, der er es mir ermöglichte, diese Arbeit in seiner Arbeitsgruppe anzufertigen. Ich danke ihm für Unterstützung und die Diskussionsbereitschaft in den letzten Jahren.

Dr. Gunhild Layer danke ich für ihr Interesse an meiner Arbeit und ihre Bereitschaft das Zweitgutachten dieser Dissertation zu übernehmen, sowie für ihre stete Hilfsbereitschaft bezüglich der Analyse von Eisen-Schwefel Proteinen.

Prof. Dr. Ralf Mendel danke ich für die Übernahme des Vorsitzes der Prüfungskommission.

Ganz besonderer Dank gilt Dr. Martina Jahn für die ausgezeichnete Betreuung während meiner Doktorarbeit, die hilfreichen Diskussion und ihre immer positive Einstellung.

Anna-Lena Kaufholz, Claudia Schulz, Dagmar Zwerschke, Ilka Heinemann, Lars Remus, Melanie Burghartz, Nina Diekmann, Vanessa Hering und Vera Haskamp aus Labor 212 danke ich für ihre Zusammenarbeit, die hilfreichen Diskussionen und die wirkliche schöne Atmosphäre im Labor.

Allen Mitgliedern des Instituts für Mikrobiologie der TU Braunschweig danke ich für die vielen kleinen und großen Hilfen im Laboralltag und das angenehme Arbeitsklima.

Meinen Freunden danke ich für ihre Unterstützung und ihr Verständnis in allen Lebenslagen.

Ein ganz besonderer Dank gilt meiner Familie, besonders meinen Eltern, ohne die diese Arbeit nicht möglich gewesen wäre. Vielen Dank für eure Unterstützung und euer Vertrauen!

Heiko danke ich für sein Verständnis, seine aufmunternden Worte und dafür dass er immer für mich da ist.

APPENDICES

Tab. 15: Characterization of detected interaction partners of *P. aeruginosa* HemH, KatA and BfrA on protein level.

clone	length of homolog protein [aa]	Coverage of the homolog protein by the interacting protein fragment [aa]	Identity [%]	homolog gene
pKT25-hemH				
1.1	173	42 - 117	86	PA1442
1.6	511	29 - 44	87	PA3984
1.8	415	49 - 102	100	PA0605
1.9	250	63 - 250	90	PA3851
1.10	446	9 - 53	97	PA2687
1.11	128	95 - 128	100	PA0540
1.12	395	235 - 252	61	PA2236
1.17	229	1 - 69	98	PA4034
1.19	81	1 - 81	100	PA0738
1.24	173	42 - 117	86	PA1442
1.27	156	58 - 137	98	PA3689
2.26	367	33 - 115	77	PA4002
2.33	69	27 - 69	100	PA1548
2.34	155	1 - 155	60	PA3536
2.36	212	1 - 181	84	PA0885
2.49	250	91 - 190	99	PA3851
2.53	212	1 - 112	100	PA0885
2.60	328	1 - 74	100	PA2254
2.73	309	158 - 309	100	PA4811
2.82	212	1 - 181	84	PA0885
2.92	352	1 - 77	76	PA3360
2.95	207	1 - 164	81	PA5042
2.117	391	11 - 222	66	PA3303
2.121	480	275 - 480	82	PA1262
2.128	117	1 - 117	100	PA0563
2.132	422	1 - 174	85	PA1131
2.147	250	63 - 92	76	PA3851
pKT25-katA				
1.5	183	1 - 36	100	PA3248
1.6	183	1 - 60	92	PA3248

clone	length of homolog protein [aa]	Coverage of the homolog protein by the interacting protein fragment [aa]	Identity [%]	homolog gene
pKT25-bfrA				
1.9	924	523 - 638	87	PA0595
1.22	264	255 - 264	100	PA3382

Figures

Tables